Ti(CN) BASED CERMET SYSTEMS FOR THE IMPROVED WEAR AND MACHINING PERFORMANCE

Ph.D. THESIS

by

VIKAS VERMA

**DEPARTMENT OF METALLURGICAL & MATERIALS ENGINEERING
INDIAN INSTITUTE OF TECHNOLOGY ROORKEE
ROORKEE-247667 (INDIA)
JULY, 2017**

Ti(CN) BASED CERMET SYSTEMS FOR THE IMPROVED WEAR AND MACHINING PERFORMANCE

A THESIS

Submitted in partial fulfilment of the
requirements for the award of the degree

of

DOCTOR OF PHILOSOPHY

in

METALLURGICAL & MATERIALS ENGINEERING

by

VIKAS VERMA

DEPARTMENT OF METALLURGICAL & MATERIALS ENGINEERING
INDIAN INSTITUTE OF TECHNOLOGY ROORKEE
ROORKEE-247667 (INDIA)
JULY, 2017

INDIAN INSTITUTE OF TECHNOLOGY ROORKEE
ROORKEE

CANDIDATE'S DECLARATION

I hereby certify that the work, which is being presented in the thesis entitled "Ti(CN) BASED CERMET SYSTEMS FOR THE IMPROVED WEAR AND MACHINING PERFORMANCE" in partial fulfilment of the requirements for the award of the degree of Doctor of Philosophy and submitted in the Department of Metallurgical and Materials Engineering of the Indian Institute of Technology Roorkee, Roorkee, is an authentic record of my own work carried out during a period from July, 2012 to July, 2017 under the supervision of Dr. B. V. Manoj Kumar, Associate Professor, Department of Metallurgical and Materials Engineering, Indian Institute of Technology Roorkee, Roorkee.

The matter presented in this thesis has not been submitted by me for the award of any other degree of this or any other institute.

(Vikas Verma)

This is to certify that the above statement made by the candidate is correct to the best of my knowledge.

B. V. Manoj Kumar
(Supervisor)

The Ph.D. Viva-Voice Examination of Mr. Vikas Verma, Research scholar, has been held on 23rd October 2017.

Chairman, SRC

External Examiner

This is to certify that the student has made all the correction in the thesis.

Supervisor
Dated: 23/10/17

Head of the Department
प्रोफेसर एवं विभागाध्यक्ष/Prof. & Head
धातुकर्म एवं पदार्थ अभियांत्रिकी विभाग
Metallurgical & Materials Engg. Deptt.
भा॰ प्रौ॰ सं॰ रुड़की/I.I.T Roorkee

Abstract

Ti(CN)-based cermets are reported to possess a unique combination of properties like low density, high hardness and reasonable toughness, ability to undergo plastic deformation, superior wear and corrosion resistance, high strength, high thermal and electrical conductivity. They are proved to be more promising for high speed machining purposes. They possess light weight, superior mechanical properties, resistant to wear, provide improved surface finishing and offer superior geometrical work-piece accuracy than conventionally used tools. The composition of Ti(CN)-based cermets significantly influences properties and the performance. Addition of WC enhances densification during sintering. WC gets readily wetted by both molten nickel and cobalt, thus improving sinterability. Nickel is the basic binder having the highest wettability effect with hard phase. The grain size of the hard phase becomes finer with addition of cobalt. The cobalt addition also improves machinability and decreases solubility of TiN in metallic melt providing the stability of carbonitrides. The literature indicates that TiCN-Ni with WC is the preferred composition for superior wear resistance. Further improvement in the performance of TiCN-based cermets in wear or machining conditions can be achieved with design of new composition. Addition of TaC cermet is expected to improve the high temperature wear resistance because of its thermal shock resistance and the deformable characteristics. The major aim of the present study is to develop TiCN-Ni/Co-WC-TaC cermets for the improvement of performance in wear and machining conditions.

The work presented in the present thesis can be broadly divided into three parts: (i) preparing newly designed Ti(CN)-based cermets and their characterization; (ii) understanding tribological behavior of the sintered cermets in sliding wear conditions and; (iii) estimating performance of the selected cermets in dry machining conditions. The major mechanisms of material removal in wear and machining conditions are particularly elucidated.

Ti(CN) based cermets with compositions Ti(CN)-5WC-20Ni, Ti(CN)-5WC-20Ni-5TaC, Ti(CN)-5WC-10Ni-10Co, and Ti(CN)-5WC-10Ni-10Co-5TaC were processed via conventional sintering and spark plasma sintering (SPS) techniques. The microstructure of the sintered cermets was characterized in terms of carbides (core + rim) size, ceramic contiguity and mean free path of the binder. Hardness and indentation toughness were

estimated for the sintered cermets. High densities are obtained for cermets prepared via SPS than conventional sintering than conventional sintering. Addition of TaC in Ti(CN)-WC-Ni/Co cermets resulted in high hardness and indentation toughness. Refined size and least fraction of adjacent ceramic phase are attributed for improved properties of spark plasma sintered Ti(CN)-5WC-10Ni-10Co-5TaC.

To understand the friction and wear behavior of sintered Ti(CN) based cermets, unlubricated sliding wear behavior at different loads was studied. Three different commercially available counterbody balls (steel, cemented carbide and silicon carbide) were selected. The dominant mechanisms of material removal on the worn cermet discs as well as counter bodies in the selected sliding conditions were elucidated as function of cermet composition and sintering technique. It was found that among the investigated cermets, the Ti(CN)-5WC-10Ni-10Co-5TaC cermet exhibited stabilized friction and reduced wear due to formation of a strongly adherent tribochemical layer and is found to be more promising for superior performance in sliding wear conditions against any counterbody and load. Debris particles were collected after wear tests and their shape and size also studied to obtain a better understanding of friction and wear behavior of the investigated cermets.

Continuing, performance of the sintered Ti(CN) based cermets was studied in machining conditions against 304 stainless steel rod and compared with commercially available cemented carbide tool. Turning operations were performed at different cutting speeds and time intervals for a given feed rate, depth of cut and cutting force was recorded. Dominant crater wear mechanisms were studied on the Ti(CN) based cermets tools and carbide tip tool. Increased intensity of crack, grain pull-out and fracture is observed in conventional sintered Ti(CN)-5WC-20Ni cermet tool, whereas increased resistance against crack or fracture is observed in conventionally sintered and Spark plasma sintered Ti(CN)-5WC-10Ni-10Co-5TaC cermet tools. Further damage during turning is restricted in spark plasma sintered Ti(CN)-5WC-10Ni-10Co-5TaC cermet tool due to formation of adhered layer beneath the tool face.

Summarizing, the present study essentially demonstrates the potential of newly designed cermet composition of Ti(CN)-WC-Ni-Co-TaC for superior performance in wear and machining conditions. Particularly, the design of new composition and degradation mechanisms in sliding wear and turning conditions are highlighted. In other words, an attempt is made to understand the relation of sintering conditions, composition,

microstructure, mechanical properties, wear behavior and tool performance of newly designed TaC added Ti(CN)-WC-Ni/Co cermets.

Acknowledgements

I would like to express my heartiest thanks and deepest gratitude to my respected supervisor Dr. B. V. Manoj Kumar, Associate Professor, Department of Metallurgical and Materials Engineering (MMED) for his inspiration and expert guidance at every stage of this thesis work. This thesis could not have been completed without his support and encouragement. His timely help, constructive criticism, positive attitude, painstaking efforts, humanistic and warm personal approaches made me capable to compile the thesis in its present form. Dr. B. V. Manoj Kumar spent his precious time and efforts directing the research work. I believe that the things that I learned from him will benefit me over the course of my lifetime.

I am highly grateful to Prof. Anjan Sil, Head, MMED, IIT Roorkee and all faculty members of the department for their help and support throughout the course of my research work. Profound sense of appreciation acknowledged to all the members of my Student Research Committee (SRC), Prof. G. P. Chaudhari (Chairman), Prof. Tapas Kumar Mandal, Department of Chemistry (External member) and Prof. Anjan Sil (Internal member) for their valuable suggestions, encouragement and motivation to improve the quality of my research work. Deep sense of admiration acknowledged to the Head, Institute Instrumentation Centre (IIC), for their cooperation in extending the necessary facilities and supports during the course of characterization work. A special thanks to all the IIC technical staff members for giving their full assistance for all characterization facilities. I would like to thank all the technical and administrative staff of MMED for their corporation during the tenure of the work.

Sincere appreciation and special thanks to all my friends and colleagues for their moral support and for helping me directly or indirectly during the entire period of this work.

I would like to express heartiest gratitude to my parents for showering their blessings over me.

Above all, I express my sincere thanks to GOD for giving the strength and patience to accomplish my research work.

I would like to dedicate my thesis to God, my Supervisor and my parents whose presence were always there for me for every moment during my PhD period.

Roorkee

Dated:

(VIKAS VERMA)

Table of Contents

Chapter 3.

Chapter 4.

List of Tables

Chapter 4.

Chapter 5.

Chapter 7.

List of Abbreviations

Al	Aluminium
Al_2O_3	Aluminium oxide
BCC	Body centred cubic
C	Carbon
Co	Cobalt
Cr	Chromium
CDH	Central Drug House
Cr_3C_2	Chromium carbide
CrN	Chromium nitride
Cu	Copper
Fe	Iron
ΔG_f	Gibbs free energy
GPa	Giga Pascal
Hf	Hafnium
HV	Hardness Vickers
HfC	Hafnium carbide
HfN	Hafnium nitride
HIP	Hot isostatic pressing
HP	Hot pressing
K_{Ic}	Indentation toughness
Mo	Molybdenum
Mo_2C	Molybdenum carbide
MPa	Mega Pascal
N	Nitrogen
NaCl	Sodium Chloride
Nb	Niobium
NbC	Niobium carbide
NbN	Niobium nitride
Ni	Nickel
O	Oxygen
Si_3N_4	Silicon nitride
SPS	Spark plasma sintering

Si	Silicon
Ta	Tantalum
TaC	Tantalum carbide
TaN	Tantalum nitride
Ti	Titanium
TiC	Titanium carbide
Ti(CN)	Titanium carbonitride
TiN	Titanium nitride
TRS	Transfer rupture strength
V	Vanadium
VC	Vanadium carbide
VN	Vanadium nitride
WC	Tungsten carbide
Zr	Zirconium
ZrC	Zirconium carbide
ZrN	Zirconium nitride

Award and List of Research Publications

Awards and Achievements

1. Best paper Award in IMME17, International Conference organized by the Department of Metallurgical and Materials Engineering, National Institute of Technology (NIT), Tiruchirappalli, India (10-12.March.17)

Publications in PhD

Papers in refereed Journals from PhD thesis work

1. Vikas Verma, B. V. Manoj Kumar. Processing of Ti(CN)–WC–Ni/Co Cermets via Conventional and Spark Plasma Sintering Technique. Transactions of the Indian Institute of Metals, 2017; 70(3):843–853. doi 10.1007/s12666-017-1069-y.Impact Factor: 0.502

2. Vikas Verma, B. V. Manoj Kumar. Sliding wear behavior of SPS processed TaC containing Ti(CN)-WC-Ni/Co cermets against Silicon Carbide. Wear, 2017; 376-377:1570-1579. doi 10.1016/j.wear.2017.02.013. Impact Factor: 2.323.

3. Vikas Verma, B. V. Manoj Kumar. Effects of binders (Ni-Co) and ternary carbide (TaC) on friction and wear behavior of Ti(CN) based cermets, Ceramic Transactions, Wiley online library 2017; 263: 353-364.doi: 10.1002/9781119407270.ch34

4. Vikas Verma, B. V. Manoj Kumar, Shinhoo Kang. Sliding wear behavior of TaC-containing Ti(CN)-WC-Ni/Co cermets. International Journal of Applied Ceramic Technology, 2016; 13(6):1033-1042. doi:10.1111/ijac.12583. Impact Factor: 1.534.

5. Vikas Verma, B. V. Manoj Kumar. Tribological characteristics of conventionally sintered Ti(CN)-WC-Ni/Co cermets against cemented carbide. Ceramics International. 2016; 43(1):368-375. doi.org/10.1016/j.ceramint.2016.09.167. Impact Factor: 2.758.

6. Vikas Verma, B. V. Manoj Kumar. Tribological behavior of Ti(CN) based cermets against steel and cemented carbide. Materials Today: Proceedings., 2016; 3(9):3130-3136, doi: 10.1016/j.matpr.2016.09.029

Papers in refereed journals from other than PhD thesis work

1. Vikas Verma, B. V. Manoj Kumar. Processing of Alumina based Composites via Conventional Sintering and their Characterization. Materials and Manufacturing

Processes. 2016; 32(1): 21-26, doi: 10.1080/10426914.2016.1198023. Impact Factor: 1.63.

2. Vikas Verma, B. V. Manoj Kumar. Synthesis, microstructure and mechanical properties of $Al_2O_3/ZrO_2/CeO_2$ composites with addition of Nickel and Titania processed by conventional sintering. Materials Today: Proceedings. 2017; 4(2):3062-3071. doi.org/10.1016/j.matpr.2017.02.189.

Participation in Conferences

1. International Conferences

1. Vikas Verma, B. V. Manoj Kumar. Oral Presentation on, "TaC-Containing Ti(CN)-WC-Ni/Co Cermets for the Improved Machining Performance". Sips2017-Sustainable Industrial processing Summit and Exhibition, Cancun, Mexico, 22-26 October, 17 (Paper Accepted)

2. Vikas Verma, B. V. Manoj Kumar, Oral presentation on, "Microstructure effect on mechanical properties of advanced TiCN based cermet system". AMPCO-2017 Advanced Materials and Processes: Challenges and Opportunities. Indian Institute of Technology, Roorkee, India, 30.Nov.-02.Dec.2017 (Accepted)

3. Vikas Verma, B. V. Manoj Kumar. Poster Presentation on, "Tribological characteristics of conventional and spark plasma sintered Ti(CN) based cermets". (Presented by PhD Guide Sir). 12th Pacific Rim Conference on Ceramic and Glass Technology (PACRIM 12), including Glass & Optical Materials Division Meeting (GOMD 2017). Hawaii, USA, 21-26.May.2017.

4. Vikas Verma, B. V. Manoj Kumar, Conference Volunteer and Poster Presentation on, "Sliding wear behavior of SPS processed TaC-containing Ti(CN)-WC-Ni/Co cermets against Silicon Carbide". WOM 17-21st International Conference on Wear of Materials, Long Beach, California, USA, 26-30 March 2017

5. Vikas Verma, B. V. Manoj Kumar, Oral presentation on, "Sliding wear behavior of conventional processed Ti(CN) based cermets against WC-Co". HTCMC 9—in conjunction with GFMAT 2016 (High Temperature Ceramic Matrix Composites and Global Forum on Advanced Materials and Technologies for Sustainable Development. Toronto, Canada. 26. June - 1.July.2016.

6. Vikas Verma, B. V. Manoj Kumar, Oral presentation on, "Processing of Ti(CN)-WC-Ni/Co cermets via Conventional and Spark Plasma Sintering Technique" IMME17, International Conference organized by the Department of Metallurgical and Materials Engineering, National Institute of Technology (NIT), Tiruchirappalli, India. 10- 12.March.17.

7. Vikas Verma, B. V. Manoj Kumar, Oral presentation on, "Processing of Densified Ti(CN)-WC-Ni/Co based Cermets via Conventional and Spark Plasma Sintering and their Characterization" . PM 16 International Conference on Powder

Metallurgy & Particulate Materials + exhibition & 42nd annual technical meeting of PMAI, Pune. 18-20.Feb.2016.

8. Vikas Verma, B. V. Manoj Kumar, Oral presentation on," Tribological Behavior of Ti(CN) based Cermets against Steel and Cemented Carbide" Advances in Refractory and Reactive Metals and Alloys (ARRMA), International Conference BARC Bombay. 27-29.Jan.2016.

9. Vikas Verma, B. V. Manoj Kumar, Oral presentation on," "Effect of TaC and Co addition on the sliding wear behavior of Ti(CN)-Ni-WC cermets" (Presented by PhD Guide Sir). 11th International Conference of Pacific Rim Ceramic Societies (PacRim-11), Jeju Island in Korea. 30.Aug-4.Sep.2015

2. National Conferences

1. Vikas Verma, B. V. Manoj Kumar, Oral Presentation on "Tribological Characterization of Ti(CN)-10Ni-10Co-5WC-5TaC cermet". 53rd National Metallurgist's Day, The Indian Institute of Metals NMD ATM 2015. Int. Symp. On "Vision 2025 - Global Challenges & Opportunities in Steel Industry" and 69th Annual Technical Meeting of the Indian Institute of Metals. New Horizons in Materials Processing and Applications. PSG, Coimbatore. 13-16. Nov.2015

2. Vikas Verma, B. V. Manoj Kumar, Oral presentation on, "Advanced Cermet systems for improved Tribological performance". 52nd National Metallurgist's Day. The Indian Institute of Metals NMD ATM 2014. Redefining the Horizons of Metallurgy/Materials, Focus on Automotive, Aerospace, Defense and Energy. And 68th Annual Technical Meeting of the Indian Institute of Metals. College of Eng. Pune. 12-15.Nov.,2014

3. Vikas Verma, B. V. Manoj Kumar, Poster presentation on, "Tribological behavior of Ti(CN) based Cermets. 51st National Metallurgist's Day. The Indian Institute of Metals NMD ATM 2013. 67th Annual Technical Meeting conducted by The Indian Institute Of Metals, IIT BHU, Varanasi, 12-15.Nov., 2013.

Chapter-1
Introduction

1.1 Background

Structural ceramics are preferred for cutting tool inserts as they have low density, high hardness, high-temperature sustainability and high resistance against corrosion, wear, and thermal shock [Kim et al. 1999, 2005; Terao et al. 2002; Eom and Kim, 2010; Basu and Kalin, 2011]. However, they are difficult to sinter and possess moderate toughness. The addition of metal binder helps in reducing sintering temperature and increasing the toughness. The composites made up of ceramics and metallic binders are known as cermets. Cermets are materials with high temperature sustainability and superior resistance against oxidation and wear [Chicardi et al., 2016a]. They have high melting point, chemical stability, oxidation resistance, ductility and high thermal conductivity [Ettmayer and Lengauer, 1989; Kumar et al. 2008; Obra et al. 2017b]. Cermets are commonly used in cutting tool industry (for milling, turning, grooving or semi-finishing of stainless steels and carbon alloy) and making of dies [Kumar et al. 2007; Peng et al, 2013].

Ti(CN)-based cermets were invented in 1931 [Krupp, 1931]. But boom of the production really started in 1968-1970 [Kieffer, 1971]. Ti(CN) based cermets are proved to be more promising in finishing and high speed cutting tools machining purposes [Kwon et al., 2004]. A photograph of Ti(CN) based cermet cutting tools is shown in **Figure 1-1.** Ti(CN)-based cermets are reported to possess a unique combination of properties like low density, high hardness, reasonable toughness, ability to undergo plastic deformation, superior wear and corrosion resistance, high strength, high thermal and electrical conductivity [Zhang, 1993; Ettmayer et al., 1995; Zhang et al., 2006].

Ti(CN) based cermet cutting tools are superior from conventionally used WC tools. They are more resistant to wear and inert against corrosion in comparison to WC tools [Ettmayer et al., 1995; Kumar et al. 2008]. Ti(CN) based cermet cutting tools are light in weight [Zhang, 1993]. A lower cost was expected because of the abundance and low price of raw materials [Pastor, 1987]. When compared with conventional WC-Co tool materials, Ti(CN) based cermets were found to provide improved surface finishing and offer superior geometrical workpiece accuracy [Kwon et al., 2004].
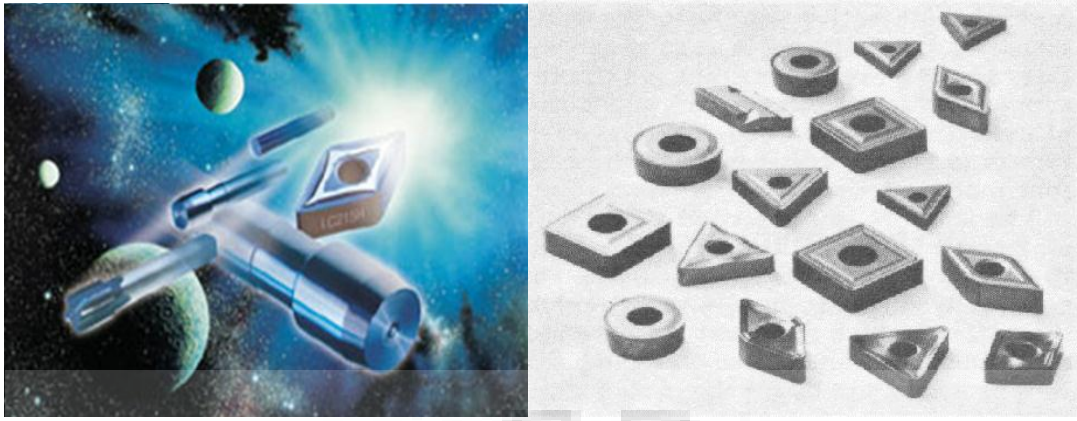
Figure 1-1: Ti(CN) based cermet cutting tool [Lengfeng Metallica, 2016]

Ti(CN) based cermets can be prepared by many sintering techniques like conventional (pressureless) sintering, hot pressing (HP), hot isostatic pressing (HIP) and novel processing route of spark plasma sintering (SPS). Sintering transforms powdered compact into solid mass by heat or pressure or by both [German, 1996]. When there is no application of external pressure, it is called conventional sintering. It is a popular inexpensive processing method that can produce different sintered geometries. Most of the studies highlight the processing of Ti(CN) based cermets by conventional sintering. High productivity, excellent geometrical precision, surface finish and efficient use of material are some of the primary advantages of the conventional sintering [Zhang et al. 2000; Castro, 2012]. It is widely believed that one can achieve better mechanical properties by restricting the grain growth during sintering, whereas conventional sintering, HP or HIP, leads to considerable coarsening of grains. In this aspect spark plasma sintering technique (SPS) has emerged as a novel processing route by employing rapid rate of heating and lowering the holding time at sintering temperature [Jain et al. 2010; Cordoba et al., 2013; Obra et al. 2017a]. In SPS, high pressure and electric current permit localized necking. Due to Joule heating effect, temperature raises very fast and densification completes within few minutes Relatively low sintering temperature with rapid processing time allows a tight control of the grain growth [Jain et al., 2010; Reddy et al., 2010a & 2010b; Guillon et al., 2014]. Thus, it has the advantage of reduced sintering time, good grain to grain bonding and clean grain boundaries resulting in improved physical and mechanical properties. The fabrication of various shapes is possible using SPS with the use of suitable dies.

From the past decade, extensive research has been carried out to understand the composition and wear or friction behavior of structural ceramics, composites, polymeric composites and cermets [Krishna et al. 2006; Bijwe et al. 1990; Bijwe and Rattan, 2007; Kumar et al. 2008; Ramkumar et al. 2011]. Ti(CN) based cermets over a wide range of

experimental conditions and several grades of Ti(CN)-based cermets are being investigated for their tribological behavior [Kumar et al. 2008, Jin et al. 2017a, 2017b]. Over the years, efforts have been made in development of titanium carbonitride-based cermets having different ceramic hard phases and metallic binders as shown in **Table 1-1.**

Table 1-1: A list of reported compositions of ceramic hard phase and binder phase of Ti(CN) based cermets.

Hard phase	Binder phase	References
Ti(C, N)	Ni(Co, Fe)	(Krupp, 1931)
Ti(C, N)	Ni-Mo	(Kieffer, 1971)
(Ti, Mo)(C, N)	Ni-Mo	(Pastor, 1987)
TiC-TiN- WC- TaC	Ni-Co-Mo	(Zhang, 1993)
TiC–TiN–WC	Ni–Mo	(Ning et al, 1994)
(Ti,Mo,W,Ta,Nb)C,N	Co/Ni	(Ettmayer et al., 1995)
TiN–WC–TiC	Ni–Mo	(Zhang et al, 1997)
Ti(CN)–WC– (Ti,W)C	Ni–Co–Mo	(Zackrisson and Andren, 1999)
TiC–TiN–WC	Ni	(Ahn and Kang, 2000)
TiC–TiN–WC	Co	(Zackrisson et al., 2001)
Ti(CN)–x(WC)	Ni	(Jeon et al., 2002)
Ti(CN)–Al$_2$O$_3$	Ni–Mo	(Liu et al., 2004)
Ti(CN)–xWC–(ZrC, ZrN, HfC)	Ni.	(Kwon et al., 2004)
(Ti,W)(C,N)	Ni	(Park and Kang, 2005)
Ti(CN)–WC–TiN	Mo–Ni	(Liu at al., 2006)
Ti(CN)-(W,Nb,Ta,Hf)C	Ni	(Kumar and Basu, 2008)
Ti(CN)–WC	Co–Ni	(Xiong et al., 2008)
Ti(CN)	Ni	(Cardinal et al., 2009)
Ti(CN)–WC	Ni–Co	(Zhang et al., 2010)
(Ti, Mo, W, V)(C, N)	Ni–Co	(Liu et al., 2011)
Ti(C,N)/(Ti,W)(C,N) –	Ni	(Kim et al., 2012)

WC,Mo$_2$C, TaC, NbC		
(Ti, Ta, Nb, V, W, Mo)(C, N)	Ni-Cr	(Yokoo, 2016)
TiC–TiN–WC	Ni–Mo	(Liu et al., 2016)

The composition of Ti(CN)-based cermets significantly influence properties and the performance of the cermet. **Figure 1-2** shows the compositional design of Ti(CN) based cermets. Hardness of the cermet increases with increasing TiC and TiN contents, whereas additions of (Ta, Nb)C appear to increase thermal shock resistance in the cermets thus improving machinability. Densification increases during sintering with the increased WC and Mo$_2$C content. Addition of Co/Ni increases indentation toughness of the cermets as they have highest wettability with ceramic phases.

The rationale for different constituents of cermets used in the present study is as follows:

Titaniumcarbonitride (Ti(CN)): Ti(CN) is a complex structure consisting of TiN and TiC bonds in a crystalline matrix. It is preferred for cutting tool inserts as it is harder than various carbides and nitrides provides wear and abrasion resistance on precision components holds sharp edges and corners and generates low friction while operation.

Tungsten Carbide (WC): WC can be pressed and given different shapes for use in industrial machinery, cutting tools, abrasives, other instruments and tools. WC gets readily wetted both nickel and cobalt molten melt and thus improves sinterability [Kwon et al., 2004].

Tantalum Carbide (TaC): TaC is considered for the consistent mechanical behavior among transition metal carbides. Resistance to crack propagation also increases due to addition of TaC as it behaves plastically deformable before breaking [Rowcliffe and Warren, 1970; Rowcliffe and Hollox, 1971; Rolander et al., 2001].

Nickel (Ni): Nickel is the basic binder having the highest wettability effect with hard phase. The contact angle is the least at high temperature providing complete wetting of carbide particles with nickel. It is used as binder phase in the cermet. It improves the indentation toughness of the cermet [Zhang, 1993].

Cobalt (Co): Cobalt is also used as metal binder phase in the cermet material. It improves the resistance to grain pull-out from the base cermets. Co addition leads to grain refinement of the hard phase. Co addition provide the stability of carbonitrides by decreasing Ti solubility in Ni. Addition of Co improves machinability [Zhang, 1993].

During sintering of TiCN based cermets, there is formation of nitrogen-rich nuclei around which the dissolved carbides will precipitate in the course of a dissolution-reprecipitation process. Co decreases the solubility of Ti in Ni as Cobalt has low solubility with TiN in comparison to TiC. So TiC dissolution rate in Ni melt is faster than TiN dissolution. The reason being as heats of formation (ΔH_f) at 298 K (kJ/mol) of TiC and TiN are -183.7 and -338 KJ/mol. So as TiC has low negative heats of formation it has the lowest wetting angle or best wettability with liquid metals (Co/Ni) in comparison of TiN [Ettmayer et al, 1995].
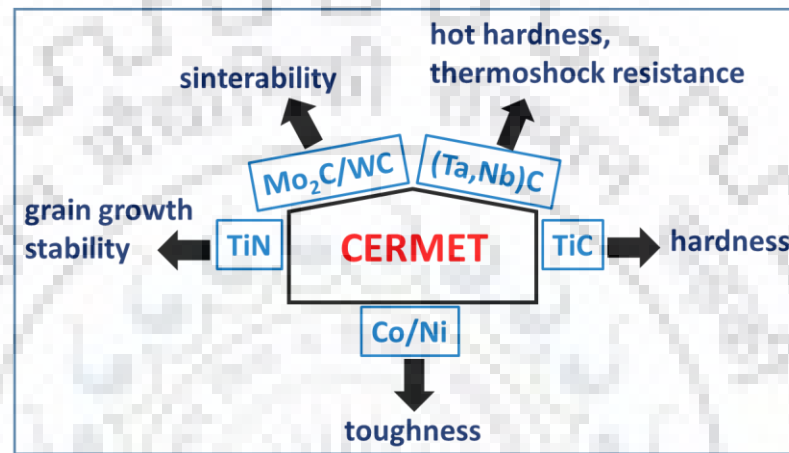
Figure 1- 2: Compositional design of Ti(CN) based Cermets [Ettmayer et al., 1995]

Wear is a phenomenon of progressive damage which result in loss of materials [Gahr, 1987]. Wear can be classified on the basis of types of relative motion of contacting solid surfaces. The most common motion is sliding and Sliding wear can be performed at the laboratory scale by using several test configurations viz. pin-on-disc, ball-on-disc, block-on-ring, etc [Quercia et al., 2001; Wood et al., 2005; Krishna et al., 2003, 2015; Stewart and Plucknett, 2015]. Sliding behavior of Ti(C,N)-based cermets is influenced by their heat treatment, microstructure and mechanical properties [Pirso et al., 2006].

Major wear mechanisms operative in sliding conditions are adhesion, abrasion, surface fatigue, oxidation or tribochemical wear and fretting [Bhushan, 2013]. Adhesion wear occurs during sliding due to the interactions of surfaces in contact and due to the welding of asperities. Kayaba et al., 1986 mentioned that the wear fragments may transfer to the mating surface, may remain adhered to a surface or may detach as large loose wear particles. Sliding of hard particles or hard asperities over a softer body results in abrasive wear. There occurs damage at the interface by fracture or by plastic deformation. The surface fatigue, initiation and propagation of cracks in surface region present due to

repeated tribological stress cycles (e.g. reciprocatory motion at a loaded tribocontact). According to Suh, 1973; Suh, 1977 cracks can originate below the surface and propagate parallel to the surface. Tribochemical wear results due to removal of material and reaction products from the contacting surfaces. Tribochemical wear process occurs mainly in four sequential instances. The metallic debris due to adhesion of metallic contacts gets oxidized. Protective surface layers forms due to chemical reaction of the metals with the environment. Further, localized high pressure or microfatigue situations leads to cracking of the protective layers [Gahr, 1987].

With regards to the improvement in performance, several grades of Ti(CN)-based cermets are being investigated for their tribological behavior [Sarkar et al., 2004; Kumar et al. 2008; Jin et al. 2017b]. In cutting, major properties that are to be desired are high hardness, indentation toughness, wear resistance, thermal stability at higher or elevated temperature, shock resistance at impact loading etc. The physical and mechanical behavior of the cermets are controlled by adding different binder phases like Ni or Co and various carbides such as WC, TaC, HfC, NbC etc [Moskowitz and Humenik, 1966; Pastor, 1987; Dusza et al., 1987; Kwon et al., 2004]. Dry machining is preferred over wet machining as it has the advantages of non-polluting the environment and offers no danger to health, whereas wet machining includes lubricants having compounds harmful for human health and environment. Their consumption in the industrial environment can have serious respiratory effects and also ecological problems [Byrne and Scholta, 1993; Suliman et al., 1997; Sreejith and Ngoi, 2000; Mijanovic and Sokovic, 2001; Dahmus and Gutowski, 2016].

In the present research, in order to improve mechanical properties and wear performance of Ti(CN)-based cermets, novel Ti(CN) based compositions were designed with addition of TaC as ternary carbide with Ni/Co as binders. The effect of TaC with Ni/Co as binders on physical and mechanical properties of Ti(CN)-based cermets were investigated. Ti(CN) based cermets were processed via two techniques: (i) low cost conventional sintering technique and (ii) spark plasma sintering (SPS).

Further to understand the friction and wear behavior of processed Ti(CN) based cermets, unlubricated sliding wear study was done. Three different commercially available counter bodies: bearing grade steel of 7 GPa hardness, cemented carbide of 17 GPa hardness and silicon carbide of 25 GPa hardness respectively were selected for the sliding wear tests. Tests were performed at different loads (5, 10 or 20 N). The dominant mechanisms of material removal on the worn cermet discs as well as counter bodies in the

selected sliding conditions were elucidated. Debris particles were collected after wear tests and their shape and size were studied and compared to develop a better understanding of friction and wear behavior.

Continuing, machining performance study of the processed Ti(CN) based cermets were done and were compared with commercially available tool to study the wear mechanisms on worn cutting edges. Turning operations were performed against 304 Stainless steel rod. Cermet discs were shaped in machining tool geometry. Turning operations were performed at different cutting speeds and time intervals for a given feed rate and depth of cut. Similar machining tests were performed using a commercially available cemented carbide tip. Cutting force was recorded for different cutting speed and time intervals. Dominant crater wear mechanisms were studied on the cutting edges of Ti(CN) based cermets tools and carbide tip tool. Study of chip morphology was also done to understand the machining performance.

1.2 Objectives of the study

The major aim of the present thesis is to design a new Ti(CN) based cermet composition for improved performance in wear and machining conditions. The following factual objectives are identified for the present work:

1. Preparing novel composition of Ti(CN)-WC-Ni/Co cermets with or without addition of TaC by conventional sintering as well as spark plasma sintering.
2. Studying phase analysis, microstructural features and evaluation of mechanical properties of sintered cermets.
3. Understanding the tribological behavior of sintered cermets in sliding conditions as a function of sliding load and counter body.
4. Studying mechanisms of material removal in sliding wear conditions.
5. Estimation of machining performance of cermets as cutting tools and studying wear mechanisms in unlubricated conditions of machining.
6. Understanding the relation of cermet processing, composition, microstructure, physical and mechanical properties, wear behavior and tool performance of novel Ti(CN) based cermets.

1.3 Structure of the thesis:

In order to envisage the above objectives, the thesis is structured as per the following:

Chapter-2   Literature review

This chapter presents a comprehensive review of the published available literature in different areas that are directly relevant to the study being undertaken. The literature

7

review has been presented broadly in following segments; history and present status of Ti(CN) based cermets, processing via conventional sintering and spark plasma sintering techniques, friction and wear behavior and machining performance. A review of mechanical properties, tribological behavior, machining study and effect of different constituents on the properties of Ti(CN) based cermets has been presented.

Chapter-3   Experimental Procedure

It deals with the experimental procedures employed in the present work and describes the details of powders used, compositions investigated, processing and fabrication methods. Details of various instruments used to investigate density, microstructural features, mechanical properties and wear behavior of the investigated cermets are described. Tool processing and experimental details pertaining to machining study of Ti(CN) based cermets are also given.

Chapter-4   Processing and characterization of Ti(CN) based cermet via conventional sintering and SPS.

In this chapter, details of characteristics of conventional sintering and SPS used for processing of Ti(CN) based cermets are discussed. Also major observations in microstructure and mechanical properties of the investigated cermets are provided.

Chapter-5   Tribological behavior of conventional sintered cermets against steel and cemented carbide balls

This chapter deals with major results obtained on friction and wear properties of conventionally sintered Ti(CN) based cermets against steel ball and cemented carbide counterbodies.

Chapter-6   Tribological behavior of Spark plasma sintered cermets against silicon carbide ball

The salient observations on friction and wear properties of Spark plasma sintered Ti(CN) based cermets against hard silicon carbide ball as counterbody are discussed in this chapter.

Chapter-7   Machining studies of Ti(CN) based cermet tools

Results obtained in turning of Ti(CN) based cermet tools against 304 stainless steel are discussed. Particularly dominant crater wear mechanisms responsible for material removal from the tool edge of Ti(CN) based cermet with or without TaC are discussed and compared with that of commercial cemented carbide tip.

Chapter-8   Conclusions and future scope

In this chapter, the important conclusions drawn from the present thesis work are described. Also future directions in which studies can be extended are suggested.

The outline of the doctoral investigation is shown in **Figure 1-3.**
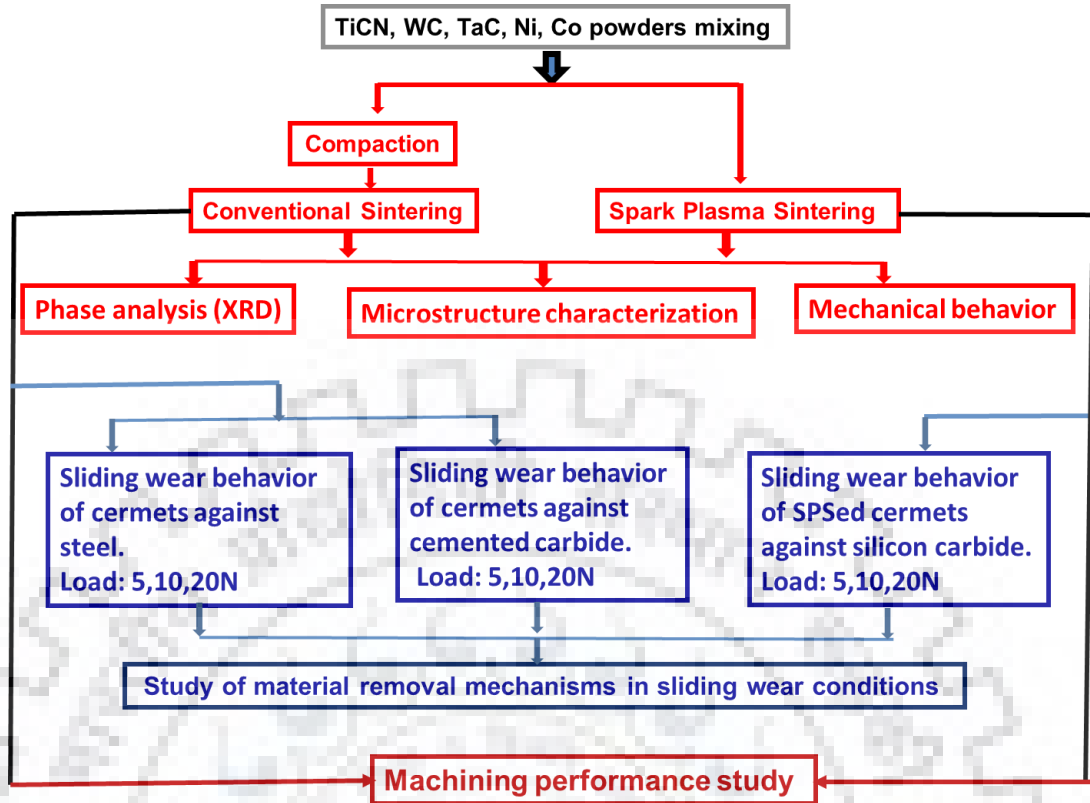
Figure 1-3: A pandect of the doctoral investigation

<div align="right">

Chapter-2
Literature Review

</div>

This chapter presents a comprehensive review of published available literature in different areas that are directly relevant to the present study. The literature review is presented broadly in following segments; history and present status of Ti(CN) based cermets, processing via conventional sintering and spark plasma sintering techniques, friction and wear behavior and machining performance. A review of mechanical properties, tribological behavior, machining studies and effect of different constituents on the properties of Ti(CN) based cermets is presented.

2.1. Background

A cermet is made up of two materials, a hard ceramic and a soft metal binder. Ceramics can survive at high temperature, exhibit superior wear resistance and are chemically stable. Metals have high ductility and high thermal conductivity. Metals like nickel, molybdenum or cobalt are used as binders for an oxide, boride, or carbide ceramics. Cermets consist of nitrides and carbides of the transition metals and exhibit unique physical and mechanical properties [Santhanam, 1996]. A summary on properties of Group IV-VI transition metals, carbides or and their nitrides is shown in **Table 2-1**. Group IV-VI transition metals carbides and nitrides are refractory materials having very high melting points (2000-4000°C). They are extremely hard (1200-3000 kg/mm^2) and have high elastic modulus (300-700 GPa). Their hardness is retained to very high temperatures, they have low chemical reactivity and retain good corrosion and wear resistance at high temperatures so they are in industrial use as cutting tools [Santhanam, 1996]. Properties of Group IV-VI transition metals, carbides and nitrides are shown in **Table 2-1.**

Table 2-1: Properties of Group IV-VI transition metals, carbides and nitrides [Santhanam, 1996; Toth, 1971].

	Crystal Structure	Melting Point (K)	Micro-Hardness (kg/mm^2)	Modulus of Elasticity (GPa)
Group IV				
Ti	Hexagonal	1940	-	110
TiC	FCC	3370	3000	451

TiN	FCC	3220	2000	612
Zr	Hexagonal	2120	-	95
ZrC	FCC	3670	2700	348
ZrN	FCC	3250	1500	460
Hf	Hexagonal	2490	-	138
HfC	FCC	4170	2600(2700 $HfC_{0.99}$)	352
HfN	FCC	3660	1600	380
Group V				
V	BCC	2170	-	130
VC	FCC	2970	2900	422
VN	FCC	2450	1500	-
Nb	BCC	2740	80	101
NbC	FCC	3870	2000 (2400$NbC_{0.99}$)	338
NbN	FCC	2470	1400	-
Ta	BCC	3250	110	186
TaC	FCC	4070	1800 (2500 $TaC_{0.99}$)	285
TaN	FCC	3360	1050	-
Group VI				
Cr	BCC	2130	-	248
Cr_3C_2	Orthorhombic	2070	1400	373
CrN	Hexagonal	1770	1100	-
Mo	BCC	2890	210	325
Mo_2C	Hexagonal	2770	1500	533
W	BCC	3670	400	345
WC	Hexagonal	3070	2350	696

Compared to conventional WC-based hard materials, titanium carbide or nitride based cermets have higher hot hardness, chemically inert, thermal stability, resistance to plastic deformation at high temperatures, wear resistance, performance reliability, give a better surface quality finish and better edge strength [Zhau et al., 2009]. Because of their superior physical and mechanical properties they are used in machining of high strength steel grades and ductile cast irons [Salem, 2009; Liu et al., 2005]. A glance to the history of TiC or TiN based cermet development is shown in **Table 2-2.**

Table 2-2: Overview of titanium carbonitride-based cermets development (Zhang, 1993)

Year	Hard phase	Binder phase
1931	Ti(C, N)	Ni(Co, Fe)
1970	Ti(C, N)	Ni-Mo
1974	(Ti, Mo)(C, N)	Ni-Mo
1980-83	(Ti, Mo, W)(C, N)	Ni-Mo-Al
1988	(Ti, Ta, Nb, V, Mo, W)(C, N)	(Ni, Co)-Ti_2AlN
1988	(Ti, Ta, Nb, V, W)(C, N)	Ni-Co
1991	(Ti, Ta, Nb, V, W, Mo, etc)(C, N)	Ni-Cr

Comparatively, titanium carbonitride-based cermets have high hot hardness, better oxidation resistance, high transverse rupture strength, and higher thermal conductivity **(Table 2-3).** [Tobioka et al, 1988; Matsubara and Sakuma, 1988]. Ti(C,N)-based cermets exhibit superior surface finish, high tolerance with improved cutting performance and long tool life (Pastor, 1988).

Table 2-3: Comparison of properties between TiC-based cermets and Ti(C,N)-based cermets [Gruss, 1993]

Cermets	1000°C Microhardness ($kgmm^{-2}$)	900°C Strength (TRS) (MPa)	Weight gain during oxidation tests at 1000°C ($mg.cm^{-2}h^{-1}$)	Therm. Cond ($Wm^{-1}deg^{-1}$)
TiC-16.5Ni-9Mo	500	1050	11.8	24.7
TiC-20TiN-15WC-10TaC-5.5Ni-11Co-9Mo	600	1360	1.6	42.3

2.2. Titanium carbonitride based cermets

Titanium carbonitride is an alloy of titanium carbide (TiC) and titanium nitride (TiN). The crystal structures of TiC and TiN are illustrated in **Figure 2-1**, which shows a NaCl crystal structure formed by titanium ions, with C or N occupying octahedral sites.
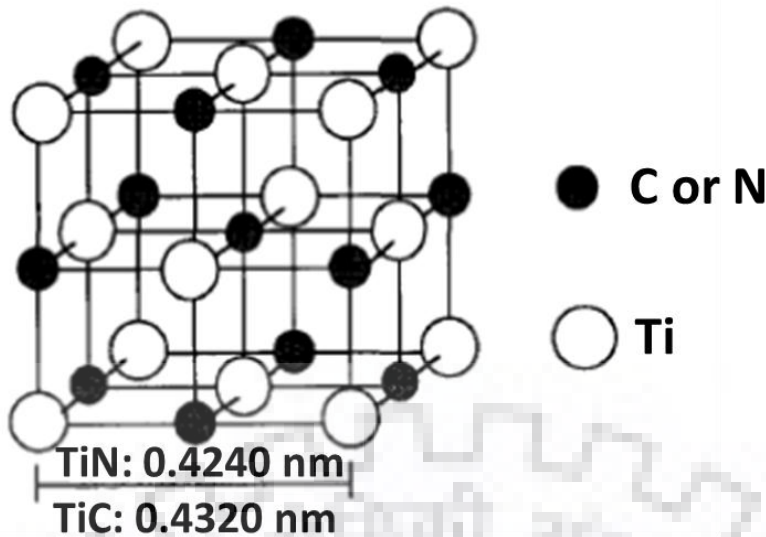
Figure 2-1: Crystal structure of Ti(C,N) [Zhang, 1993]

Brittleness and low breaking strength of titanium carbonitride limit its use as cutting tools or wear resistance machine parts. So metal binders like Ni, Co or both are added to form the cermet material [Zhang, 1993]. Groups IVb (Zr, Hf),Vb (V, Nb, Ta) or VIb (Cr, Mo, W) of the periodic table elements (carbides, nitrides or carbonitrides) are generally added as additional hard phases. These elements (i.e. Mo,V,W,Nb,Ta,Zr,Hf and Cr) form carbonitride solid solutions which improve hot hardness, improve the sinterability and thermal shock resistance. Increasing TiC and TiN contents increases hardness, addition of Ta/Nb improve cutting performance and Mo_2C and WC improve sinterability of the cermet (Rowcliffe and Warren, 1970; Ettmayer et al., 1995; Zhang et al., 1994; Zhang, 1995; Kang and Kang, 2010).

2.3. Microstructure of Ti(C,N) based cermets

Many researchers identified that the key to optimize mechanical properties of Ti(C,N)-based cermets lies in its complex microstructure. Ti(CN)-based cermets show core-rim morphology of the hard phase. Equiaxed fine grains are wetted in tough metallic binder [Parikh and Humenik, 1957; Rynemark, 1992; Ahn and Kang, 2000; Ahn and Kang, 2001; Ahn et al. 2001; Wang et al., 2017]. Usually, the cores are partially dissolved and the rim structures develops through dissolution reprecipitation processes around them. Kumar et al., 2008 prepared Ti(CN)–Ni-based cermets with addition of secondary carbides WC, NbC, TaC, and HfC. **Figure 2-2 (a)** shows a scanning electron microscope (SEM) [backscattered electron (BSE)] image of a Ti(CN)–20Ni–10WC cermet processed by Kumar et al., 2008 and **Figure 2-2 (b)** shows a schematic microstructure of a commercial Ti(C,N)-based cermet, which consists of black undissolved cores of Ti(C,N) which are

13

surrounded by grey (Ti, W, Mo, Nb, Ta,…)(C, N) complex carbonitride solid-solution rims [Kang et al., 2000].
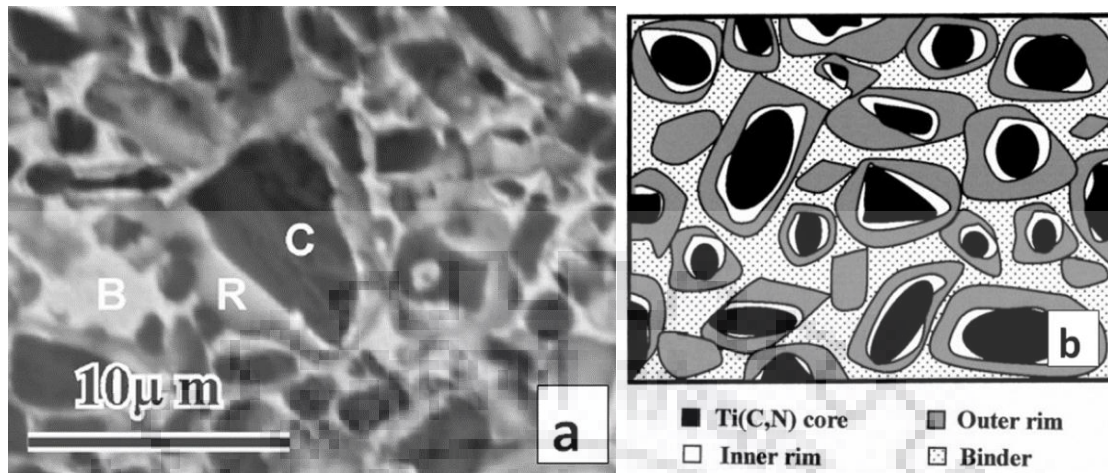
Figure 2-2: (a) BSE SEM image of the polished (unworn) surface of the Ti(CN)–20Ni–10WC cermet. The core, rim, and binder phases are represented by the labels C, R, and B, respectively [Kumar et al., 2008] (b) Schematic representation of an SEM image of a Ti(C,N)-based cermet [Ahn and Kang, 2000].

Cermets are composite materials, thus their properties depend strongly on their constituent materials. The characteristics of the microstructure (in terms of size/shape of the core-rim structure and chemical composition) are influenced greatly by the starting materials. The undissolved cores of Ti(C,N) exhibit high wear resistance, while rim structure and the binder phase solid solution determine toughness of the cermets [Ahn and Kang, 2000; Ahn and Kang, 2001; Chaoa et al., 2005, Li et al., 2012]. Investigations by Lindahl et al., 2000 supported the theory that the physical properties of the cutting tools depend strongly on the starting materials which significantly enhance the indentation toughness and wear resistance of the sintered cermet. With regard to the binder, it is important that the amount of binder is sufficient to achieve high density during liquid phase sintering and produce cermets with good machining characteristics. High binder content also deteriorates the mechanical properties of the material. Xiong et al., 2007 suggested that a lower binder content is required in Ti(C,N)-based cermets used as finish machining tools. Senthil et al., 2003 reported that that hardness decreases with increasing concentrations of metallic binder. This trend is easily explained when considering that the hardness of the individual metallic binder elements (Ni and/or Co) is smaller than that of Ti(C,N). Thus increasing metallic phase content lowers the overall hardness of the cermet

14

material. Many authors [Senthil et al., 2003; Rolander et al., 2001] studied the effect of addition of secondary carbide on the microstructure and properties of Ti(C,N)-based cermets. Ahn and Kang, 2001 studied the effect of secondary carbides on the dissolution behavior of Ti(C,N). Typical microstructures of cermets sintered using different secondary carbides are shown in **Figure 2-3**. The size and shape of core-rim differ based on the secondary carbide. With HfC, the Ti(C,N) core size was the least was the smallest whereas with TaC or WC, the frequency and size of the Ti(C,N) cores are increased, and the rim size reduced. Effect of carbon addition in Ti(C,N)-based cermets shows that the hard phase core becomes refine when the carbon contents increases. With 0.8 wt.% carbon addition Ti(C,N)-based cermets gives minimum wear loss (Wei et al., 2014).
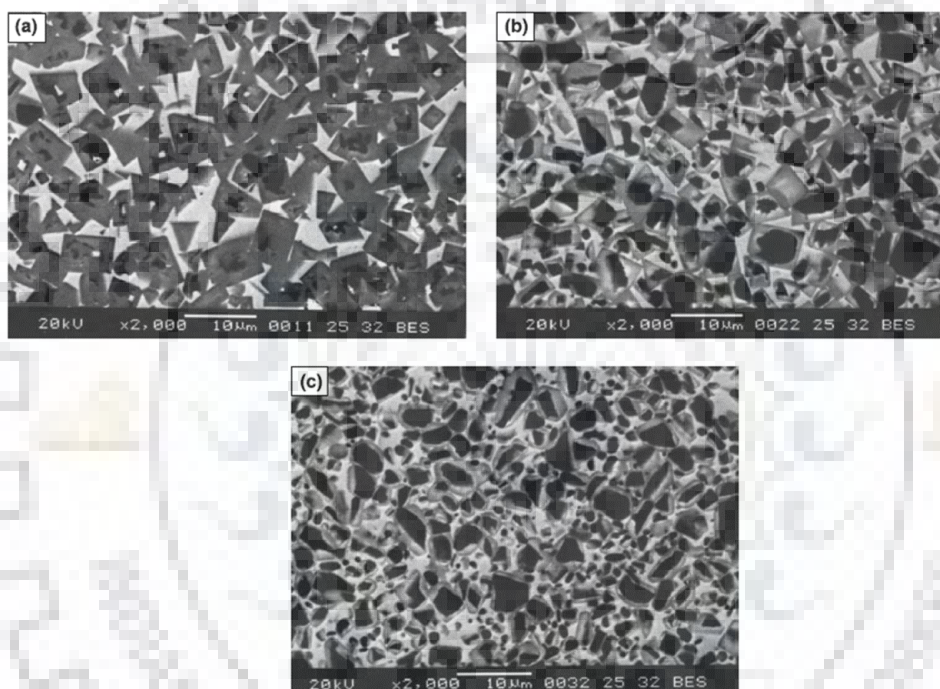
Figure 2-3: SEM (BSE) micrographs of Ti(C,N)-10MC-30Ni, where MC is (a) HfC, (b) TaC and (c) WC [Ahn and Kang, 2001]

These results support the theory that Ti(C,N) solubility in the binder phase controls grain growth during sintering. Generation of different Ti(C,N) core-rim sizes is reported to relative affinity with secondary carbides towards nitrogen from Ti(C,N). The free energy of formation, ΔG_f of HfN, TaN and WN are respectively -238, -114 and +51kJ/mol (at 1500°C) according to thermodynamic tables (Chase, 1998),. This shows that Hf and Ta have a higher tendency of forming a nitride as compared to W. Thus, smaller solid-solution rim is formed as a result of WC addition. Furthermore, the dissolution of Ti(C,N) in the Ti(CN)-Ta/Ti(C,N)- Hf systems is facilitated more by the crystal structure similarities

between the Ti(C,N) and Ta/Hf (which are all FCC), compared to W (which is HCP) [Dizaji et al., 2007].

The microstructural variations directly influence the mechanical properties of the material. Kumar et al., 2007 studied refractory carbides influence on Ti(C,N)-based cermets machining performance. Addition of metal carbides effect on the mechanical properties of these cermets is illustrated in **Table 2-4**. The metal carbides (i.e. WC, NbC and TaC) addition increases the hardness of the cermet. Kumar and Basu, 2008 reported that tantalum carbide added cermets provide the greatest increase in hardness ($\approx$2.6 GPa). It was concluded that cermets containing TaC phases exhibited lowest tool wear compared to WC and NbC containing cermets. Thus, TaC addition allows the wear resistance of the baseline Ti(C,N) cermet to be retained while subsequently improving mechanical properties of the material.

Table 2-4: Physical and mechanical properties of Ti(C,N)-based cermets compositions in wt. %. [Kumar et al., 2007; Kumar and Basu, 2008]

Ti(C,N) Cermets	Density (g/cm^3)	Hardness HV30 (GPa)	K_{Ic} (MPa.m$^{1/2}$)	Wear rate (x10^{-6} mm^3/Nm)
Ti(CN)-20Ni	5.33	9.9 ± 0.5	18.3 ± 0.9	3.2
Ti(CN)-10WC-20Ni	5.87	11.8 ± 0.6	17.3 ± 0.9	5.0
Ti(CN)-10NbC-20Ni	5.52	10.9 ± 0.5	13.4 ± 0.7	5.2
Ti(CN)-10TaC-20Ni	5.48	12.5 ± 0.6	16.1 ± 0.8	3.5

2.4. Processing of Ti(C,N)-based cermets

The most suitable method for processing titanium carbide based cermets is the low cost conventional sintering technique. Highly dense (>99%) Ti(CN) based cermets were prepared via conventional sintering with the addition of Ni, Co, Ni-Co, Ni-Mo or Ni-Co-Mo as binders and WC, NbC, HfC or TaC as secondary carbides. Zhang, 1993 sintered Ti(C, N)-Ni/Co cermets with addition of Mo and TaC, at 1400°C - 1600°C in presence of nitrogen and achieved hardness of 16.5 GPa and indentation toughness of 8.5 MPam$^{1/2}$. Short sintering time prevents grain coarsening and restricts degradation of mechanical properties [Zhang, 1993]. Ettmayer et al., 1995 processed fully dense (Ti/Mo/W/Ta/Nb)C,N-Co/Ni cermet via conventional sintering at 1550°C in nitrogen atmosphere and achieved hardness of 14.40 GPa and indentation toughness of 8.5 MPam$^{1/2}$. Hussainova et al, 2003 sintered dense (>98%) TiC-Ni/Mo cermets at 1420°C in N$_2$. They found that increasing Ni and Mo content, cermet hardness reduced to 9 GPa from 14 GPa

and indentation toughness raised to 22.9 MPam$^{1/2}$ from 12.1 MPam$^{1/2}$. Pastor, 1988 fabricated TiC$_{1-x}$ N$_x$-(Ni-Mo) and (Ti, Mo)(C$_{1-x}$ N$_x$) (Ni-Mo) alloys by hot pressing at 1700°C temperature in presence of nitrogen and achieved density higher than 95% with hardness of 13.8 GPa and indentation toughness of 14.7 MPam$^{1/2}$. Kwon et al., 2004 fabricated Ti(C$_{0.7}$ N$_{0.3}$)-xWC-20Ni (x = 5 - 20 in wt.%) cermet sintered at 1510 °C for 1 h in vacuum. They obtained hardness of 13 GPa for cermet having 10 wt. % WC and 20wt. % Ni. Indentation toughness of 13 MPam$^{1/2}$ was obtained for the cermet having 5 wt.% WC and 20 wt.% Ni. Kim et al., 2012 prepared Ti(C,N) based cermets with the addition of secondary carbides WC and Mo$_2$C and observed fine grain structure with hardness of 11.79 GPa and indentation toughness of 9.5 MPam$^{1/2}$. Kumar and Basu, 2008 processed Ti(CN)–Ni-based cermets with addition of secondary carbides WC, NbC, TaC, and HfC, sintering at 1510 °C for 1 h under vacuum. Addition of 10 wt.% TaC in Ti(CN)–20Ni increased the hardness from 9.9 GPa to 12.5 GPa. Jeon et al., 2002 processed Ti(CN)–x(WC)–20Ni cermets at 1510°C for 1 h in vaccum with different Ti(CN) particle size. With Ti(CN):WC having 75:5 ratio and 0.70 – 0.95 μm Ti(CN) particle size, the cermet has 13.6 GPa hardness and 7.25 MPam$^{1/2}$ indentation toughness. With Ti(CN):WC having 55:25 ratio and 3–5 Ti(CN) particle size, hardness reduced to 7 GPa.

Spark plasma sintering (SPS) is a fast sintering technique. It sinters the material at low sintering temperature in a short time. Borrell et al., 2012 processed Ti(CN)–15 wt.%Co cermets via spark plasma sintering (SPS) technique at different temperatures (1200–1400 °C) for 1 min in vacuum under a uniaxial load of 80 MPa. Material sintered at 1300°C had 17.1 GPa hardness, 5.51 MPa m$^{1/2}$ indentation toughness and 904 MPa bending strength. Lower sintering temperature resulted in a decrease in mechanical properties due to poor cohesion between the ceramic and binder phases. Alvarez and Sanchez, 2007 processed Ti(CN) cermets with intermetallic binder phases. Ti(CN)- Mo$_2$C–Ni and Ti(CN)-Mo$_2$C–Ni–TiAl$_3$ with full density were prepared via SPS at 100 MPa uniaxial pressure for 2 min at 1400°C. The presence of ultrafine Ti(CN) grains led to a combination of 18 GPa hardness and 7.5 MPam$^{1/2}$ indentation toughness for Ti(CN)-Mo$_2$C–Ni–TiAl$_3$ cermet. High hardness is related to the compositional difference, particularly because of presence of (Al,Ti) rich oxides due to the addition of TiAl$_3$. Ping et al., 2004 Spark plasma sintered Ti(C,N)-Mo/Ni cermets at 1050°C - 1450°C for 3min at 30MPa with a heating rate of 200°C /min and cooled down to 700°C in 2-3min. It was observed that samples sintered below 1350°C were perfect in their external appearance, whereas for samples sintered at 1450°C crack appeared on the sintered samples surface. The porosity decreased sharply below 1200°C sintering temperature. Gong et al., 2003

processed Ti(C,N) cermets with addition of Al_2O_3, Mo and Ni at 1450°C for 2 min via SPS at 50 MPa and achieved high hardness of 17 GPa. Zheng et al., 2005 obtained dense Ti(CN) cermets with addition of WC, Ni, Mo, VC and graphite via SPS at 1350°C and 20 MPa.

In addition, Kumar et al., 2007 observed that the hardness of Ti(CN)-20Ni cermets increased from 9.9 GPa to 12.5 GPa with 10 wt.% TaC addition. Park et al., 1999 found that TaC produces cubic carbides in the microstructure during sintering which lead to higher indentation toughness. Tretyakov and Mashevskaya, 1999 reported the effect of tantalum in the Ti(C,N)-Ni-Mo-WC system and found that the tantalum addition increased the bending strength as a result of the formation of a complex carbonitride phase with higher strength. It is also observed that the Compared with TiC-based cermet, Ti(CN) based cermets much higher transverse rupture strength (TRS), have higher hot hardness, high oxidation resistance and higher thermal conductivity (Gruss, 1989; Monteverde and Bellosi, 2002, Chicardi et al., 2016a & 2016b). It is found that TiC-20TiN- 15WC- 10TaC- 5.5Ni- 11Co-9Mo cermet has 600 kg/mm^2 microhardness when sintered at 1000°C and 1360 MPa strength when sintered at 900°C whereas TiC-16.5Ni-9Mo cermet is found to have 500 kg/mm^2 microhardness at 1000°C and 1050 MPa strength at 900°C [Gruss, 1989]. It is also reported that molybdenum carbide additions produce cermets with a microhardness of 1650 Kg/mm^2, indentation toughness of 8.5 MPam$^{1/2}$ and bending strength of 1500 MPa. However tantalum additions, known as tantalum toughened Ti(C,N) cermets, produce a little lower hardness but result in higher strength and indentation toughness values, as compared in **Table 2-5.**

Table 2-5: Typical properties of Ti(C,N)-based cermets [Gruss, 1989]

Cermets	Hardness (Kgmm^{-2})	MOR (MPa)	K_{Ic} (MPam$^{1/2}$)	Youngs Modulus (GPa)
(Ti, Mo/W)(C,N) - based cermets	1650	1500	8.5	450
(Ti, Mo/W, Ta)(C, N) - based cermets	1500	1800	10	410

Rolander et al., 2001 studied the effect of tantalum addition in (Ti-W)(C,N)-Co cermets on machining performance. Ta additions increased the resistance against plastic deformation, which in turn reduced flank wear during metal cutting operation. Hence, the

tantalum addition to Ti(C,N) shows great promise for the production of a cermet with high hardness, which still exhibits a considerable toughness.

2.5. Tribology

Tribology is primarily the study of friction, wear and lubrication and is now widely accepted as, "the science of interacting surfaces in relative motion and practices related there to." The word, "tribology" came from the Greek word tribos, means rubbing [Ghar, 1987; Basu and Balani, 2011; Bhushan, 2013].

2.5.1. Sliding wear behavior of Ti(C,N)-based cermets

When two contacting surfaces are in relative movement, the friction induced damage occurred on either or both surfaces is known as sliding wear. It is the predominant type of motion between tribological parts. According to Gahr, 1987 the wear and induced friction of any sliding couple are contributed by several properties, such as surface finish, load, speed, shape and dimensions of the coupled solids, adsorption of atoms, type and nature of surface films, temperature, humidly, lubrication, material composition and metallurgical parameters. Sliding wear can be performed at the laboratory scale by using several test configurations viz. pin-on-disc, ball-on-disc, block-on-ring, etc [Quercia et al., 2001; Wood et al., 2005; Krishna et al., 2003, 2015; Stewart and Plucknett, 2015]. Sliding behavior of Ti(C,N)-based cermets is influenced by their heat treatment, microstructure and mechanical properties [Pirso et al., 2006]. The condition of two surfaces in relative motion under load leads to the friction induced damage on either surface is generally known as sliding wear.

Many researchers correlated the sliding characteristics of TiC or Ti(CN) based cermets with test parameters. All the relevant information so far available in this area is summarized in **Table 2-6**. Literature survey shows that majority of experiments were performed at room temperature (25±5°C) with relative humidity (RH) of 40-50% in air [Lancaster, 1990; Williams, 2005]. Based on the experimental and material parameters, the complex tribological behavior of Ti(CN)-based cermets in sliding wear is widely characterized by adhesion, abrasion, tribochemical wear, oxidation, plastic deformation and/or fracture. A wide range of COF values from 0.2 to 1.2 and wear rate from 10^{-7} mm^3/Nm to 10^{-3} mm^3/Nm are reported [Rigney, 1984; Arenas et al., 2003; Engqvist et al., 2000; Pirso et al., 2004a; Meng et al. 2006; Östberg et al. 2006; Kumar et al., 2007; Kiani et al., 2015].

Table 2-6. The summary of tribological characteristics of Ti(CN) based cermets during sliding against different counterbodies in dry (in air) conditions

Cermet composition	Counter body	Dry (in air) sliding wear test conditions	COF	Wear rate (mm^3/Nm)	Dominant Wear mechanism	References
(Ti(CN)– 20Ni)- WC/NbC/TaC/ HfC	steel	300 rpm; 5, 20 or 50 N	0.4-0.7	10^{-6}-10^{-7}	Tribolayer removal	Kumar et al., 2008
TiC–NiMo	steel	2.2m/sec; 40N	0.2-0.3	3.8×10^{-7}- 13×10^{-7}	Tribolayer removal	Pirso et al., 2004a
(WC-Co)–TiC, TaC/NbC	steel	1500-3000 rpm; 40 N- 350 N	0.2-0.7	-	Tribofilms removal	Engqvist et al., 2000
Ti(CN)–Ni- WC	steel	0.1m/sec at 5; 20 or 50 N	0.27– 0.73	2.7×10^{-7}- 3.4×10^{-6}	tribolayer removal & delamination	Kumar et al., 2007
Ti(CN)–Ni– Mo	Si_3N_4	0.5m/sec; 5N	0.8	10^{-7}	Micro fracture	Meng et al., 2006
Ti(CN)– Al_2O_3–Ni–Mo	Si_3N_4	0.5m/sec; 5N	1.0	10^{-7}	Tribolayer removal	Meng et al., 2006

It can be noted from **Table 2-6** that the sliding wear behavior of various Ti(CN) based cermets have been extensively studied against steel ball, probably due to the application of tools in machining steel. Kumar et al., 2008 studied the sliding wear behavior of Ti(CN)–Ni-based cermets with WC addition slid at 0.1 m/sec velocity at different loads against 100Cr6 steel. COF varied from 0.7 to 0.3 and wear rate varied in the order of 10^{-7} to 10^{-6} mm^3/Nm. Worn surfaces revealed increased abrasion at low loads and severe fracture of the tribooxide layer at high loads. The increased tribolayer formation can be noted at a load of 50N in **Figure 2-4 (a)** on Ti(CN)–20Ni cermet worn surface. The appearance of abrasion grooves are noted for the Ti(CN)–20Ni–10NbC cermet in **Figure 2-4 (b)** at a 20N load. Severe abrasion occurred due to debris entrapped in the sliding contact at a load of 20N.
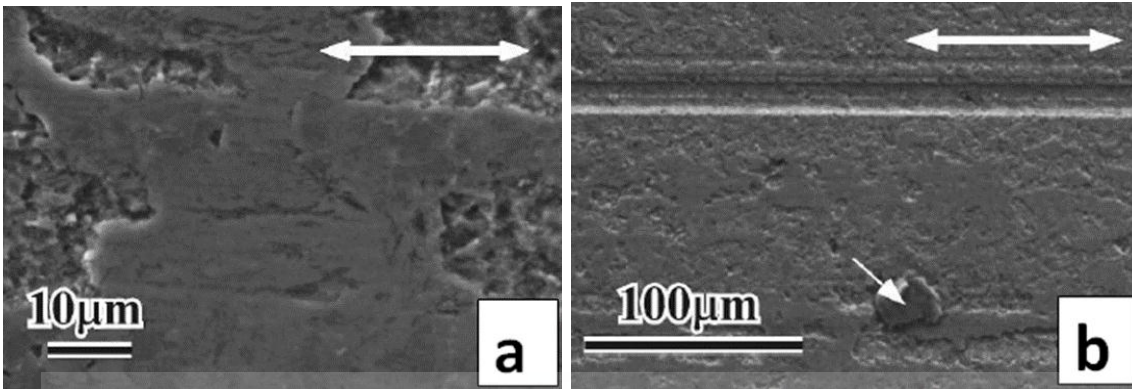
Figure 2-4: (a) SEM images of the worn Ti(CN)–20Ni cermet slid against a steel ball at 50N and **(b)** Ti(CN)–20Ni–10NbC cermet at 20N [Kumar et al., 2008].

Pirso et al., 2004a in their study found microabrasion (polishing) and adhesive wear as main wear mechanisms for TiC–NiMo cermets slided against steel at a velocity of 2.2 m/s and a load of 40N shown in **Figure 2-5**. COF varied from 0.2 to 0.3 and wear rate varied in the order of 10^{-7} mm^3/Nm. When slid against Si_3N_4 at 0.5m/sec and 5N load, Meng et al., 2006 observed dominant micro fracture on Ti(CN)–Ni–Mo cermets worn surfaces, whereas tribolayer formation is observed in Ti(CN)–Al_2O_3–Ni–Mo cermet COF varied from 0.8 to 1.0 and wear rate in the order of 10^{-7} mm^3/Nm. Engqvist et al., 2000 studied the wear behavior of (WC-Co)–TiC- TaC/NbC against steel at 1500-3000 rpm 40 or 350 N load. COF varied from 0.2 to 0.7 and tribolayer formation is observed in all the materials.
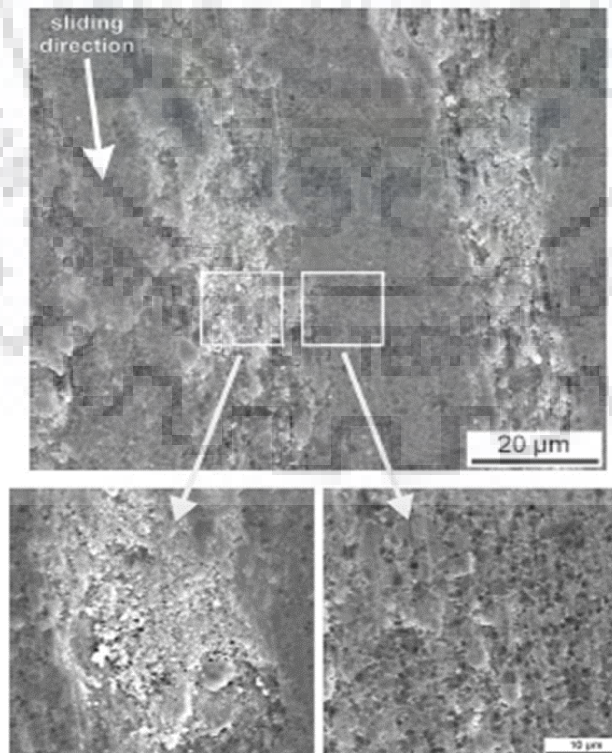
Figure 2-5: Smeared transfer film on the TiC–20% NiMo cermet wear track after 4 km run against steel [Pirso et al., 2004a]

2.6. Machining studies using cermet cutting tools:

The term machining is defined as an operation in which material is removed from workpiece by cutting tool in the form of chip or swarf, a thin layer of metal and specifically to cutting tools. The classic definition of wear is the loss of material caused by some tribological phenomenon. Cook, 1973 stated that a tool considerably fail when it either does not cut or it cuts in a manner grossly different from a sharp tool. Failure of a tool can be categorised as fracture or chipping under severe conditions of cutting force or shock. When the wear rate increases due to the cutting conditions, tool softening leading to gross and rapid loss of entire cutting zone.

Dry machining is preferred over wet machining as it has the advantages of non-pollution of the atmosphere (or water) and no danger to health, whereas wet machining includes lubricants having compounds, the consumption of which may lead to serious respiratory effects [Byrne and Scholta 1993; Sreejith and Ngoi 2000]. Moving to dry machining is also required because of strict rules enforcement while using cutting fluids or lubricants [Narutaki et al. 1997]. Vieira et al., reported that the cutting fluids accelerates the thermal cracks and accelerate their nucleation process, thus reducing the tool's life regardless of the type of cutting fluid used. The major limitation of dry machining is that it increases tool wear because of increased friction and adhesion between tool and workpiece which results in shortening of tool life. So either heat generation has to be controlled or tool material properties have to be improved for superior performance in dry machining [Sreejith and Ngoi 2000].

Cermet cutting tools are used to machine a variety of materials at relatively higher speed than carbide tools. The cermet cutting tools are used in extremely unfavorable conditions during machining various materials like cast iron, steel, stainless steel in their hardened conditions. Adverse conditions that damage these tools are high cutting temperatures, chemical attacks, compressive and shearing stresses, variable cyclic thermal and mechanical loads. Therefore, it is crucial to understand the process of tool damage. In this part of the review, machining studies conducted using cermet cutting tool materials on various types of work materials and the performance of the cutting tools are discussed from the available literature. Due to superior properties of high hot hardness, chemical stability and better oxidation resistance, Ti(C,N) cermet material is considered over other materials for machining steel and cast iron for the high speed milling, roughing or semi-finishing operations [Zhang, 1993; Li and low, 1994; Watanabe et al., 1996; D' Errico et al., 1997; Pastor, 1998; Zhang, 1998]. Different metal carbides are added to Ti(C,N) based cermets as discussed earlier to improve their properties [Ettmayer et al., 1995; Zhang.,

1995; Qi and Kang, 1998; Rolender et al. 2001]. Improvement in interrupted cutting performance occurs on adding NbC or TaC as they impart hot hardness and thermal shock resistance (Kang, 1996; Qi and Kang, 1998; Rolender et al. 2001). Strain misfit between different microstructural phases can be reduced by addition of HfC or ZrC [Mun and Kang, 2016]. WC imparts densification and indentation toughness to Ti(C,N) based cermets [Ahn and Kang, 2000; Ahn et al. 2001; Kwon et al. 2004]. Compared to cemented carbide cutting tools, Ti(CN) based cermet has high temperature hardness, resistance to oxidation and better chemical stability, as reported by Kwon et al. 2004; Liu, 2005. D' Errico et al., 1999 further stated that the performance of ceramic tool materials outperformed other cutting tool materials like cubic boron nitride (CBN) and polycrystalline diamond (PCD). Kwon et al., 2004 studied the effect of Group IV (ZrC, ZrN or HfC; 1 wt. %) addition on the microstructure and cutting performance of Ti(C,N)– (5-20 wt.%) WC– (20 wt.%) Ni systems. It was observed that ZrC, ZrN and HfC addition enhanced the high-temperature strength of the cermet system. In general, inserts containing 20 wt.% WC showed the longest tool life for milling and those containing 15 wt.% WC exhibited the longest tool life for turning. Ti(C,N)–14WC–20Ni (wt.%) cermets showed the best cutting performance among the various cermet compositions Low strain energy developed between core and rim interfaces resulted in improved performance.

Wear in a cutting tool is a complex phenomenon comprising several wear mechanisms. Tool wear mechanisms, as discussed before include abrasion, adhesion, diffusion, plastic deformation, fatigue failure, micro spalling, chipping, cracking and/or fracturing. An understanding on the nature of wear of a tool helps in better utilization of the cutting tools [Czichos, 1984, Tonshoff et al., 1994]. Slavko Dolinšek et al., 2001 reported that the cutting tool wear results due to mechanical (thermo-dynamic wear i.e. abrasion, adhesion) and chemical (thermo-chemical wear, where elevated temperatures enhance the chemical reactions, i.e. diffusion, oxidation) interactions between the tool and workpiece. It is reported that tool wear during machining occurs as abrasion at low speeds/temperatures, adhesion at moderate speeds/temperatures and diffusion at high speeds/temperatures [Opitz and Konig, 1967; Hastings and Oxley, 1976; Lim et al., 1999; Arsecularatne et al., 2006].

Tool wear results in damage to the work piece, reduced dimensional accuracy of the finished product, residual stress generation or decreased surface integrity. So it is important to review and evaluate tool wear and to predict tool life [Devillez et al., 2004]. Dominant wear mechanisms of different cermet tools during machining is summarized in **Table 2-7**.

Table 2-7. The summary of dominant wear mechanisms of different cermet tools during machining.

compositions (wt.%) for tool materials	workpiece	Opera-tion	Cutting speed (V_c) m/min	feed (f)	Dominant Wear mechanism (tool)	References
WC-TiC-Ta(Nb)C-Mo$_2$C- TiN-(Co, Ni)- VC	Quenched & tempered steel	turning	150-400	0.1-0.3 rev/min	abrasion	Thoors et al., 1993
WC-TiC-Ta(Nb)C-Mo$_2$C- TiN-(Co, Ni)- VC	Ball bearing steel	turning	150-400	0.1-0.3 rev/min	abrasion	Thoors et al., 1993
Ti(C, N), WC, (Co,Ni)	carbon steel	milling	470–600	0.12–0.06 mm/tooth	Abrasion, thermal cracks	Bellosi et al., 2003
WC-Co-(Ti(CN)/HC/Ta/LC)	steel	turning	300, 475	0.3 mm/rev	Plastic deformation	Östberg et al., 2006
WC, Co, (Ti/Ta/Nb)	titanium alloy	milling	100	0.15 mm/tooth	Adhesion Attrition, galling	Nouari and Ginting, 2006
TiN coated cermet	Stainless steel	turning	300-700	0.05-0.4	microcracking	Khan et al., 2006
Ti(CN)-20Ni-(5-10)wt.% WC	boiler grade steel`	turning	47,74,104	0.075, 0.113, 0.175 mm/rev.	adhesion	Kumar et al., 2007
Ti(CN)-20Ni-(>10)wt.% WC	boiler grade steel	turning	47,74,104	0.075, 0.113, 0.175 mm/rev.	Abrasive grooves, pull outs	Kumar et al., 2007
TiC-TiN-Ni-Mo-WC	Steel	turning	323, 432.1, 567.8	0.1,0.3, 0.5	ceramic grains removal, abrasive wear	Shi et al., 2007

Tool may undergo wear as crater wear on the rake face, flank wear on the flank face or a notch at nose [Astakhov, 2004]. The flank wear of the tool is caused by the abrasive, oxidation and diffusive wear at high cutting speed [Zhang et al., 2007]. Flank wear occurs on the relief face of the cutting tool and affects the workpiece dimensional tolerance [Senthil et al., 2003]. This is caused by abrasive and/or adhesive wear and affects the tool material properties and workpiece surface [Kumar et al., 2006]. Koren et al., 1991 designed and performed experiments for turning operations with varying depth of cut and concluded that the difference between the estimated and actual flank wear is less than 0.05 mm during the entire cutting cycle and it is a promising result for practical applications. Thoors et al., 1993 reported the active wear mechanisms for Ti(CN) based cermet during turning of steel. SEM observations of worn tools (**Figure 2-6)** revealed that the rake

surface of the tools were covered with abrasive tracks over the greater part of the contact length, except very near the cutting edge.
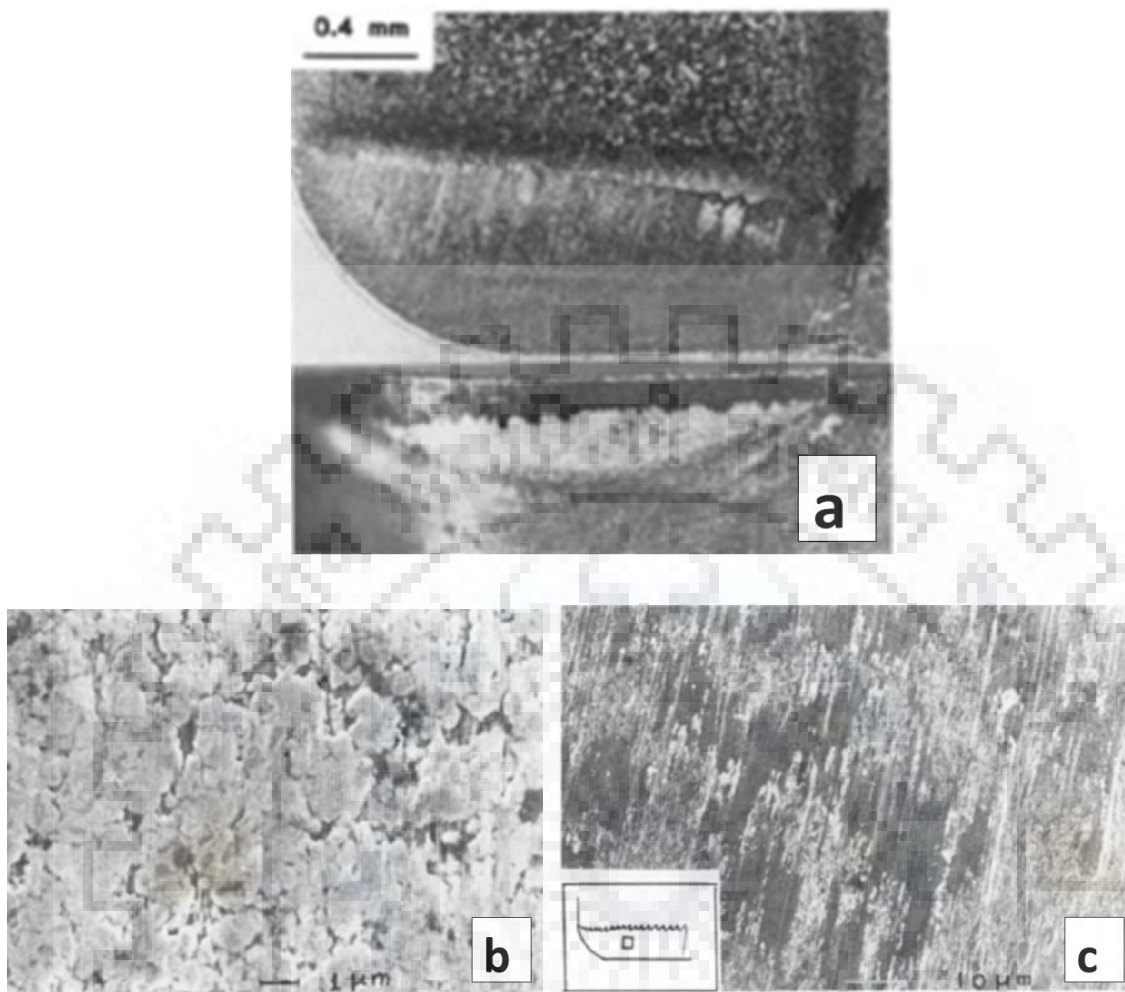
Figure 2-6 (a) Appearance of worn Ti(CN) based cermet tool after machining steel (b) rake surface very near cutting edge - no sticking layers or abrasive tracks (c) crater region showing sticking layers and abrasive tracks [Thoors et al., 1993].

Kumar et al., 2007 studied the crater wear mechanisms of Ti(CN)-20Ni-(5-15)wt.% WC cermet cutting tools against boiler grade steel during dry machining. It was found that cutting performance of Ti(CN)-Ni cermet tool improved with WC content upto 10 wt.%. The adhesion of tribochemical layer was dominant with limited WC content, whereas the presence of abrasive grooves and pull-outs were observed for Ti(CN)–20Ni cermets containing higher amount of WC (>10wt.%) on rake face of the tool, as shown in **Figure 2-7.**
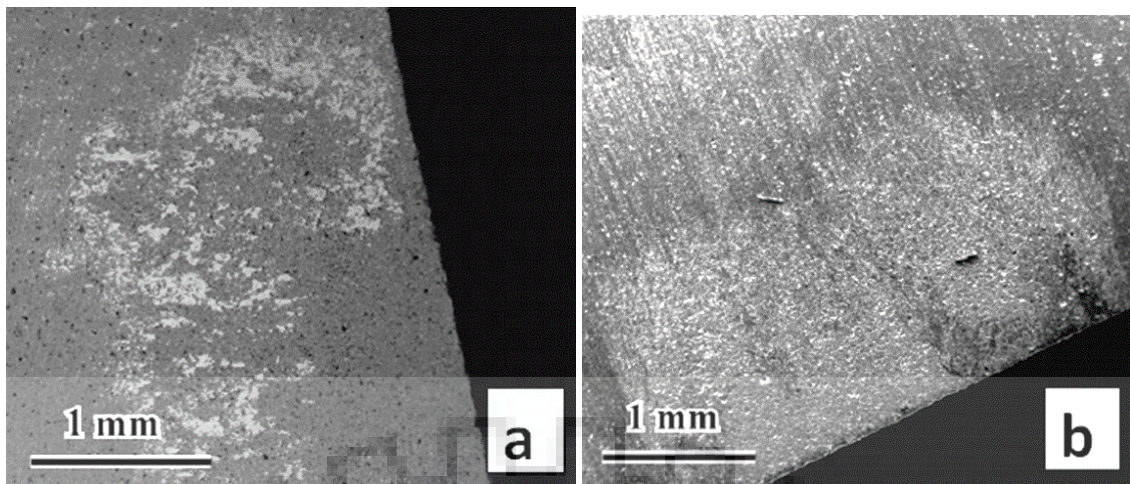
Figure 2-7: (a) Rake surface of Ti(CN)–20Ni–5WC tool revealing tribolayer, (b) Severe abrasion and grain pull-outs in Ti(CN)–20Ni–15WC tool surface [Kumar et al., 2007].

Bellosi et al., 2003 observed abrasion and fatigue on the cutting edge of Ti(CN)-WC-(Ni-Co) cermet tool used against carbon steel in dry machining as shown in **Figure 2-8.** Besides abrasion and fatigue wear, the most critical phenomena are diffusive and oxidative processes. Oxidation induced formation of molten and/or volatile products causing alteration of the surface and further internal oxidation. These processes favor the growth of (micro)-cracking, and lead to the failure of the cutting edge.
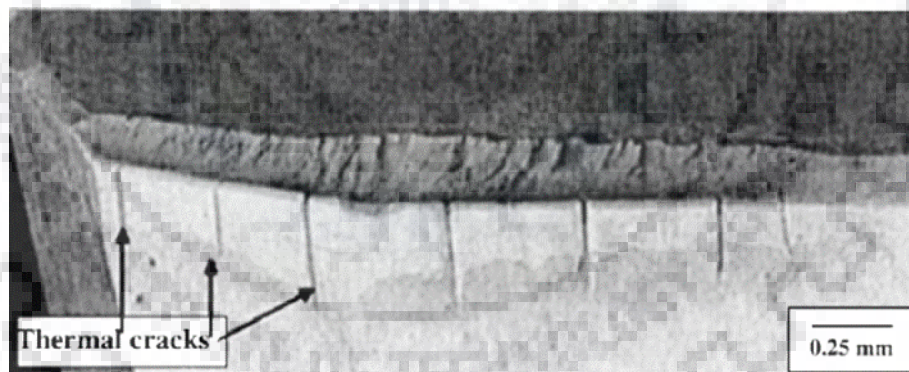
Figure 2-8. Thermal cracks on the flank and crater of tool after milling [Bellosi et al., 2003].

In cermet tool machining, flank face generally undergoes abrasive wear and is characterized by development of grooves and ridges in the direction of chip sliding against the rake face or tool sliding against a newly machined surface of the work piece. Abrasive wear also occurs when a third particle harder than the surfaces in contact is trapped at the interface. During machining, high stresses generated at the tool-chip/workpiece interface cause many abrasive grooves and ridges on rake and flank faces [Hastings and Oxley,

26

1976]. According to Trent and Wright, 2002 tool wear mechanisms are based on the stress and temperature on the rake face of the cutting tool. They pointed out that when machining steel materials, abrasion and oxidation are dominant at relatively high cutting speeds. For chemically stable cutting tools such as cermet, plastically deformed grooves and ridges account for most of the rake and flank face wear. De Melo et al., 2006 pointed out attrition is frequently treated as adhesion. It usually happens due to the irregular flow of chip material on the rake face and associated with a high temperature/high pressure on the cutting edge at low cutting speeds. The adhesion can also be accelerated depending on the chemical affinity between tool and workpiece materials. A built- up edge and notch wear are commonly observed on rake face. Built up edge is a dynamic structure, with successive layers from the chip welded to the tool. It can be sheared off and this causes the tool material to break away from the cutting tool edge. Attrition consists basically adhesion of workpiece material on the cutting tool surfaces. Tool of cemented carbide (**Figure 2-9**) shows an example of a notch wear occurred on flank face after machining Inconel 901 [Machado., 1990]. Notch wear occurs mainly when machining materials with poor thermal properties such as nickel alloys, titanium, cobalt and stainless steel and it can develop either on the flank face or on the rake face of a cutting tool. According to Trent and Wright, 2002 this type of wear generally occurs in regions where sliding condition persists and involves abrasion and attrition, and sufferes by strong influence of the atmosphere, mainly the amount of oxygen.
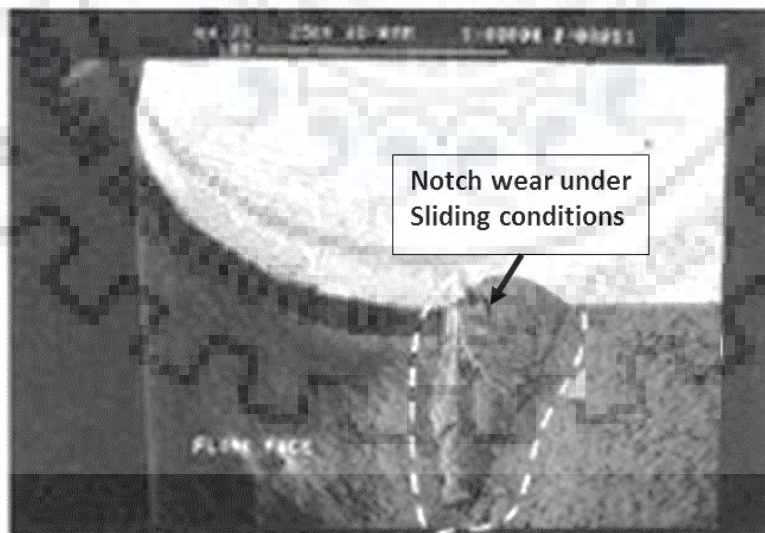
Figure 2-9 Notch wear observed on the flank face of a cemented carbide cutting tool [Machado, 1990].

Nouari and Ginting, 2006 found that alloyed uncoated carbide tools during dry machining of the titanium alloy Ti-6242S was worn by adhesion wear (attrition or galling)

and diffusion wear. Arsecularatne et al., 2006 investigated cutting tools wear mechanisms for WC/steel and polycrystalline cubic boron nitride (PCBN)/hardened-steel tool/work combinations and reported that the tool wear was greatly influenced by the temperature and the most dominant tool wear mechanism was diffusion for WC and chemical wear for PCBN. Diffusion wear occurs due to activation of chemical reaction between the cermet tool and the workpiece by pressure and high temperatures mainly at the tool-chip (rake face) interface. Machado, 1990 observed crater wear on the rake face close to the cutting edge during machining Ti-6Al-4V alloy against cemented carbide cutting tool as shown in **Figure 2-10.** Crater wear on cemented carbide cutting tools is normally formed due to diffusion, where interchange of atoms occurs between rake face and chip root at the seizure zone, and it is strongly dependent of temperature, time and solubility of the involved elements. This form of wear is mainly associated with crater wear and, to a less extent, flank and notch wear. Subramanian and Strafford, 1993 reported that crater wear occurs due to the dissolution of tool material by diffusion in the region of maximum temperature rise.
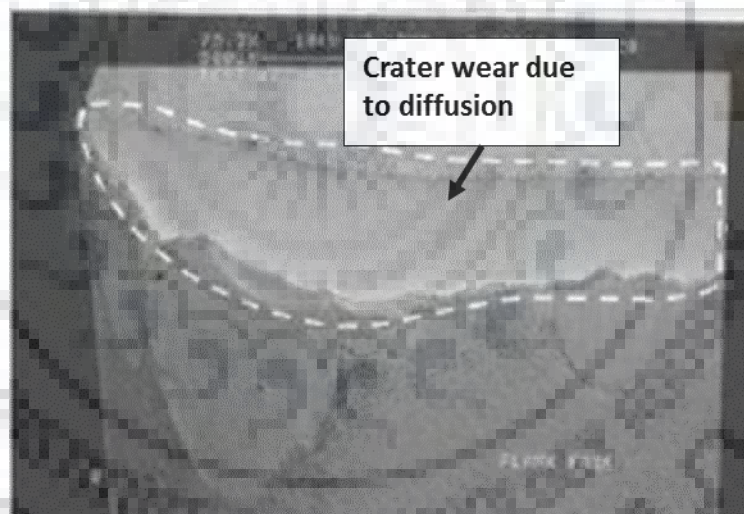
Figure 2-10 Rake face wear of a cemented carbide cutting tool [Machado, 1990]

Plastic deformation of WC-TaC-Co cermet tool takes place as a result of high temperatures and high pressures along the cutting edge. The plastic deformation in the cobalt phase results in tearing-off of the grains of carbide from deforming cobalt layers, "ploughing" this deforming layer by hard inclusions contacting the work material, and "spreading" of the tool material on the chip and workpiece contact surfaces. **Figure 2-11** shows an example of plastic deformation under compressive stress [Ostberg et al., 2006]. The cutting edge of a WC-TaC-Co cemented carbide cutting tool after turning steel shows plastic deformation.
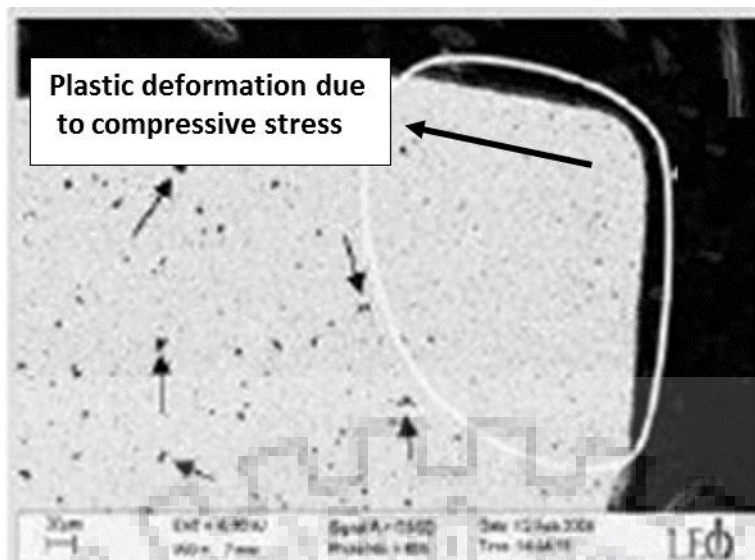
Figure 2-11 SEM micrograph of the deformed WC-TaC-Co cemented carbide [Ostberg et al., 2006].

King and Wheidon, 1966 reported that the damage due to fatigue accumulates over a period of time before a tool fails as evidenced by the numerous micro cracks on the wear land and in the crater area. The cutting tool tip is subjected to compressive stresses due to the cutting forces from orthogonal directions. The compressive stresses in the cermet cutting tools inhibit the propagation of fatigue cracks. In this case, the fatigue damage can accumulate in the ceramic to a great extent prior to the destruction of ceramic by a catastrophic fracture. King and Wheidon, 1966 have conducted tests with various tool materials having different grain sizes and found that sometimes removal of whole grains or small aggregate of grains from the cutting tool material occurs, resulting in microspalling. The cermet cutting tools are susceptible to chipping, cracking and fracturing, especially when it is used in interrupted machining operations. A thin layer of tool material is stripped off the tool rake face or flank face due to mechanical interactions between tool and workpiece [Dolinsek et al., 2001]. Shi et al., 2007 observed flank wear mechanisms when Ti(C, N)-based cermet cutting tools were tested in dry machining of normalized medium carbon steel (AISI1045) under various cutting conditions. Abrasive wear and removal of the ceramic grains were the main source of tool failure. Abrasion wear on cutting tools occurs when tool material gets removed or dislocated by hard particles. Hard particles can be loose, between chip and rake face, or emerge from workpiece material and/or from cutting tool material. In addition, adhesion and oxidation were also observed. Bellosi et al., 2003 observed Ti(C, N)–WC-based cutting tools prepared by hot pressing performed better than commercial (TiC+TiN) based cermet inserts, when tested in milling and turning operations on C45 carbon steel at different cutting conditions. Khan et al., 2006 used

29

titanium nitride coated cermet tool inserts (SNMG 120408-HM, grade 200) against 304 austenite stainless steel at 300, 400, 500, 700 m/min cutting speeds, depth of cut were 0.1,0.2,0.3,0.5 mm with 0.05,0.1,0.2 and 0.4 mm/rev feed rates. Result shows a fracture of a depth of 80µm at the cutting edge (see **Figure 2-12**) after 10min of machining at 300 m/min cutting speed, 0.05 mm/rev feed rate and 0.1 mm depth of cut. As the cutting conditions becomes severe, depth of the crater becomes larger and further catastrophic failure of the cutting edge occurs at only after 2.5 min. of machining time at 700 m/min cutting speed, 0.4 mm/rev feed rate and 0.5 mm depth of cut. Low indentation toughness and low thermal conductivity are also attributed for tool failure, as under severe cutting conditions heat generation rate at cutting zone becomes very high in cermet tools.
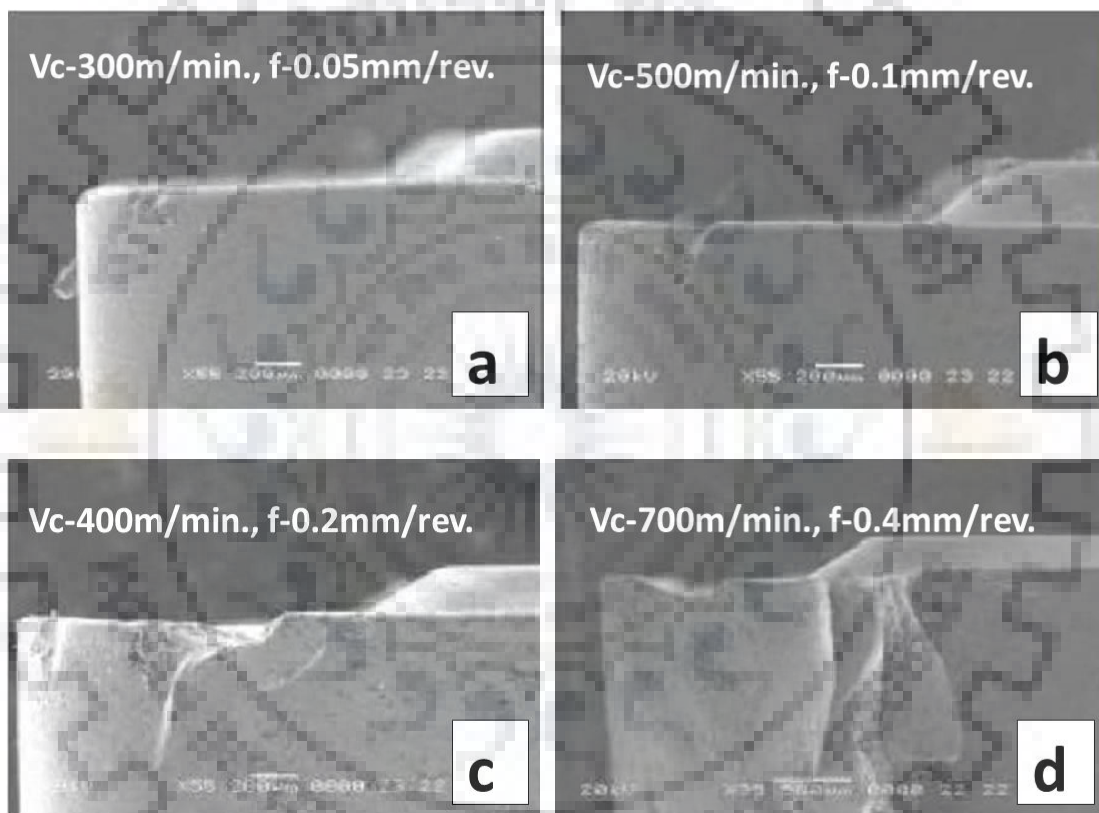
Figure 2-12 Cermet tools failure mode: (a) depth of cut=0.1mm; (b) depth of cut=0.2mm; (c) depth of cut=0.3mm; (d) depth of cut=0.5mm [Khan et al., 2006].

Literature review indicates that a more systematic study of processing, friction and wear, and machining performance is required to explore Ti(CN) based cermets. It is observed that preliminary work is done with a routine pattern of steps and without much change in experimental parameters for estimating wear and understanding wear mechanisms for Ti(CN) based cermets. Particularly, the understanding on the relation between the cermet composition, microstructure, mechanical properties, wear behavior and machining performance is limited.

This chapter deals with the powders used, sintering routes adopted for processing Ti(CN) based cermets. Details of friction and wear test, tool machining test are also discussed. Detailed experimental procedures employed for characterization and testing of the cermets compositions for various studies in the present study are given.

3.1 Material selection

In this study, cermet compositions for the present work were prepared using powders of Ti(CN) (1-2 μm, Sigma Aldrich, USA) Lot # MKBT1042V; WC (2 μm, Sigma Aldrich, USA) Lot # MKBN6834V, Ni (100 mesh size, Central Drug House (CDH) New Delhi, India) Lot # 01016 and Co(3-5 μm, The Metal Powder Company Ltd. (MEPCO) Thirumangalam Madrai Dt. India) Lot # 3; TaC (<5 μm, Sigma Aldrich, USA) Lot # 10807PHV. All results are with concern to $TiC_{0.5}N_{0.5}$ with C:N = 0.5:0.5. Four batch compositions of Ti(CN) based cermets: Ti(CN)-5WC-20Ni, Ti(CN)-5WC-20Ni-5TaC, Ti(CN)-5WC-10Ni-10Co, Ti(CN)-5WC-10Ni-10Co-5TaC were prepared and designated as C1, C2, C3, C4. Numerals in the batch compositions indicate content in wt. % (see Table 3.1).

Table 3.1: Ti(CN) based cermet compositions (wt.%) investigated in present study

Designation	Cermet Compositions
C1	Ti(CN)-5wt% WC-20wt% Ni
C2	Ti(CN)-5wt% WC-20wt% Ni-5wt% TaC
C3	Ti(CN)-5wt% WC-10wt%Ni-10wt%Co
C4	Ti(CN)-5wt%WC-10wt%Ni-10wt%Co-5 wt% TaC

3.2 Material Fabrication

The steps involved in the processing route employed for fabrication of cermets for various studies are described below:

3.2.1 Powder mixing

According to the compositions shown in **Table 1,** individual powders were carefully taken on a butter paper via spatula and weighed on an electronic balance (shown

in **Figure 3-1**). Powder blend was manually mixed in a mortar pestle. In this way, for every composition a powder blend was prepared for compaction. To facilitate homogenization, powders were uniformly mixed using a high energy ball mill (PM100, Retsch, Germany), (shown in **Figure 3-2**). in a tungsten carbide vial at 250 rpm for 8 h with a tungsten carbide balls to powder ratio of 10:1.
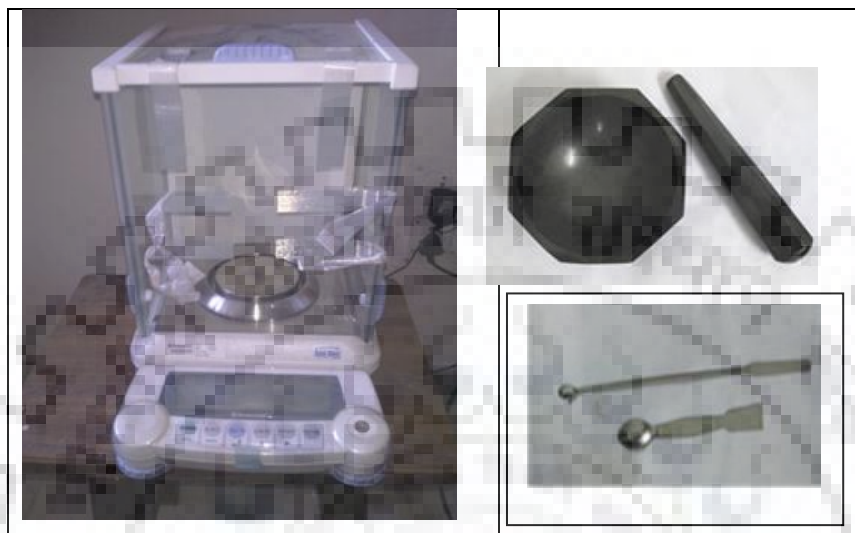
Figure 3-1: Weighing balance, mortar crusher and spatulas.
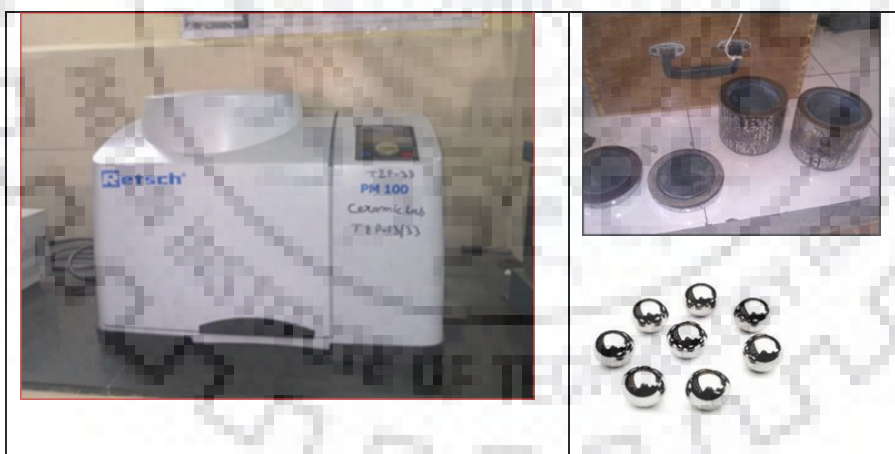
Figure 3-2: Planetary ball mill machine with WC jar and WC-balls

3.2.2 Powder compaction

For the conventional sintering, the mixed powder was compacted in a hydraulic press (EIE, Instrument Private Ltd, India) (shown in **Figure 3-3**). at 100 MPa and discs of 21 mm diameter and 5-6 mm thickness were obtained.

Figure 3-3: Hydraulic machine, die steel die-punch, compacted pellet

3.2.3 Sintering

Powder compacts were placed in alumina crucible, in a horizontal tubular furnace (Naskar & Company, India) **(Figure 3-4)** having $MoSi_2$ heating elements and sintered at 1550°C temperature for 2 h holding time in flowing argon. Thickness of the sintered cermet disks varied between 3 and 5 mm.

For spark plasma sintering (SPS), the powder mixtures were compacted in a graphite die of 20 mm diameter and 5-6 mm thickness and were sintered in (Dr. Sinter SPS-625, Fuji Electronic Industrial Co. Ltd., Japan) at 1400°C for 3 min at 70 MPa in Ar atmosphere. The general procedure for sample preparation of weighing the sample, filling the die, tapping and set punches for SPS is shown in **Figure 3-5.** A 0.2 mm thick graphite paper was used to make a liner for the inner area of the die and protect the sample from deterioration that may occur during the sintering process. To reduce the amount of radiant heat transfer to the machine, the entire die and punch assembly were wrapped with carbon felt. A photograph of the SPS facility is shown as **Figure 3-6.** The temperature of the inner surface of the upper graphite piston was monitored by a digital pyrometer. Heating was done at 100°C/min, while cooling was done at 200°C/min.

Figure 3-4: High temperature tubular sintering furnace
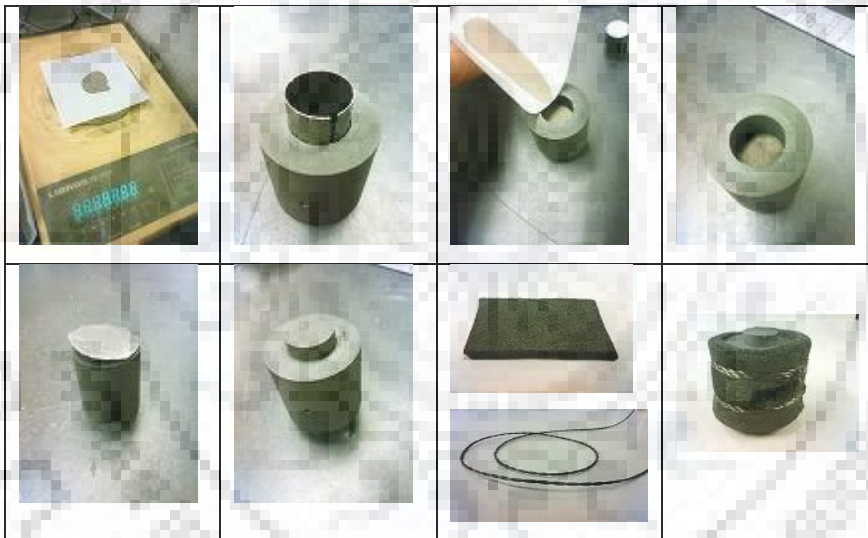
Figure 3-5: General procedure for sample preparation for Spark plasma sintering

Figure 3-6: Spark plasma sintering machine

3.2.4 Sample polishing

The samples processed via conventional and SPS were polished. Initially, graphite layer was removed from the surface of the sample by using belt polishing (**Figure 3-7**). Sintered cermet surfaces were further polished using emery papers embedded with abrasive particles of 9, 6, 3, or 1 μm size. Further sintered samples were polished on auto polisher (**Figure 3-7**) by using diamond suspension to obtain a scratch free mirror like finish.

The surface roughness was measured using a profilometer (Mitutoya Surfest SJ-401, Japan) as shown in **Figure 3-8.** and obtained an arithmetic average surface roughness (Ra) of 20-70 nm. The roughness of polished surfaces is found to be 0.06±1 μm.

Figure 3-7: Belt polisher, auto polisher
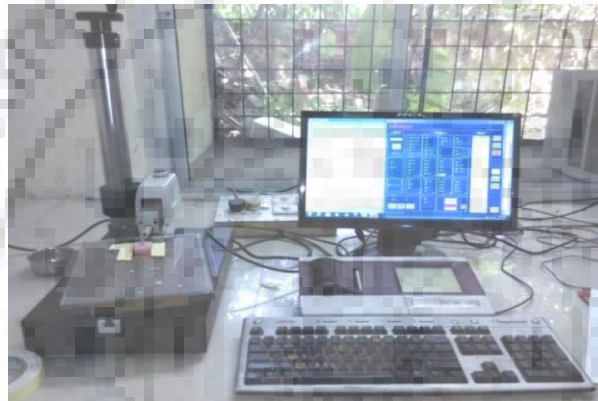
Figure 3-8: Stylus tip profilometer

3.3 Characterization

3.3.1 Powder characterization

The ball milled powders after sieving through a fine sieve to achieve free flow of powders, were sputter coated with gold, and subjected to microstructural characterization using scanning electron microscopy (FESEM; Quanta 200 FEG, Eindhoven, the Netherlands or SEM Zeiss, EVO18, Oberkochen, Gemany) (**Figure 3-9**). Working distance, voltage, probe current etc are kept constant while taking SEM/EDS. Working distance is kept 8-12 mm accordingly to focus the surface, voltage is 20 KV and probe current is 3 pA is kept constant. Particle size distribution of ball milled powders was determined using a particle size analyzer (ANKERSMID LFC-101 computerized inspection system) (**Figure 3-10**). The system used laser light beam scattering technique through a dispersed particulate sample. A known quantity of powder sample was dispersed in a 5 ml glass cover with distilled water and placed into the analyzer chamber of the

36

detector. Particle sizes were reported in micrometer by the instrument software package which analyze the scattering data.

Figure 3-9: Scanning electron microscope

Figure 3-10: Particle size analyzer

3.3.2 Density measurement

The density of the sintered cermets was measured by Archimedes method. For calculating theoretical densities of cermet compositions using inverse rule of mixture, theoretical densities (g/cc) of as received powders were considered as per the following formula

$$\frac{1}{D} = \frac{x_1}{d_1} + \frac{x_2}{d_2} \tag{3.1}$$

where

D= Density of cermet

x₁, x₂ = mass fractions of respective powders.

d₁, d₂ = theoretical densities of respective powders

The relative density was further determined. Samples were weighed in air (m_a) and distilled water (m_w) by placing on a stainless steel pan. This pan along with the sample was freely suspended by a wire attachment in a glass beaker filled with distilled water. Water level in the beaker and depth of immersion of the compact holding pan were kept constant. The materials were assumed to be perfectly solid and completely insoluble in water at the measured condition. At least three identical specimens were carried out at 25°C, where water density was considered as 0.99704 g/mL, to compute the density. The density (ρ = g/cc) was determined by using the formula [Kwon et al., 2004].

$$\rho = \frac{m_a}{ma - m_w} \tag{3.2}$$

3.3.3 Phase analysis

The polished specimens were subjected to X-ray diffraction using a D8-Advance Bruker, Diffractometer (**Figure 3-11**), fitted with goniometer with Cu-Kα radiation of wavelength 0.154 nm to identify different phases. The vertical θ-θ goniometer had a range of 0°-360° (2θ). The detector moves around the sample and measures the intensity and position of peaks which satisfy Bragg's law. An Expert High Score Plus™ software which has inbuilt inorganic JCPDS (Joint Committee on Powder Diffraction Standards) was used to index the peaks of various phases present in the pattern.

Figure 3-11: X-Ray Diffraction Machine

3.3.4 Microstructural analysis

There is development of core rim binder phase morphology visible in SEM micrographs of sintered cermets with black, grey and white contrast. ImageJ Analyzer was used to estimate the average size of core and rim in microstructures of the cermets. The microstructural parameters were further evaluated by linear intercept method for each cermet microstructure. The average number of intercepts per unit of length was determined for $N_{ceramic/ceramic}$ grain boundaries and $N_{ceramic/binder}$ interfaces, and used to estimate the contiguity (C) of the ceramic particles and the mean free path (λ) of the binder phase [Lee and Gurland, 1978].

$$C = \frac{2N_{ceramic/ceramic}}{[2N_{ceramic/ceramic} + N_{ceramic/binder}]} \tag{3.3}$$

$$\lambda = \frac{\phi_{ceramic}}{N_{ceramic/binder}} \tag{3.4}$$

where $\phi_{ceramic}$ is the mean ceramic particle size.

3.3.5 Hardness and Indentation toughness measurement

The hardness and indentation toughness of sintered cermets were estimated by Vickers hardness tester (FEI, Kolhapur, India) (**Figure 3-11**) at 10 kg for 15s. All the readings of hardness were taken at different locations. Normally, an average of 10 readings of hardness is reported. Hardness was determined using the following equation [Smith and Sandland, 1922].

$$\text{Hardness (GPa)} = \frac{(1.8544 * P)}{d^2} \tag{3.5}$$

where P is load (N), d is average of two diagonals of the indentation in mm.

Indentation toughness was determined using the following equation [Shetty et al, 1985]. In the present study, Shetty formula is used for measuring fracture toughness via Vickers indentation as a wedge-loaded crack system. The plastic zone was treated rigid and ideally plastic, the displaced hardness impression volume was assumed to be accommodated in the plastic zone. In reality apart of the hardness impression, volume is taken up by some displacement of the material to the surface (surface pile-up). The plastic zone also probably undergoes some elastic compression. Residual indentation plastic zone acts as a wedge or compressed spring so the plastic zone undergoes some elastic compression [Shetty et al, 1985].

$$\text{Fracture toughness} = 0.025 \left(\frac{E}{H} \right)^{0.4} (\text{H.W})^{0.5} \qquad\qquad (3.6)$$

$$W = \frac{P}{4a} \qquad\qquad (3.7)$$

where, P=Load in N, 4a=2xAvg. Length of diagonal of the indentation (d) in mm, H=hardness in GPa, E is elastic modulus of the cermet in GPa estimated by rule of mixture.

Figure 3-12: Vicker's Hardness Tester

Nano hardness measurement was done to study the mechanical behavior of core and rim phases using a Triboindenter (Hysitron TI950 Hysitron Inc, USA) (**Figure 3-12)** equipped with three-sided Berkovich diamond indenter with a tip radius of 100 nm. A maximum normal load of 3000µN was applied for 2 sec.

Figure 3-13: Nano Hardness Tester and Indentor

3.4. Dry sliding wear test

Dry sliding wear tests were carried out using a ball-on-disk type tribometer (TR-201E-M2TM DUCOM, Bangalore, India (**Figure 3-14**). A schematic diagram for sliding wear is shown in **Figure 3-15**. The samples were fixed on the sample holder of wear testing machine with glue so that it should not get loosened during the continous sliding. Also after the wear test sample was removed by keeping the holder on hotplate and due to heat glue is removed and sample is easily taken from the holder.

Figure 3-14: Sliding wear test set up
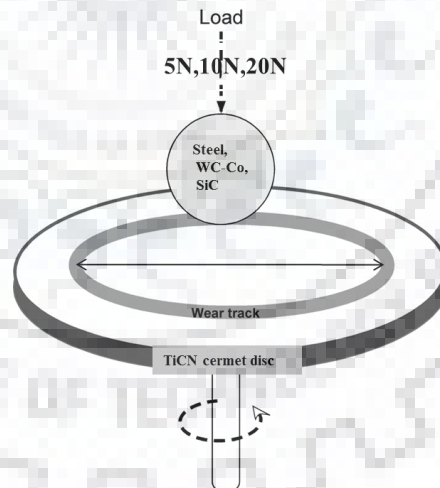
Figure 3-15: Schematic diagram for sliding wear test set up

Polished Ti(CN)-based cermets were subjected to sliding tests in unlubricated ambient conditions ($25 \pm 5^{\circ}C$ and 30-35 % RH). Commercially available bearing grade Chrome steel, cemented carbide or SiC balls of 10 mm diameter of ~7.40 GPa, 17 GPa, 25 GPa, respectively were used as counterbody. Properties and composition of balls as provided by the supplier, Jayashree Spheres and Measures, Jayashree Neelayam, Mahadevnagar, S.No. 95/4B/1/5 Post: Manjari Farm, (Hadapsar AM College Road), Pune 412307, India.

Table 3.2: Properties of counter balls used for wear against processed Ti(CN) based cermets

Balls	Composition elements	Grade	Roughness (µm)	Hardness (GPa)	Young's modulus	Poissons ratio
Chrome steel	C, Cr, Mn, Si, S, P	AFBMA G24	0.05	7.4	200	.29
Cemented carbide	WC, Co	AFBMA G10	0.025	17	630	.24
SiC	SiC, C	AFBMA G24	0.05	25	476	.19

Table 3.3: Chemical analysis of counter balls used for wear against processed Ti(CN) based cermets

Balls	Chemical analysis (wt.%)	
Chrome steel	Carbon	1.02%
	Chromium	1.42%
	Manganese	0.31%
	Silicon	0.30%
	Sulphur	0.006
	Phosphorous	0.009
Cemented carbide	Tungsten Carbide	94%
	Cobalt	6%
SiC	Silicon Carbide	99.9%
	Carbon	0.1%

Both the cermet discs and the balls were cleaned ultrasonically in ethanol and dried. The ball was fixed to make a track radius of 5.0 mm from the central axis and cermet discs were rotated at a fixed rotational speed of 500 rpm (linear speed of 0.22 m/s) for 20 min against steel ball and for 40 min against cemented carbide or SiC balls. A load of 5, 10 or 20 N load was applied on the ball that resulted in a maximum Hertzian (initial) contact stresses of 1.0, 1.1 or 1.3 GPa with steel; 1.15, 1.45 or 1.82 GPa with cemented carbide and 1.07, 1.35 or 1.70 GPa with SiC balls, respectively. Following assumptions were made in estimating the initial maximum Hertzian contact stress:

a. The strains are small and within the elastic limit.

b. The area of contact is much smaller than the characteristic radius of the body.

c. The surfaces are continuous and non-conforming (i.e. initial contact is a point or a line).

The initial maximum Hertzian contact stress (Pmax in GPa) was estimated by the following [Jhonson, 1955]:

$$P_{\max} = 1.5 \left(\frac{W}{\pi a^2} \right)$$

(3.8)

$$a = \left(\frac{3WR}{4E} \right)^{1/3}$$

(3.9)

Where applied load (W=5 N, 10 N or 20 N) and 'a' is the initial contact area. R is equivalent radius of contact bodies. E is the equivalent elastic modulus, μ is Poisson's ratio which can be estimated by using following expression:

$$\frac{1}{E} = \frac{\left(1 - \mu_1^2 \right)}{E_1} + \frac{\left(1 - \mu_2^2 \right)}{E_2}$$

(3.10)

The tangential frictional force at the contact was measured online and the coefficient of friction (COF) was estimated. The width and depth of wear scar formed on the cermet disc were measured using a stylus-tip profilometer. The morphologies of worn surfaces of all the samples were studied using scanning electron microscope (SEM) to understand the dominant wear mechanisms. At least 10 orthogonal measurements per track and three tracks for each composition were made to obtain average values of width and depth of wear scars. Results of width and depth were used for quantification of the extent of volumetric wear damage in the disk (V in mm^3) [Quercia et al. 2001].

$$V = 2\pi rwd$$

(3.11)

where, r, w and d are radius, width and depth of wear track, respectively (mm). SEM was used to measure scar dimensions on worn WC balls and the wear volume (*Vb*) was calculated according to

$$Vb = \left(\frac{\pi \, d^4}{64R} \right)$$

(3.12)

where d is the average of the wear scar dimensions measured in transverse and sliding directions and R is the radius of the ball. The estimated wear volume of disks or balls were divided by applied load and total sliding distance, and reported as a specific wear rate (WR in mm^3/N-m) as per the following formula:

$$WR = \left(\frac{V}{Ps} \right)$$

<div align="right">(3.13)</div>

where P is normal load (N); s is total sliding distance (m). The average of the wear rate and the coefficient of friction data are reported after conducting at least three sliding experiments. In order to understand the wear mechanism, a detailed microstructural characterization of worn surfaces and wear debris was conducted using SEM equipped with energy dispersive X-ray spectroscopy (EDS).

3.5. Tool preparation and machining details

To study the machining performance of the processed cermets, Ti(CN) based cermet compositions Ti(CN)-5WC-20Ni and Ti(CN)-5WC-10Ni-10Co-5TaC (in wt.%) designated as C1 and C4, processed via conventional and SPS techniques were selected for the machining studies and results were compared with commercially available cemented carbide tip of 65 HRC. Dominant crater wear mechanisms responsible for material removal from the cutting edge of Ti(CN) based cermet and cemented carbide tools during machining of 304 stainless steel were observed. Photographs of cermet disc and cemented carbide tip are shown in **Figure 3-16.** Cermet disc and cemented carbide tip were shaped in machining tool geometry with rake angle: 0°; clearance angle: 5° **(Figure 3-17 (a,b))** for machining 304 stainless steel rod of 30 HRC with an initial diameter of 24.9 mm (Figure 4-16 c). Turning operations **(Figure 3-18)** were performed on lathe machine. Turning was performed at 133 rpm and 435 rpm spindle speeds for 180 sec and 60 sec, respectively at 0.5 mm/rev. feed rate and 0.9 mm depth of cut. Similar machining tests were performed by cemented carbide tip. Cutting force evolved was measured by a lathe dynamometer and dominant crater wear mechanisms were observed on Ti(CN) based cermets tools and carbide tip tool using SEM.
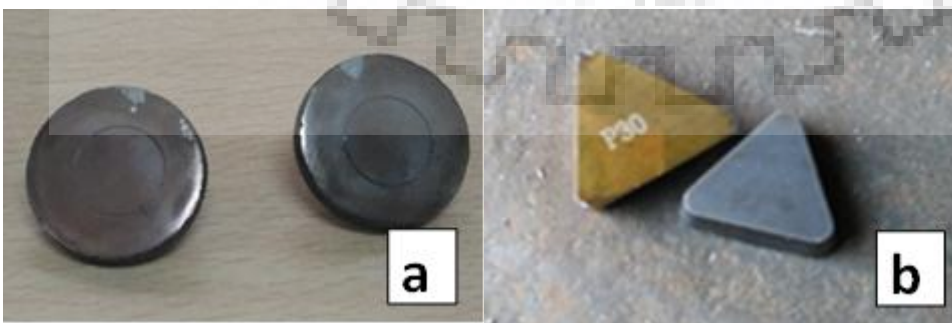
Figure 3-16. (a) Sintered Cermet disc and (b) commercially available Cemented carbide tip
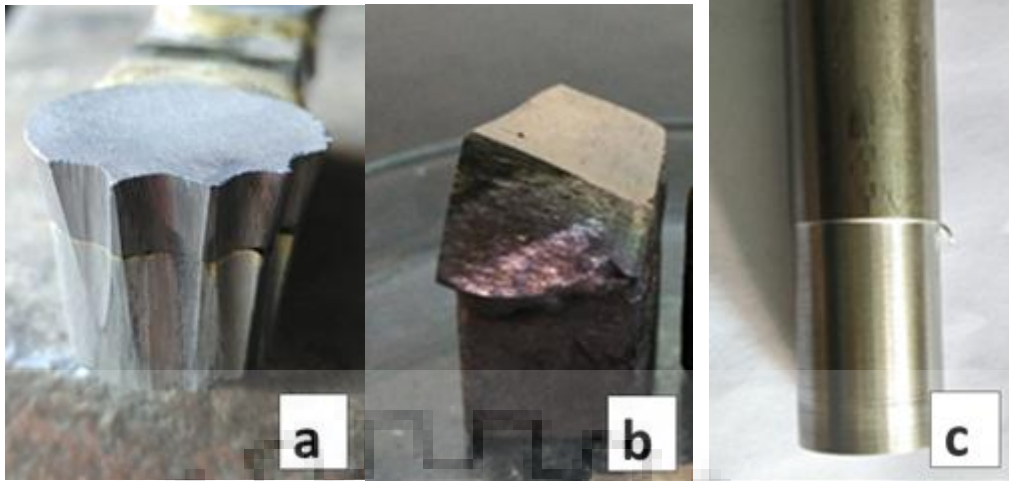
Figure 3-17. (a) Cermet disc tool, (b) Cemented carbide tool, (c) 304 stainless steel rod
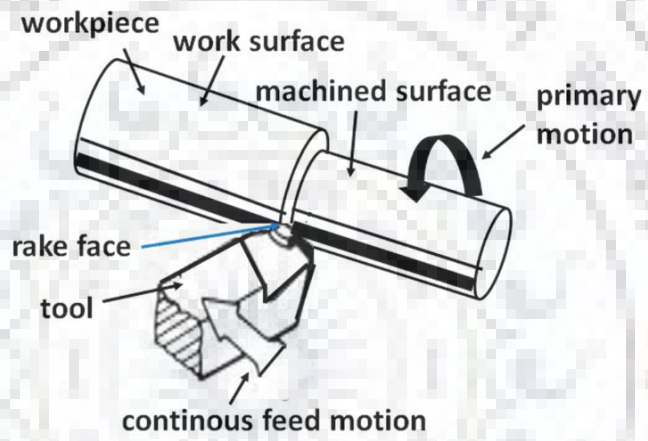
Figure 3-18: Turning machining on lathe

Processing and characterization of Ti(CN) based cermet via conventional sintering and Spark plasma sintering

In this chapter, characteristics of conventional sintering and spark plasma sintering used for processing of Ti(CN) based cermets are discussed. Also major observations in microstructure and mechanical properties of the investigated cermets are provided.

4.1 Material selection for Ti(CN)-based cermets:

For the present work following cermet compositions were designed: Ti(CN)-5WC-20Ni, Ti(CN)-5WC-20Ni-5TaC, Ti(CN)-5WC-10Ni-10Co, Ti(CN)-5WC-10Ni-10Co-5TaC (all in wt. %) and designated as C1, C2, C3 and C4, respectively. Controlled powders in terms of purity were used to have effective sintering, resulting in proper diffusion process and dense material. Also, the powders with similar size distribution were selected to facilitate uniform dispersion in mixing that would result in effective sintering. \

4.2 Ti(CN)-based cermets fabrication:

4.2.1 Powder mixing and characterization

Representative SEM images of ball milled powders of Ti(CN)-5WC-20Ni and Ti(CN)-5WC-10Ni-10Co-5TaC cermet compositions are shown in **Figure 4-1** respectively. SEM images shows that the powder particles were refined and particle size distribution was homogeneous. Some agglomerated particles are also visible. Representative results of the particle size distribution of Ti(CN)-5WC-20Ni and Ti(CN)-5WC-10Ni-10Co-5TaC ball milled powders as determined by laser scattering method are shown in **Figure 4-2 (a-b)** respectively. It was found that the large proportion of the powder samples were in submirometric range. The average particle size of ball milled powders was 0.6 ± 0.1 µm.
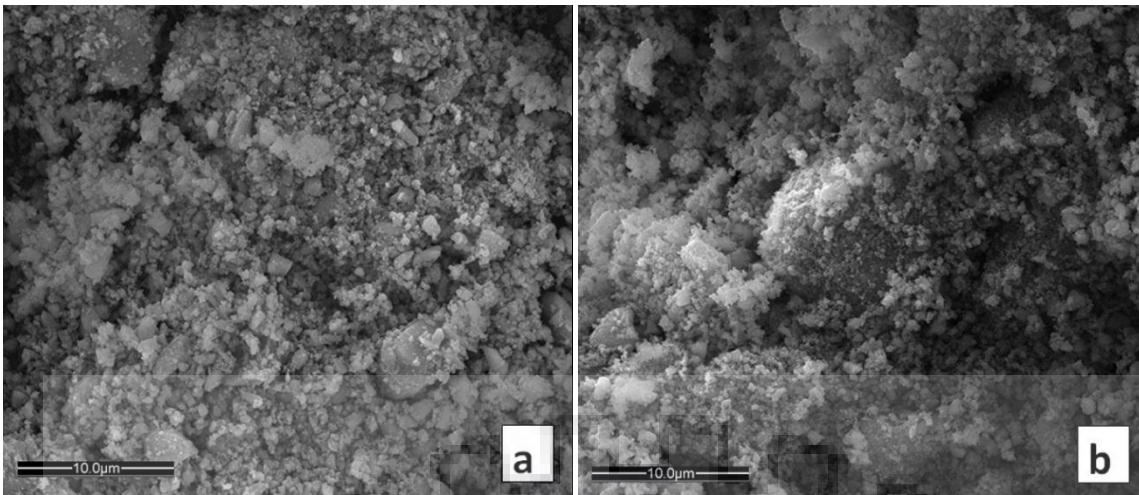
Figure 4-1. Representative SEM images of ball milled powders of (a) Ti(CN)-5WC-20Ni, (b) Ti(CN)-5WC-10Ni-10Co-5TaC
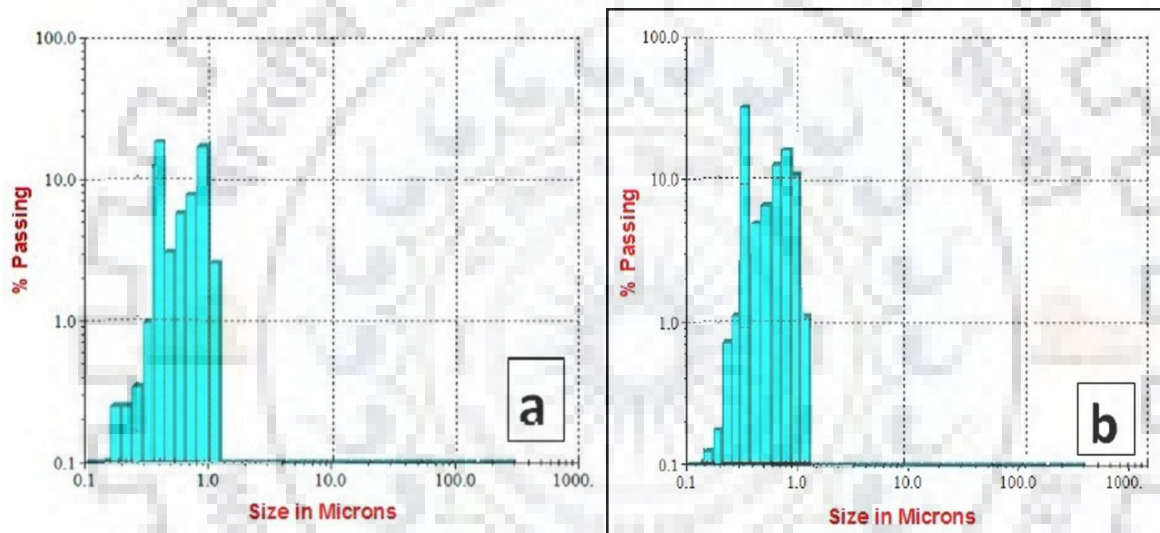
Figure 4-2. Particle size distribution of ball milled powders of (a) Ti(CN)-5WC-20Ni, (b) Ti(CN)-5WC-10Ni-10Co-5TaC respectively.

4.2.2. Sintering of Ti(CN)-based cermets

Figure 4-3 shows the sintering behavior of the samples processed via SPS. In the present single stage spark plasma sintering (SPS) the powder compact was heated directly to the final sintering temperatures of 1400°C. Temperature rose to 1400 °C in 16 min with a heating rate of 100 °C/min and pressure rose up to 70 MPa. After that, sample was held at 1400 °C temperature for next 3 min for densification. After holding for 3 min at 1400 °C, temperature was reduced with a cooling rate of 200 °C/min up to 900 °C. Most of the densification completes by the end of the holding time and at the time of holding sintering continues as thermal energy input is highest. Assuming that during holding period of SPS, most of the pores gets eliminated and leads to maximum densification. The current

47

increases sharply just before the holding stages and thereafter decreases to a lower value followed by stabilization during the rest period of the holding stage. Depending on electrical conductivity of the powder compact, the current can flow either via graphite die wall or via the powder compact. The aim was to achieve maximum density and better mechanical properties by restricting the grain growth during sintering. This can be achieved by employing rapid rate of heating and lowering the holding time at the sintering temperature. Absence of holding time generally results in non-homogenous densification, and therefore non-uniformity in material properties due to the extremely high rate of heating. The rate of heating was kept constant at 100°C/min throughout the cycles.
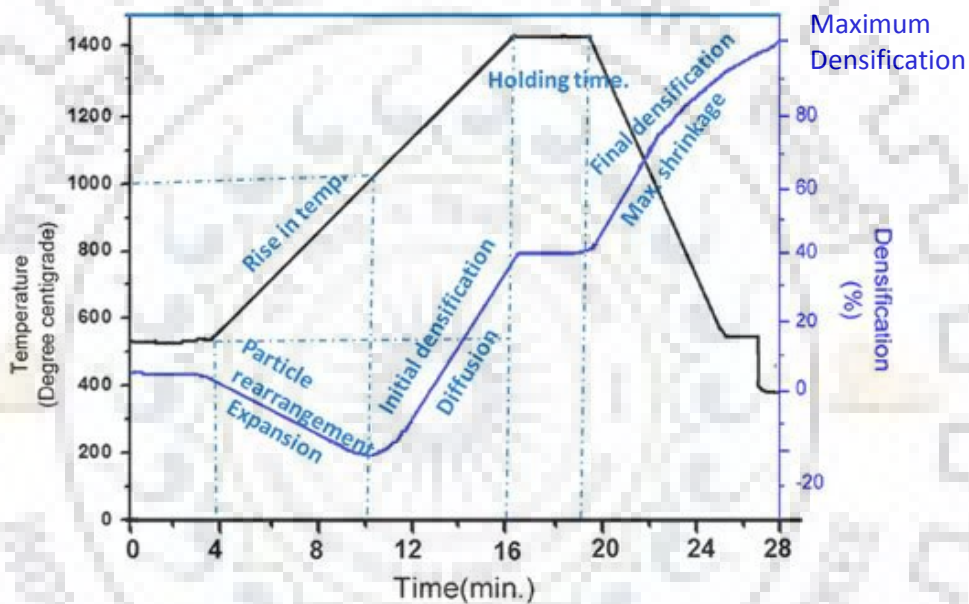
Figure 4-3. Sintering behavior of Ti(CN) based Cermets

4.3 Sample characterization:

The bulk density and relative densities for the sintered cermets are listed in **Table 4-1**. The cermets processed via conventional sintering have density (>97%) and the cermets processed via SPS technique have density (>98.5%). The liquid melt comprising of Ni and/or Co effectively dissolved Ti(CN), WC and/or TaC ceramic powders and precipitated out ceramic solid solutions. Thus, dissolution-reprecipitation process contributed for the densification [Ahn and Kang, 2000].

4.3.1. Phase analysis of sintered Ti(CN) based cermets

The phase evolution of processed Ti(CN)-based cermets via conventional and SPS is shown in **Figure 4-4.** XRD analysis for the Ti(CN)-5WC-20Ni (C1) cermets reveals the presence of Ti(CN), WC and Ni as major phases after sintering. The additional presence of

48

Co and/or TaC is observed in Ti(CN)-5WC-20Ni-5TaC, Ti(CN)-5WC-10Ni-10Co, Ti(CN)-5WC-10Ni-10Co-5TaC cermets. Sintered cermets reveal Ti(CN) core and (Ti,W)(CN)/(Ti,W,Ta)(CN) rim solid solution. Peak broadening is observed in Spark plasma sintered sintered cermets (visible in **Figure 4-4(a, b**) which confirms the evolution of refined carbide size during sintering. The selected sintering condition did not produce any other phases.
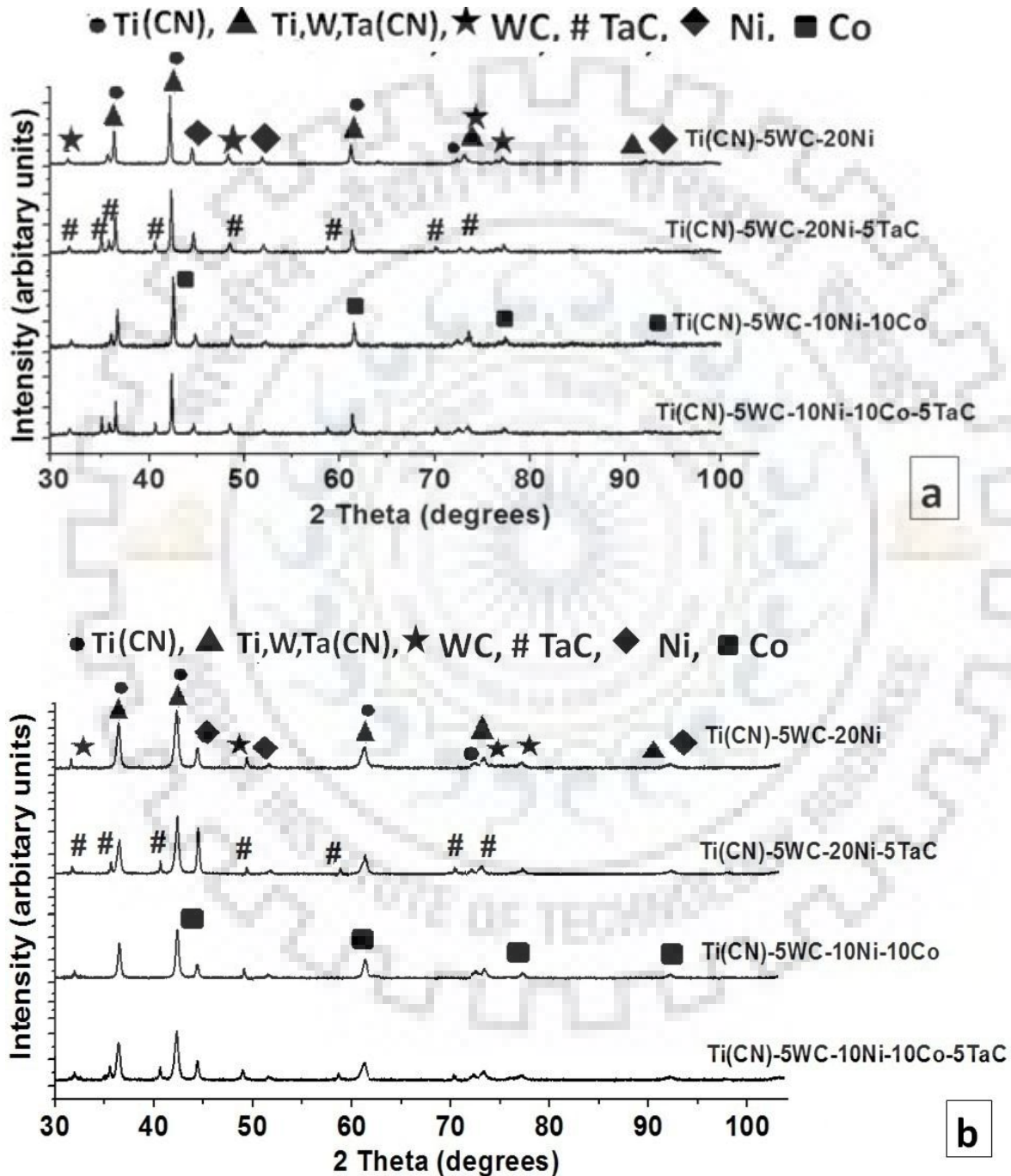
Figure 4-4 (a, b): XRD patterns of sintered TiCN based cermets processed via (a) conventional and (b) SPS technique

49

4.3.2. Microstructural characterization

In general, the back scattered SEM images of Ti(CN) based cermets C1, C2, C3 and C4 processed via conventional or SPS technique reveal three major microstructural phases of core-rim-binder with distinct difference in their contrast. Sintered cermets reveal Ti(CN) core and (Ti,W)(CN)/ (Ti,W,Ta)(CN) rim solid solution. Representative SEM (EDS) images of the polished surfaces of sintered Ti(CN)-20Ni-5WC cermet processed via conventional technique are shown in **Figure 4-5.** The EDS analysis suggests that black core phase is of Ti(CN), grey rim phase is the solid solution of (Ti, W) CN and the bright continuous phase is of Ni and NiTi solid solution. During sintering, the liquid melt of the binder phase dissolves the ceramic powders. It is reported that TiN has low solubility in metallic binder in comparison to TiC, which results in nitrogen rich undissolved TiCN core [Ettmayer et al., 1995]. The dissolved ceramic powders precipitate as solid solution rim phase around Ti(CN) core [Zhang, 1993; Ettmayer et al., 1995; Ahn and Kang, 2000]. The cores consisting of undissolved Ti(C,N) particles act as nucleation sites for the rim structure. With time and rise in temperature liquid binder phase reacts with Ti(CN) dissolving titanium carbide leaving TiN undissolved which again precipitates resulting in the formation of core-rim microstructure. Surrounding phase is the rim is a solid solution of (Ti,W/Ta)(C,N) consisting heavy metals (Zhang, 1993; Ettmayer et al., 1995; Tretyakov and Mashevskaya, 1999).
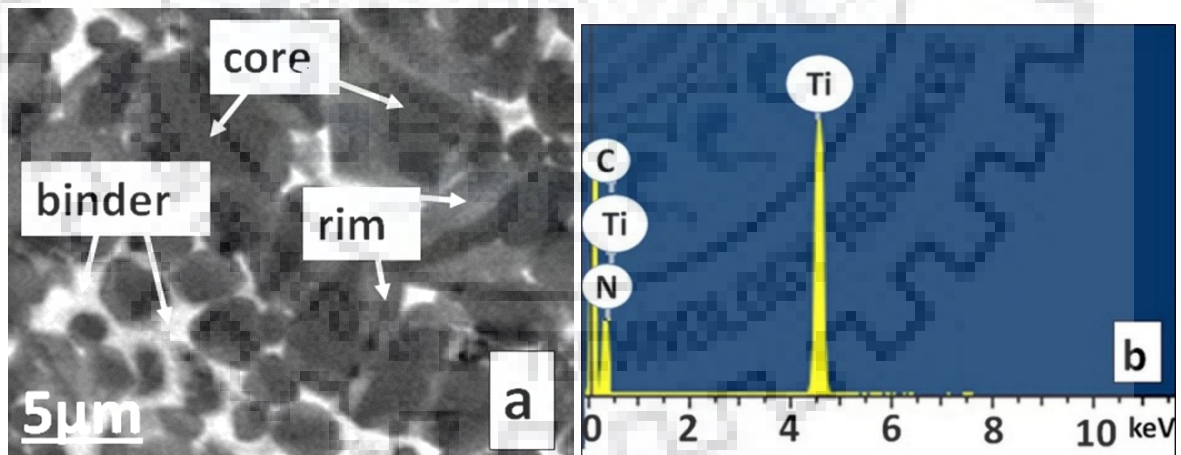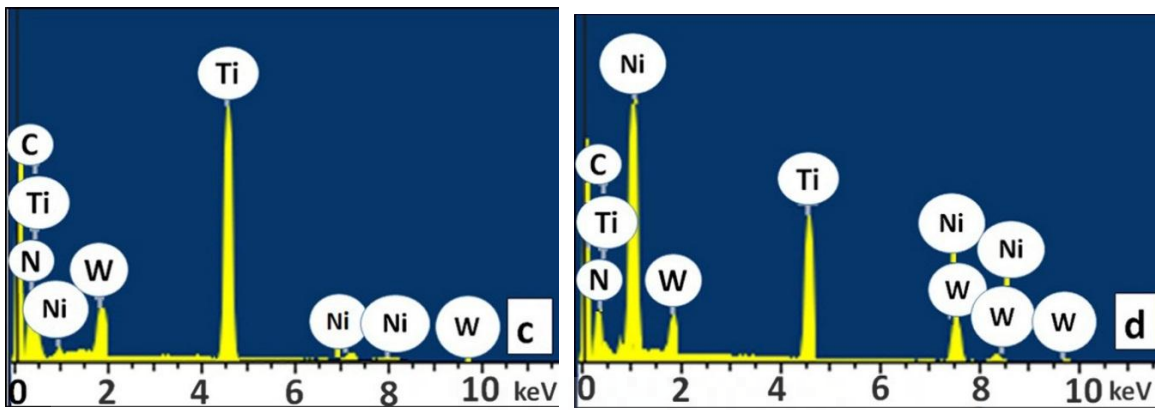
Figure 4-5: SEM image of sintered Ti(CN)-20Ni-5WC cermet processed via conventional technique. EDS analysis of core, rim and binder phases of the cermet are shown in (b), (c) and (d), respectively.

The size and the frequency of the carbide size appear to differ with the cermet composition and processing technique in the SEM (BSE) images shown in **Figure 4-6 (a-h)** of the processed Ti(CN) based cermets via conventional and SPS techniques. Microstructure of the Ti(CN) based cermets processed via SPS reveals significantly homogeneous with core/rim structure which enhances the densification of Ti(CN) based cermets. The carbide sizes (combined size of core and rim) obtained from ~200 measurements from each cermet microstructure are shown in **Table 4-1**. It is noticed that larger carbide particles and wider size distributions are obtained with conventional sintering. The carbide size varied from 1.61-2.16 μm for the cermets processed via conventional sintering and from 1.30-1.63 μm for the cermets processed via SPS. As SPS sintering process is fast, it restricts the coarsening of grains. Reduced carbide size is seen for the cermet having Ni-Co and TaC addition. C4 cermet have refined carbide size having the least (core, rim) sizes of (1.03, 0.58) μm and (0.76, 0.54) μm when processed via conventional sintering or SPS. During sintering at high temperature TiC of Ti(CN) dissolves in liquid melt of metallic binder. TiN has low solubility in comparison to TiC so undissolved nitrogen rich Ti(CN) remains. As a result, there is a formation of nitrogen rich nuclei around which dissolved TiC will precipitate in course of a dissolution precipitation process. Addition of Co restricts the solubility of nitrogen which suppress dissolution and precipitation process. As a result grain coarsening is prevented and leads to formation of refined small crystallites size. It leads to high hardness, high toughness and good machinability at the same time [Zhang, 1993; Ettmayer et al., 1995; Tretyakov and Mashevskaya, 1999]. **Figure 4-7 (a-d)** show the EDS analysis of C1, C2, C3, C4 cermets processed via SPS revealing the presence of elements present irrespective of compositions.
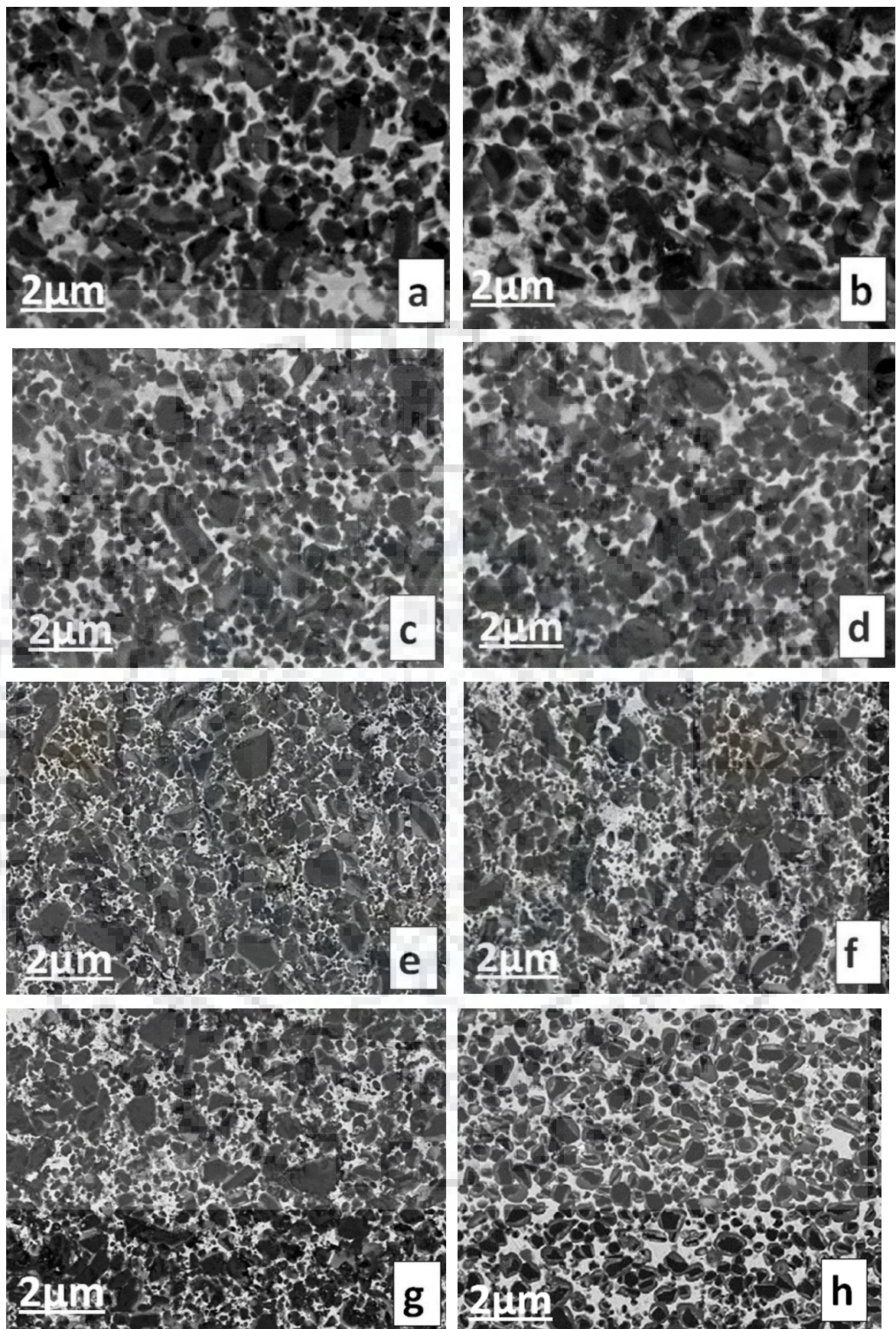
Figure 4-6: (a,b,c,d) SEM (BSE) images of C1, C2, C3, C4 cermets processed via conventional sintering. (e,f,g,h) SEM (BSE) images of C1, C2, C3, C4 cermets processed via SPS sintering
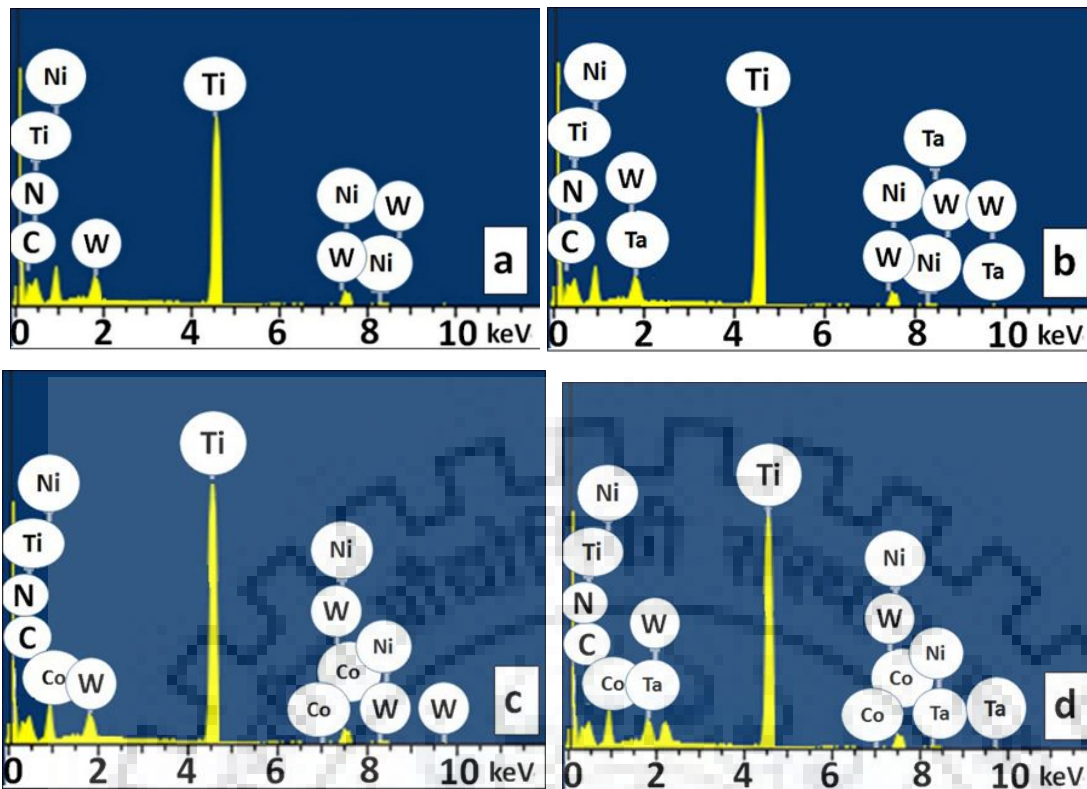
Figure 4-7: EDS analysis (a,b,c,d) of processed Ti(CN) based cermets designated as C1, C2, C3, C4

Figure 4-8 (a, b) represents the ceramic contiguity (filled square) and binder mean free path (filled triangle) for Ti(CN) based samples processed via conventional and SPS technique. Ceramic contiguity and binder mean free path are measured in order to study the effect of microstructure on the mechanical property behavior of cermets. Ceramic contiguity and binder mean free path vary from (0.41–0.45) and (1.00–1.25) μm when processed via conventional sintering and ceramic contiguity (filled square) and binder mean free path (filled triangle) vary from (0.39–0.43) and (0.94–0.99) μm respectively, when processed via SPS. Ti(CN)–5WC–10Ni–10Co–5TaC cermet has the least contiguity of the ceramic phase and largest binder mean free path among all investigated cermets. The overall metallic binder content is constant in all the four compositions i.e 20 wt.% whereas in C1, C3 it is Ni and in C3, C4 it is Ni-Co. Change in ceramic contiguity or binder mean free path is due to composition whereas the binder content is constant. Also ceramic contiguity and binder mean free path are measured in order to study the effect of microstructure on the mechanical behavior of cermets. Investigation of mechanical behavior reveals that hardness is found high for the sintered cermet having least ceramic contiguity and larger binder mean free path.

Binder mean free path decreases when there are larger ceramic particle. And it will result in decrease in fracture toughness. When ceramic particles are refined in size there will be less ceramic contiguity and higher binder mean free path. But when ceramic particles are larger in size ceramic contiguity will increase and also binder mean free path will decrease.
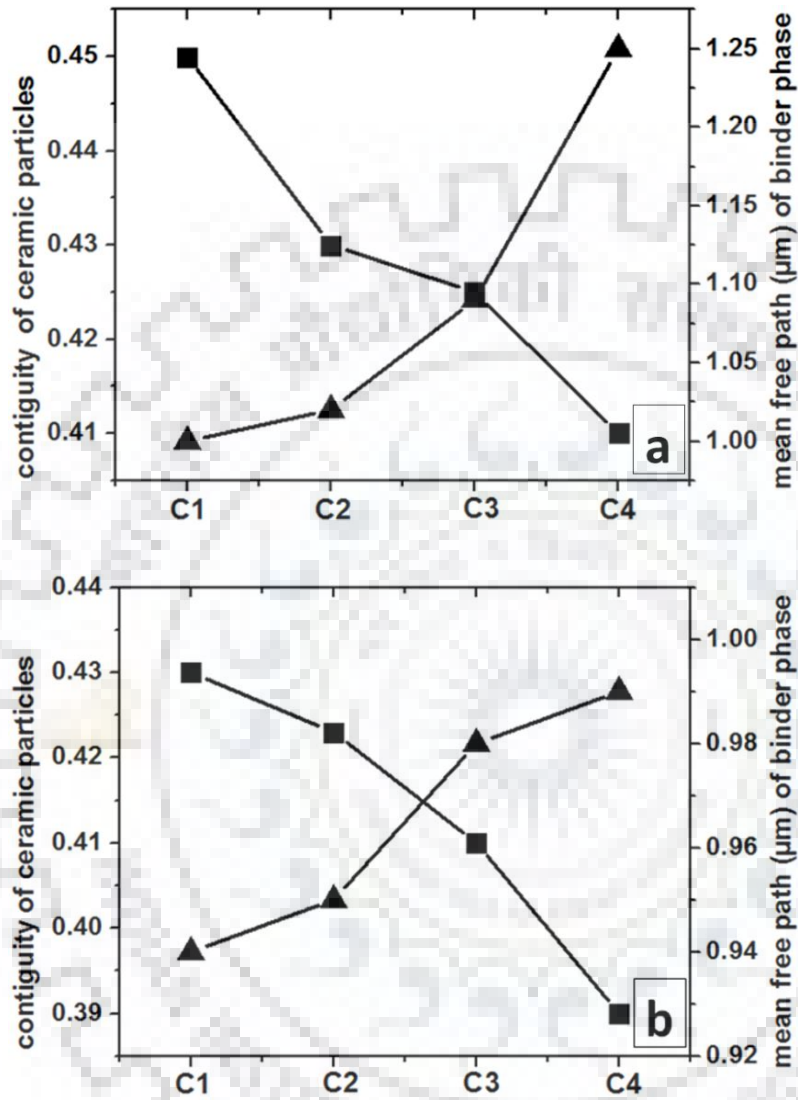
Figure 4-8: (a) Ceramic contiguity (■) and (b) binder mean free path (▲) for Ti(CN) based samples processed via conventional (a) and SPS technique (b).

Table 4-1: Designation, composition (in wt%), density and carbide size of Processed Cermets

Design ation	Composition	Density (g/cc)	Relative density %	Carbide (Core+rim) size (μm)	Density (g/cc)	Relative density %	Carbide (Core+rim) size (μm)
		Conventional sintering (100 MPa, 1550°C for 2 hr.)			Spark Plasma Sintering (70 MPa, 1400°C for 3 min.)		
C1	Ti(CN)-5WC-20Ni	5.6	97.0	2.2 ± 0.2	5.7	98.9	1.6 ± 0.1
C2	Ti(CN)-5WC-20Ni-5TaC	5.9	98.7	1.9 ± 0.1	5.9	99.1	1.6 ± 0.1
C3	Ti(CN)-5WC-10Ni-10Co	5.7	98.9	1.7 ± 0.1	5.7	99.4	1.4 ± 0.1
C4	Ti(CN)-5WC-10Ni-10Co-5TaC	5.8	98.5	1.6± 0.1	6.0	99.9	1.3 ± 0.1

EDS study of different phases was done repeatedly at five locations for microstructure of each cermet and the differences in wt% of heavy elements or metallic binders obtained from EDS analysis is shown in **Table 4-2.** The effect of cermet composition on results obtained from EDS analysis can be realized. A minimum amount of Ti in core phase is obtained for C3 or C4 cermets having Ni-Co in the composition. The Ni-Co liquid binder phase reacts with titanium carbonitride by preferentially dissolving titanium carbide leaving titanium nitride undissolved [Ahn and Kang, 2000]. Thus, it led to the high dissolution of TiC in metallic liquid melt. Also, the Ti content is more in core phases of C1 and C2 cermets. The EDS analysis conducted at various locations of rim phases of cermets reveal higher contents of Ti along with W, Ta and C in the rim phase of C4 cermet. Binder phase mainly consists of metallic binders forming liquid melt surrounding the core-rim phase of the cermets. In addition, presence of Ti, W or Ta is also observed in the binder phase of the sintered cermet (**Table 4-2**). Among binder phases of all the investigated cermet, Ni and Co are high in their content in C4 cermet. Summarizing EDS analysis, the minimum amount of Ti in core phase for C4 cermet indicates maximum

dissolution of ceramics for the cermet containing Ni-Co and TaC. The maximum presence of Ti, W, Ta, or C in rim phase in C4 cermet also confirms maximum precipitation in presence of Ni-Co and TaC.

Table 4-2. Major results obtained from EDS analysis of core-rim-binder phases of sintered cermets. Wt% of elements is shown.

Cerm-et	Core	Rim			Binder				
	Ti	Ti	W	Ta	Ni	Co	Ti	W	Ta
C1	69.1 ± 0.8	44.4 ± 0.4	18.2 ± 0.3		54.3 ± 0.6		16.1 ± 0.4	13.2 ± 0.1	
C2	66.3 ± 0.6	45.3 ± 0.2	17.3 ± 0.1	11.1 ± 0.1	43.4 ± 0.4		15.3 ± 0.3	12.1 ± 0.1	10.0 ± 0.2
C3	61.7 ± 0.4	47.4 ± 0.1	19.2 ± 0.2		27.4 ± 0.3	19.2 ± 0.5	19.1 ± 0.2	16.4 ± 0.2	
C4	59.3 ± 0.3	48.1 ± 0.2	20.0 ± 0.1	12.1 ± 0.1	30.1 ± 0.3	20.0 ± 0.3	21.1 ± 0.1	15.1 ± 0.1	11.1 ± 0.2

4.4. Mechanical properties of sintered Ti(CN) based cermets:

Investigated Ti(CN) based cermets processed via conventional sintering or SPS technique exhibit high hardness and indentation toughness values. The comparison of mechanical properties on the basis of processing technique is summarized in **Table 4-3.** Hardness and indentation toughness of the Ti(CN) based cermets prepared via conventional sintering varied from 14 to 16 GPa and 8.75 to 9.25 MPa m$^{1/2}$ and via SPS technique from 15 to 17 GPa and 8.79 to 9.51 MPa m$^{1/2}$ with variation in cermet composition. Enhanced densification attributes to improved mechanical properties of the cermets processed via SPS. The observed differences in hardness and indentation toughness with respect to compositions is probably due to the differences in strength of interface between the rim solid solution and binder phase. However, cermets prepared using nickel and cobalt or nickel, cobalt and TaC resulted in higher hardness and indentation toughness. Among transition metal carbides, TaC is considered for the consistent mechanical behavior and superior resistance against crack propagation (Rowcliffe and Warren, 1970; Rowcliffe and Hollox, 1971; Xiong et al., 2007; Kiani et al., 2015). During sintering at high temperature, liquid Ni-Co effectively spreads over the surfaces of carbide particles, resulting in good wettability. The increased metal-carbide bond strength is believed to suppress the crack propagation, improving indentation toughness. The restricted grain coarsening with the Co addition is attributed to improved hardness [Zhang, 1993; Ettmayer et al., 1995; Ahn and Kang, 2000]. Correlating with the

crystal size measurements, C4 cermet having least carbide size showed high hardness and indentation toughness.

Table 4-3: Vickers hardness and indentation toughness of Processed Cermets

Designation	HV10 (GPa)	K_{Ic} (MPa m$^{1/2}$)	HV10 (GPa)	K_{Ic} (MPa m$^{1/2}$)
	Conventional sintering (100 MPa, 1550°C for 2 hr.)		**Spark Plasma Sintering (70 MPa, 1400°C for 3 min.)**	
C1	14.0 ± 0.2	8.7 ± 0.3	15.2 ± 0.1	8.80 ± 0.02
C2	13.9 ± 0.1	8.7 ± 0.3	14.9 ± 0.2	8.70 ± 0.01
C3	15.0 ± 0.3	9.0 ± 0.4	16.0 ± 0.0	8.80 ± 0.01
C4	16.2 ± 0.5	9.2 ± 0.4	17.0 ± 0.1	9.50 ± 0.01

Nano hardness of Ti(CN) based cermets processed via conventional and SPS lie between 9.83 GPa to 25.48±0.17 GPa and 11.14 to 26.01 GPa. It is found that the Spark plasma sintered processed cermet C4 having TaC-Ni/Co addition possess the highest hardness of core, rim and binder phases as shown in **Table 4-4**.

Table 4-4: Nano hardness of core, rim and binder phases of sintered cermets

Designation	Nano hardness (GPa) at 3000µN Normal Load					
	Conventional sintering (100 MPa, 1550°C for 2 hr.)			**Spark Plasma Sintering (70 MPa, 1400°C for 3 min.)**		
	Core	**Rim**	**Binder**	**Core**	**Rim**	**Binder**
C1	23.7±0.3	16.80±0.02	10.1±0.1	24.1±0.1	18.5±0.2	11.1±0.1
C2	22.0±0.0	16.40±0.03	9.8±0.3	23.1±.0	17.3±0.3	11.2±0.4
C3	24.4±0.1	18.00±0.03	11.8±0.3	25.1±0.0	19.1±0.6	12.5±0.1
C4	25.4±0.2	20.40±0.12	12.7±0.3	26.0±0.2	21.7±0.1	13.5±0.6

The range of the average dimension (Contact area, A(nm^2) of the three-sided Berkovich diamond indenter with a tip radius of 100 nm on application of a maximum normal load of 3000μN for 2 sec. on the cermet is shown in **Table 4-5**.

Table 4-5: The range of the average dimension (Contact area, A(nm^2) of the nano indenter on application of 3000μN for 2 sec. on the cermet

Phases	The range of the average dimension (Contact area, A(nm^2) of the nano indentor of all four compositions (C1, C2, C3, C4)	
	Conventional sintered cermets	Spark plasma sintered cermets
core	$9.6 \times 10^4 – 1.05 \times 10^5$	$9.5 \times 10^4 - 1.07 \times 10^5$
rim	$1.19 \times 10^5 – 1.6 \times 10^5$	$1.17 \times 10^5 - 1.5 \times 10^5$
binder	$1.66 \times 10^5 - 2.39 \times 10^5$	$1.5 \times 10^5 - 2.3 \times 10^5$

4.5 Summary:

Ti(CN)-5WC-20Ni, Ti(CN)-5WC-20Ni-5TaC, Ti (CN)-5WC-10Ni-10Co, and Ti(CN)-5WC-10Ni-10Co-5TaC were prepared by conventional and spark plasma sintering technique in inert atmosphere of argon. Following are the major findings:

1. Ti(CN) based cermets achieved density (>97%) on processing by conventional sintering (compacted at 100 MPa and sintered at 1550 °C for 2 h) whereas density (>98.5%) is achieved on processing by SPS at 1400 °C and 70 MPa pressure for 3 min.

2. SEM (BSE) images of sintered cermets revealed Ti(CN) core and (Ti,W)(CN)/(Ti,W,Ta)(CN) rim solid solution. XRD pattern of SPS sintered cermets revealed peak broadening confirming evolution of refined carbide size during sintering. Least carbide size of 1.30 μm obtained for Spark plasma sintered Ti(CN)–5WC– 10Ni–10Co–5TaC cermet.

3. Vickers hardness and indentation toughness of the Ti(CN) based cermets prepared via conventional varied from 14 to16 GPa and 8.75 to 9.25 MPa m$^{1/2}$ and via SPS

technique from 15 to 17 GPa and 8.79 to 9.51 MPa m$^{1/2}$. Nano hardness at 3000μN of different core-rim-binder phases of sintered cermets varied between 9.83 GPa to 25.48±0.17 GPa for conventional and 11.14 to 26.01 GPa for SPS sintered cermets. Addition of TaC in Ti(CN)-WC-Ni/Co cermets resulted in high hardness and indentation toughness.

4. Refined size and least fraction of adjacent ceramic phase are attributed for improved properties of TaC added Ti(CN)-WC-Ni/Co SPS sintered cermet.

Tribological behavior of conventionally sintered cermets against steel and cemented carbide balls

---

This chapter deals with major observations on tribological behavior of conventionally sintered Ti(CN) based cermets as a function of cermet composition and sliding load (5 - 20 N).The friction and wear properties against steel and cemented carbide balls are separately discussed. At the end, a comparative note on the effect of counterbody on the sliding wear behavior of the investigated cermets is provided.

Based on the experimental and material parameters, the complex tribological behavior of Ti(CN)-based cermets in sliding wear is widely characterized by adhesion, abrasion, tribochemical wear, oxidation, plastic deformation and/or fracture and wide ranges of COF from 0.2 to 1.2 and wear rate from 10^{-7} mm^3/Nm to 10^{-3} mm^3/Nm are reported [Rigney, 1984; Arenas et al., 2003; Engqvist et al., 2000; Pirso et al., 2004a & 2004b; Kumar et al., 2007]. In order to further improve the performance of Ti (CN)-based cermets in severe wear conditions, mechanical properties and thermal shock resistance should be improved. Among transition metal carbides, TaC is considered for the consistent mechanical behavior and superior resistance against crack propagation [Rowcliffe and Warren, 1970; Rowcliffe and Hollox, 1971; Rolander et al., 2001; Xiong et al., 2007; Kiani et al., 2015].

In the present study, the effect of TaC addition on the microstructure, mechanical properties and tribological behavior of Ti(CN)-5 wt% WC-20 wt% Ni/Co cermets was investigated. For this, conventionally sintered Ti(CN)-based cermets with compositions Ti(CN)-5wt.%WC-20wt.%Ni, Ti(CN)-5wt.%WC-20wt.%Ni-5wt.%TaC, Ti(CN)-5 wt.% WC-10wt.% Ni-10wt.%Co, and Ti(CN)-5wt.%WC-10wt.%Ni-10wt.%Co-5wt.%TaC (designated as C1, C2, C3, and C4, respectively) were slid in dry unlubricated conditions at 5, 10 or 20 N load. Commercially available bearing grade EN-31 steel balls of 7 GPa of 10 mm diameter and cemented carbide balls of 17 GPa of 10 mm diameter were used as counterbodies. Friction and wear results obtained in sliding of conventional sintered cermets against steel and cemented carbide are separately discussed. The dominant mechanisms of material removal in the selected sliding conditions are elucidated

Section 5.1. Friction and wear properties of conventionally sintered Ti(CN) based cermets against steel ball

5.1.1 Frictional behavior of Ti(CN) based cermets against steel ball

When subjected to sliding against steel, the investigated cermets showed an identical evolution of friction. In general, the COF increases initially in 50–300 s (running-in-period) and thereafter reaches steady state. Typical COF plots as a function of time are shown for the baseline composition Ti(CN)-5WC-20Ni (C1) cermet and TaC - Co added Ti(CN)-5WC-10Ni-10Co-5TaC (C4) cermet slid against steel in **Figure 5-1.** The average steady state COF varied from 0.2 to 1.0 with change in the cermet composition or sliding load. The average steady state COF values for the investigated cermets are shown as a function of sliding load in **Table 5-1.** The COF decreased with increase in sliding load from 5 to 20 N. Among all investigated cermets, C4 cermet exhibits a minimum COF of 0.2 at 20 N load, the addition of TaC in Ti(CN)-5WC-10Ni-10Co reduced the friction to the minimum. The formation of smooth surface contacts for C4 cermets are explained in the later section. The frictional behavior of the investigated cermets indicates the strong influence of the addition of TaC in the cermet composition. Among cermets containing TaC, using Co and Ni binder phase is beneficial in reducing friction in selected sliding conditions.
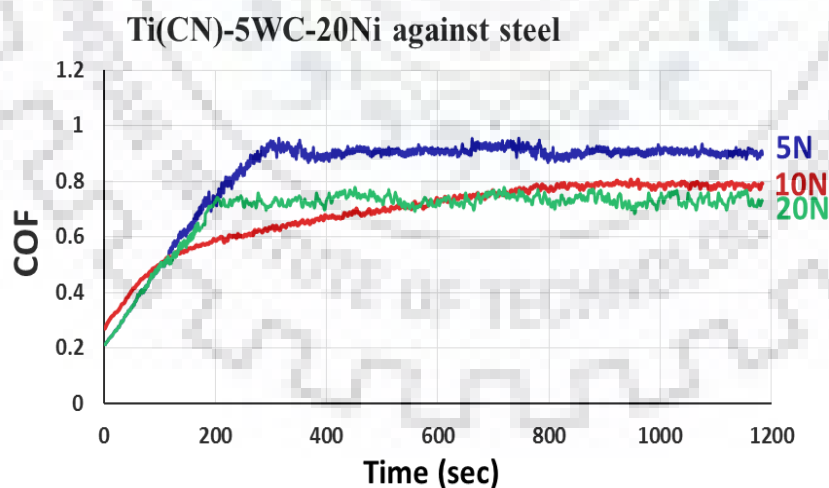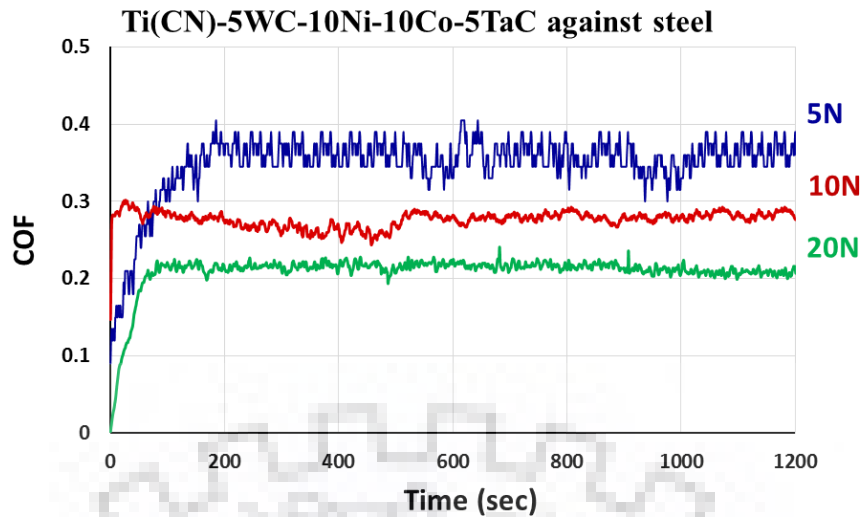
Figure 5-1 Coefficient of friction vs. time for Ti(CN)-5WC-20Ni (C1) and Ti(CN)-5WC-10Ni-10Co-5TaC (C4) cermet worn against steel ball at different loads

Table 5-1 Average steady state COF of cermets slid against steel.

Designation	Cermet Composition	Steady State COF		
		5N	**10N**	**20N**
C1	Ti(CN)-5WC-20Ni	0.90±0.05	0.79±0.03	0.73±0.03
C2	Ti(CN)-5WC-20Ni-5TaC	1.02±0.10	0.93±0.04	0.83±0.03
C3	Ti(CN)-5WC-10Ni-10Co	0.81±04	0.73±0.03	0.71±0.02
C4	Ti(CN)-5WC-10Ni-10Co-5TaC	0.37±0.02	0.29±0.01	0.21±0.01

5.1.2 Wear results

Specific wear rates of investigated Ti(CN)-based cermets and the respective steel balls are shown in **Figures 5-2 a and b**. In general, wear rate reduced with increase in load (**Figure 5a**). The C2 cermet exhibits the highest wear rate of 7×10^{-7} mm^3/Nm among the cermets at 5N, whereas the lowest wear rate of 3×10^{-7} mm^3/Nm is noted for C4 at 20 N. Wear rate of the counterbody steel ball varied in the range of 10^{-5} - 10^{-4} mm^3/Nm (**Figure 5b**). The highest and lowest wear rates of 3×10^{-4} mm^3/Nm and 7×10^{-5} mm^3/Nm are found for steel balls slid against C4 and C2 cermets, respectively. It is observed that the addition of TaC to the initial batch composition of Ti(CN)-WC-Ni did not influence the friction and wear whereas addition of TaC in Ti(CN)-WC-Ni/Co led to the minimum COF and wear of the cermet. Further, it is worth to note that wear of steel

ball slid against the least worn cermet is the maximum, whereas the wear of steel ball slid against the most worn cermet is the minimum.
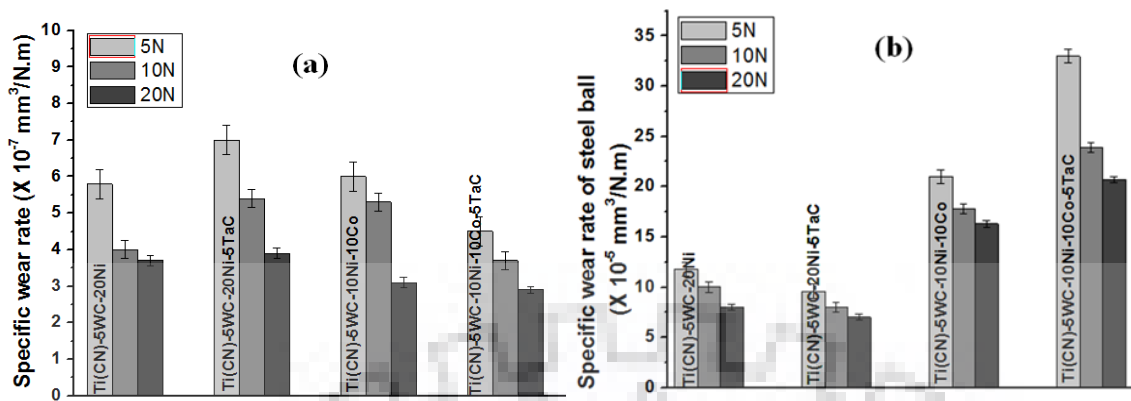
Figure 5-2 Wear rate of (a) cermets and (b) steel balls as function of composition and load.

5.1.3 Worn surface analysis against steel ball

Detailed analysis for the worn surfaces of cermets and balls was done to identify dominant mechanisms of material removal in the selected conditions of sliding. Representative SEM images of worn surfaces of investigated cermets against steel are shown in **Figure 5-3 (a-f)**. Worn surface of C1 cermet reveals characteristic grain pull-out **(Figure 5-3 (a))**. In addition, the worn surface shows adhered material, deformed in the sliding direction. Thus, there exists a combination of mechanical fracture and adhesion for the C1 cermet when slid against steel ball at 5N load. The soft binder phase is subjected to extrusion and removal followed by pull-out and fracture of carbides during sliding (Larsen Basse, 1985; Basu and Kalin, 2011; Guo et al., 2014). The pulled-out carbides are compacted, with further sliding, to form a layer on the surface. With increase in load to 20N, the worn C1 cermet surface shows increased width of wear track **(Figure 5-3 (b))** and increased fracture **(Figure 5-3(b))**. For the C2 cermet containing TaC, the surface worn at 5 N load shows increased pull-out as well as the presence of adhered layer **(Figure 5-3 (c))**. With increase in load to 20 N, the layer formation is not increased **(Figure 5-3 (d))**. When Ni and Co are used, the C3 cermet surface worn at 20 N reveals presence of layer **(Figure 5-3 (e))**. However, significant fracture of the layer exposed the underneath material for further wear. The surface of C4 cermet is completely covered with a continuous and strongly adhered layer **(Figure 5-3 (f))**. Thus, a transition in dominant wear mehcanism is observed from the fracture and carbide pull-out in C1 to the formation and removal of a layer in C4. On the other hand, typical SEM images of steel ball worn against C4 cermet at 5 N load (shown in **(Figure 5-4 (a))** primarliy reveal polishing of surface and absence of layer. The scar size reduced and thin layers found on the periphery of the scar when slid at 20 N (see **Figure 5-4 (b-c))**. EDS analysis of layers on the ball

periphery indicates the presence of small amounts of Ti along with major presence of Fe from ball. The oxygen peak from cermet suggests oxidation of the layer surface during sliding.
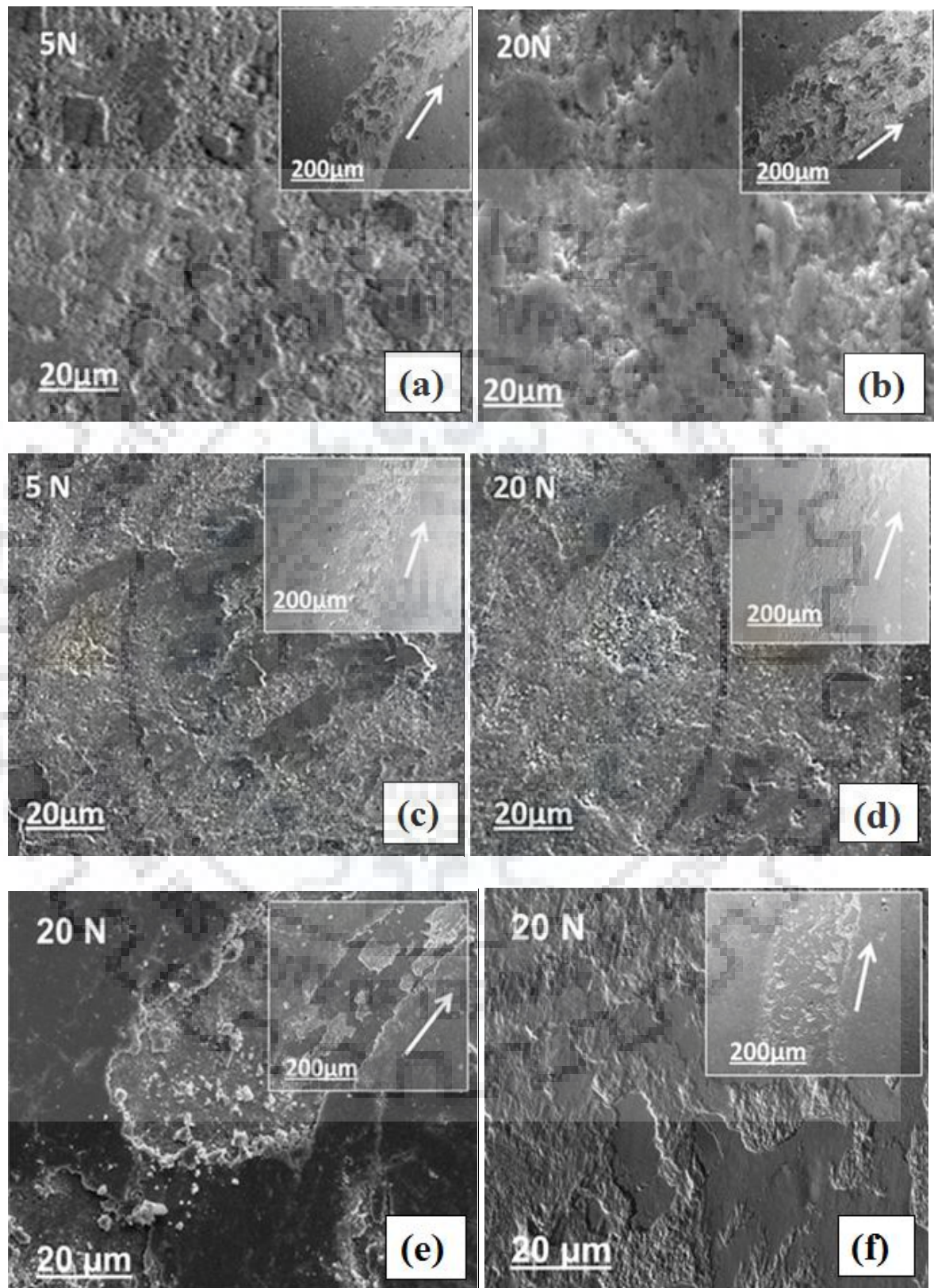
Figure 5-3. SEM images of worn cermets against steel balls: (a) Ti(CN)-5WC-20Ni at 5 N (b) Ti(CN)-5WC-20Ni at 20 N (c) Ti(CN)-5WC-20Ni-5TaC at 5 N (d) Ti(CN)-5WC-

20Ni-5TaC worn at 20 N (e) Ti(CN)-5WC-10Ni-10Co at 20 N, and (f) Ti(CN)-5WC-10Ni-10Co-5TaC at 20 N. Corresponding wear track images are shown in insets. Arrow in inset indicates sliding direction. The arrow indicating sliding direction in the inset also corresponds to the sliding direction in each primary figure.
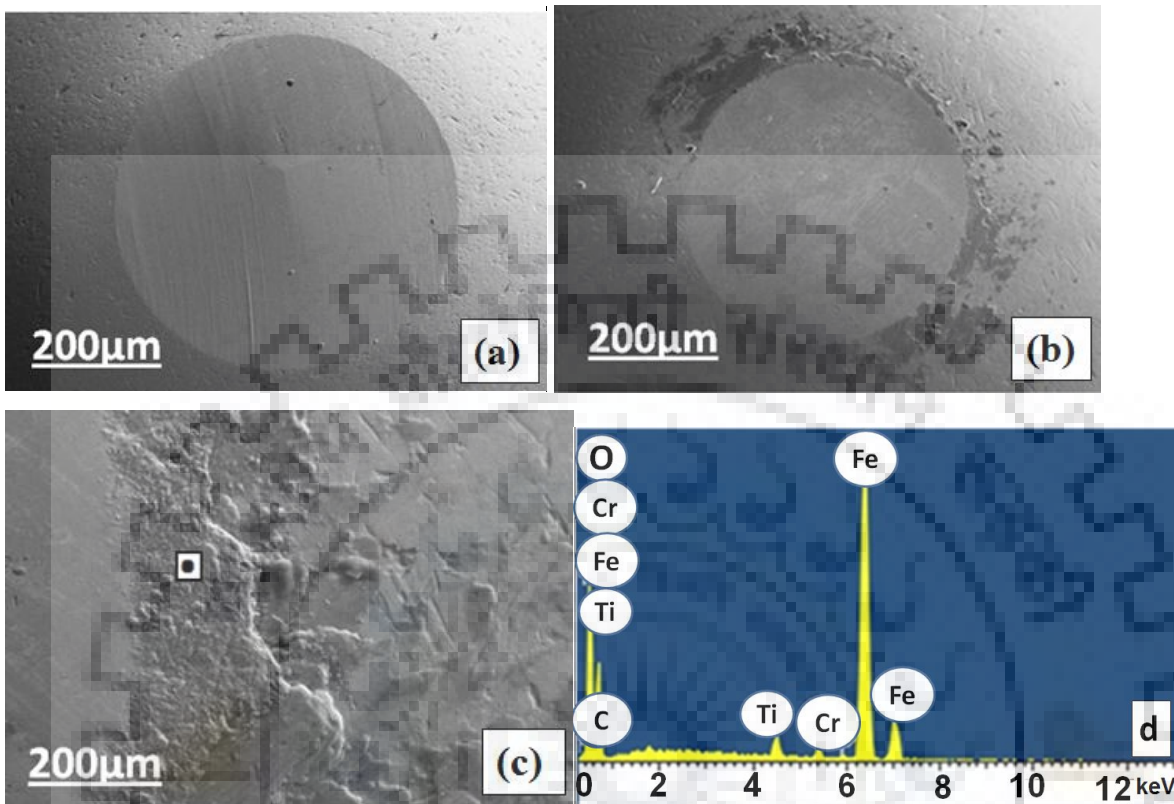
Figure 5-4. The surfaces of steel balls worn against Ti(CN)-5WC-10Ni-10Co-5TaC cermet at (a, b) 5 N and (c, d) 20 N. EDS spectrum obtained from point indicated in (c) is shown in (d).

Typical EDS spectra obtained from the layers formed on the cermet surfaces worn at 20 N load are shown in **Figure 5-5**. In general, EDS analysis shows the presence of elements of cermet i.e. Ti, W, C, N, Ni, Co and/or Ta, as well as Fe of steel ball. In addtion, the presence of oxygen suggests that the layer is composed of oxides. The formation of such mechanically mixed layer is often reported as the consequence of material transfer in the sliding wear of ceamic composites [Basu and Kalin, 2011]. However, intensities of major peaks in EDS analysis of layer surface differ to a larger extent, indicating significant difference in material transfer. In order to understand the effect of cermet composition on the material transfer, careful examination of weight percentage ratios of iron to titanium obtained from EDS analysis of cermets worn at 5 N load, and weight percentage ratios of titanium to iron obtained from EDS analysis of steel balls worn at 5 N load was carried out. EDS analysis was done repeatedly at five locations

and the average of readings is reported. A minimum ratio of 0.8 or 0.7 is found for C1 or C2 cermet, whereas a maximum ratio of 4.8 is obtained for C4 cermet (**Table 5-2**). This indicates that the iron or iron oxide removed from the steel ball is transferred to minimum extent onto the baseline cermet (C1) or the cermet containing TaC (C2). The material transfer from steel ball increased with the addition of Co, which can be attributed to high hardness of C3 cermet. The steel ball is severely abraded and iron or iron oxide transfers to the maximum extent when the hardest cermet (C4) containing TaC and Ni/Co is slid. The formation of iron oxide-rich continuous layer is responsible for the reduced wear and friction for C4 cermet.

On the other hand, the ratio of titanium to iron obtained from EDS analysis from ball surfaces worn against C2 is 0.12 and decreased to 0.03 with the addition of Co and TaC in the cermet composition (**Table 5-2**). Small ratios of titanium to iron essentially indicate negligible transfer from the cermet. Combining results obtained from EDS analysis of worn cermet and steel ball surfaces, it is clear that a significant material transfer occurs from the steel ball surfaces to the cermet discs only.

The influence of microstructural and mechanical characteristics on wear behavior of the investigated cermets can now be understood. Referring to EDS analysis, the minimum amount of Ti in the core phase and the maximum amount of Ti, W, Ta in rim phase of C4 cermet reveal the maximum dissolution and reprecipitation of carbides during sintering. Accordingly, the size of carbide is found to be refined when Co and TaC were used in the composition. In all the four investigated cermets, Ti(CN)-5WC-10Ni-10Co-5TaC (C4) has the highest hardness of 16 GPa and indentation toughness of 9.25 MPa m$^{1/2}$. During sliding, the deformation or removal of binder phase followed by the fracture or pull-out of carbides. High hardness in C4 results in restricted deformation or removal of binder phase, while increased indentation toughness can be attributed to the limited fracture of carbides. Accordingly, the wear occurred for C4 cermet is the least (refer **Figure. 5.2 a**). On the other hand, EDS analysis obtained from the stell ball surface worn against C4 cermet at 20 N reveals negligble presence of Ti (see **Figure 5-5** d).
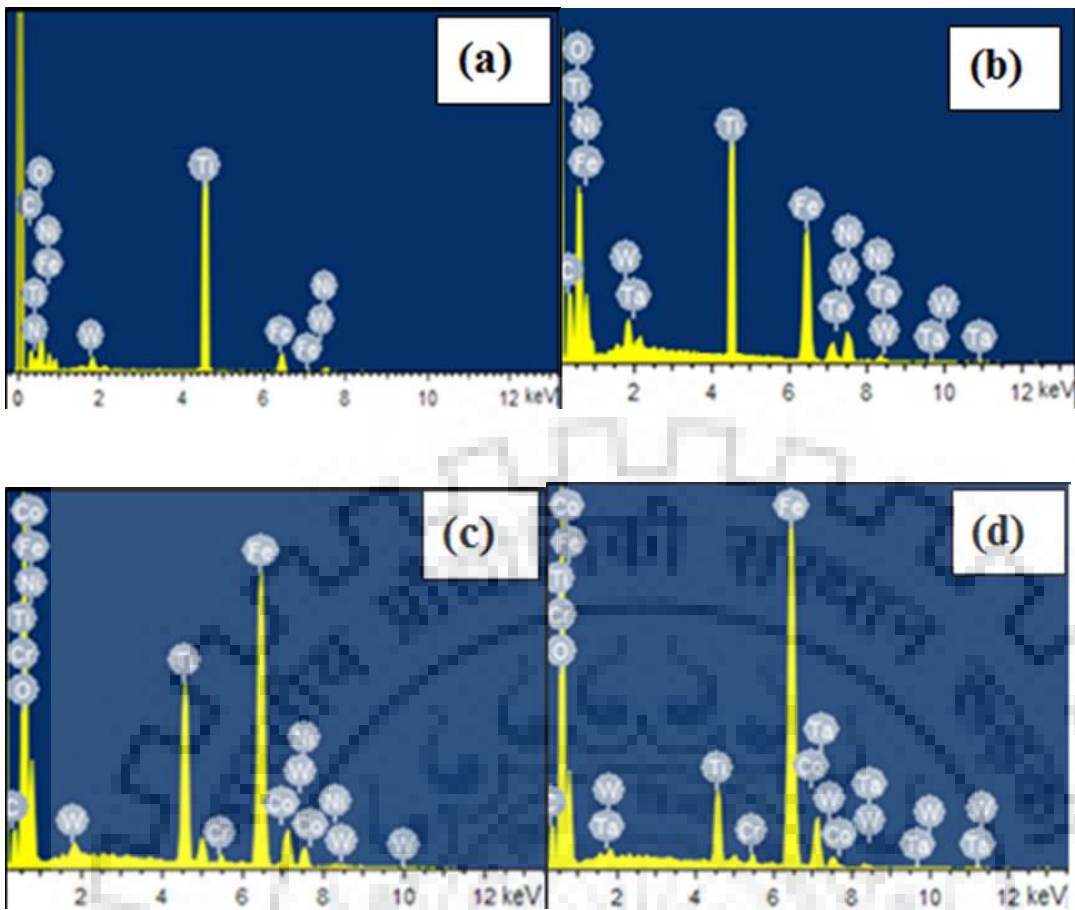
Figure 5-5. EDS analysis of cermets worn against steel balls at 20 N load (a) Ti(CN)-5WC-20Ni (b) Ti(CN)-5WC-20Ni-5TaC (c) Ti(CN)-5WC-10Ni-10Co, and (d) Ti(CN)-5WC-10Ni-10Co-5TaC.

Table 5-2: Results of material transfer studies from cermet to steel ball and steel ball to cermet worn at 5 N load as function of cermet composition

Designation	Cermet Composition	Weight ratio of iron to titanium obtained from EDS analysis of worn cermet surfaces	Weight ratio of titanium to iron obtained from EDS analysis of worn ball surfaces
C1	Ti(CN)-5WC-20Ni	0.83 ± 0.01	0.12 ± 0.02
C2	Ti(CN)-5WC-20Ni-5TaC	0.66 ± 0.01	0.14 ± 0.02
C3	Ti(CN)-5WC-10Ni-10Co	1.24 ± 0.02	0.03 ± 0.001
C4	Ti(CN)-5WC-10Ni-10Co-5TaC	4.81 ± 0.03	0.03 ± 0.002

5.1.4 Wear debris evolution

In order to understand the relation between morphology of wear debris particles and tribological performance of the investigated Ti(CN) based cermets, debris particles from worn cermets surfaces were carefully collected and subjected to SEM (EDS) analysis. Typical images of debris collected from Ti(CN)-5WC-20Ni and Ti(CN)-5WC-10Ni-10Co-5TaC cermets after sliding at 20 N load against steel are shown in **Figure 5-6 a, b.** Debris collected from worn cermet surface when slid against steel shows average size of the wear debris between 0.4 and 0.8 μm. In general collected debris particles against steel from Ti(CN)-5WC-20Ni cermet are irregular, bigger in size and in shape with sharp edges, as shown in **Figure 5-6 (a).** Debris generated for Ti(CN)-5WC-10Ni-10Co-5TaC is typically fine in size (**Figure 5-6 b).** At 20N load, a layer of iron oxide formed at periphery of worn scar **(see Figure 5.4 b and c).** EDS analysis of layer at periphery of wear scar on ball also confirmed dominant presence of Fe and O **(Figure 5.4 d**). Presence of Fe in EDS analysis for Ti(CN)-5WC-20Ni, Ti(CN)-5WC-20Ni-5TaC cermet debris particles (not shown in Figure) is due to wear of counterbody steel ball.
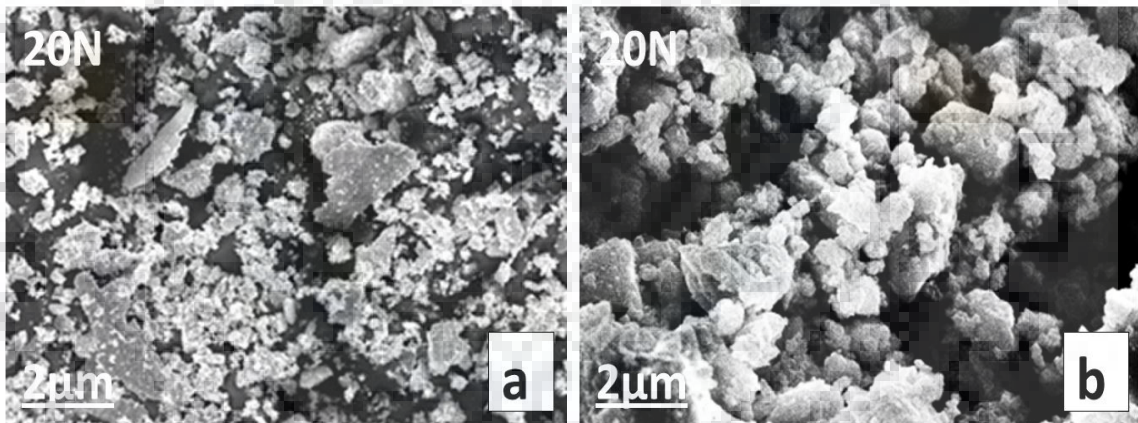
Figure 5-6 Typical SEM images of debris collected after sliding: (a) Ti(CN)-5WC-20Ni (b) Ti(CN)-5WC-10Ni-10Co-5TaC cermets against steel balls at 20 N load.

Section 5.2. Friction and wear properties of conventionally sintered Ti(CN) based cermets against cemented carbide ball

5.2.1 Frictional behavior of Ti(CN) based cermets against cemented carbide ball

When subjected to sliding against cemented carbide ball, the COF of the investigated cermets increase initially and thereafter reaches steady state. Typical COF plots as a function of time are shown for the baseline composition Ti(CN)-5WC-20Ni (C1) cermet and TaC-Co added Ti(CN)-5WC-10Ni-10Co-5TaC (C4) cermet slid against

cemented carbide in **Figure 5-7.** The average steady state COF varied from 0.25 to 1.1 with change in the cermet composition or sliding load. The average steady state COF values for the investigated cermets are shown as a function of sliding load in **Table 5-3.** The high values of COF in brittle solids are generally attributed to rough contacts generated from mechanical fracture or the formation of hard debris in the contact. Sliding against cemented carbide ball results in the formation of rough surface which increases friction. The COF against cemented carbide is found to be less at high load of 20 N. The addition of TaC in Ti(CN)-5WC-10Ni-10Co reduced the friction to the minimum. The formation of smooth surface contacts for C4 cermets is explained in the later section. Influence of counter bodies on frictional behavior is observed as cemented carbide led to the generation of rough surface which increased friction as compared to steel ball resulting in higher COF value.
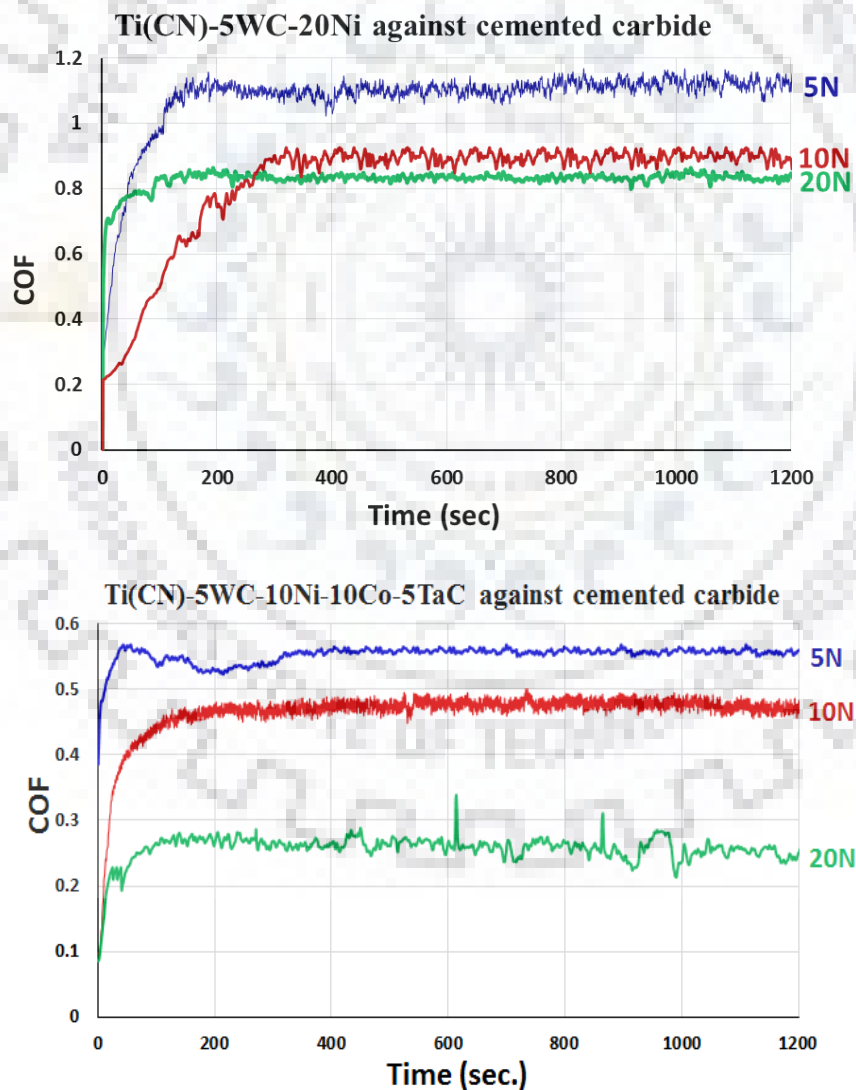
Figure 5-7 Coefficient of friction vs time for Ti(CN)-5WC-20Ni (C1) and Ti(CN)-5WC-10Ni-10Co-5TaC (C4) cermet worn against cemented carbide ball at different loads

Table 5-3 Average steady state COF values of cermets slid against cemented carbide ball

Designation	Cermet Composition	Steady State COF		
		5N	10N	20N
C1	Ti(CN)-5WC-20Ni	1.1	0.90	0.83
C2	Ti(CN)-5WC-20Ni-5TaC	0.82	0.66	0.54
C3	Ti(CN)-5WC-10Ni-10Co	0.91	0.732	0.67
C4	Ti(CN)-5WC-10Ni-10Co-5TaC	0.57	0.48	0.25

5.2.2 Wear results

Wear results obtained in sliding of the investigated cermets are shown as specific wear rate of cermets (**Figure 5-8 a**) and specific wear rates of cemented carbide balls (**Figure 5-8 b**). Ti(CN)-5WC-20Ni (C1) cermet possess highest wear rate of 7.3×10^{-6} mm^3/Nm at a load of 5N, and the least wear rate of 2.2×10^{-6} mm^3/Nm noted at 10 N for Ti(CN)-5WC-10Ni-10Co-5TaC (C4). A variation of 70 % in wear rate is found with respect to composition and load. For the cemented carbide balls used in the present study, the highest and lowest wear rates of 1.84×10^{-6} mm^3/Nm and 5.5×10^{-7} mm^3/Nm are found when slid against Ti(CN)-5WC-10Ni-10Co-5TaC (C4) and Ti(CN)-5WC-20Ni (C1) cermets, respectively. Again, the wear of the ball slid against the least worn cermet is the maximum, whereas the wear of the ball slid against the most worn cermet is the minimum.
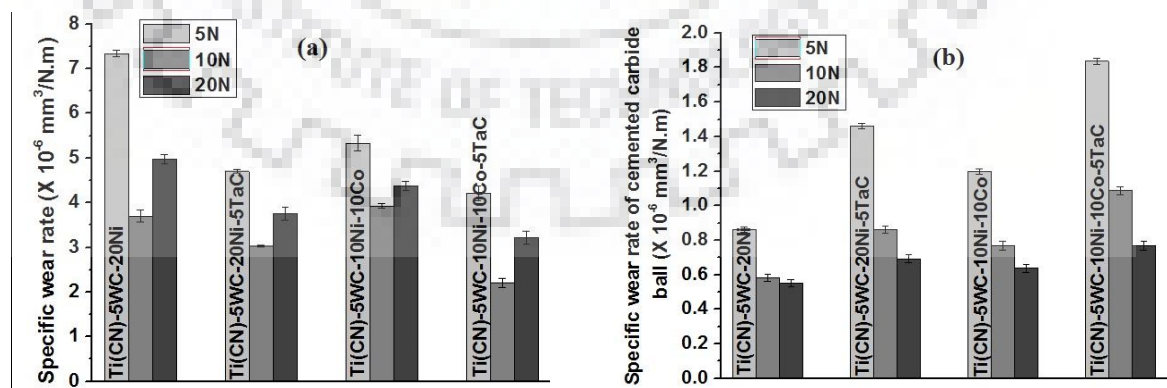
Figure 5-8 Wear rate of (a) cermets and (b) cemented carbide balls as a function of composition and load.

5.2.3 Worn surface analysis against cemented carbide ball

Typical SEM images of worn surfaces of investigated cermets against cemented carbide are shown in **Figure 5-9 (a-f).** The Ti(CN)-5WC-20Ni cermet worn at 5N reveals grain pull-out and adhered layer, similar to that observed against steel ball. However, the layer formed against cemented carbide appears thick and covers the worn surface. **(Figure 5-9 (a))**. With an increase in load to 20N, the worn Ti(CN)-5WC-20Ni cermet surface shows increased width of wear track **(Figure 5-9 (b))**. The adhered tribolayer is dominant at 20 N load (inset in **Figure 5-9 (b)**). For Ti(CN)-5WC-20Ni-5TaC cermet, the surface worn at 5 N load shows less wear with compacted layer formation (**Figure 5-9 (c)**). The worn surface of Ti(CN)-5WC-20Ni-5TaC cermet is covered with a dense tribolayer at 20N (**Figure 5-9 (d)**). This indicates that the addition of TaC resists the wear and helps in pertaining layer remain attached. At 20 N load, the worn surface of Ti(CN)-5WC-10Ni-10Co shows that the material is removed via deformation and fracture of layer (**Figure 5-9 (e)**). Ti(CN)-5WC-10Ni-10Co-5TaC cermet worn at 20 N reveals that the wear track is completely covered with a dense, continuous and strongly adhered layer (**Figure 5-9 (f)**). As Ti(CN) based cermets were slid against cemented carbide, characteristic grain pull-out and fracture of adhered material attributed to higher COF values at low load (5N) and it is observed that formation of continous and adherent layer has led to the reduction in friction and wear of the cermets at high load (20N).

In order to understand the chemistry of the layered surfaces, EDS analysis was conducted for the investigated worn cermet surfaces. The EDS analysis of the tribolayer at loads of 5 and 20N are shown as insets in **Figure 5-10 (a-d)**. In general, EDS analysis shows the presence of Ti, W, C, N, Ni, Co and/or Ta from cermet surface and W and Co from the ball surface. In addtion, the presence of oxygen indicates that the layer consist of oxides. The EDS analyis indicates significant changes in the amount of tungsten, cobalt and titanium on the layer surfaces with respect to load or composition. The EDS analysis of dense tribolayer at high load of Ti(CN) based cermets shows dominance of tungsten and titanium oxides. Therefore, it can be said that Ti(CN) based cermets slid against harder cemented carbide ball results in formation of thick tribochemical layer having increased presence of titanium oxide or tungsten oxide.
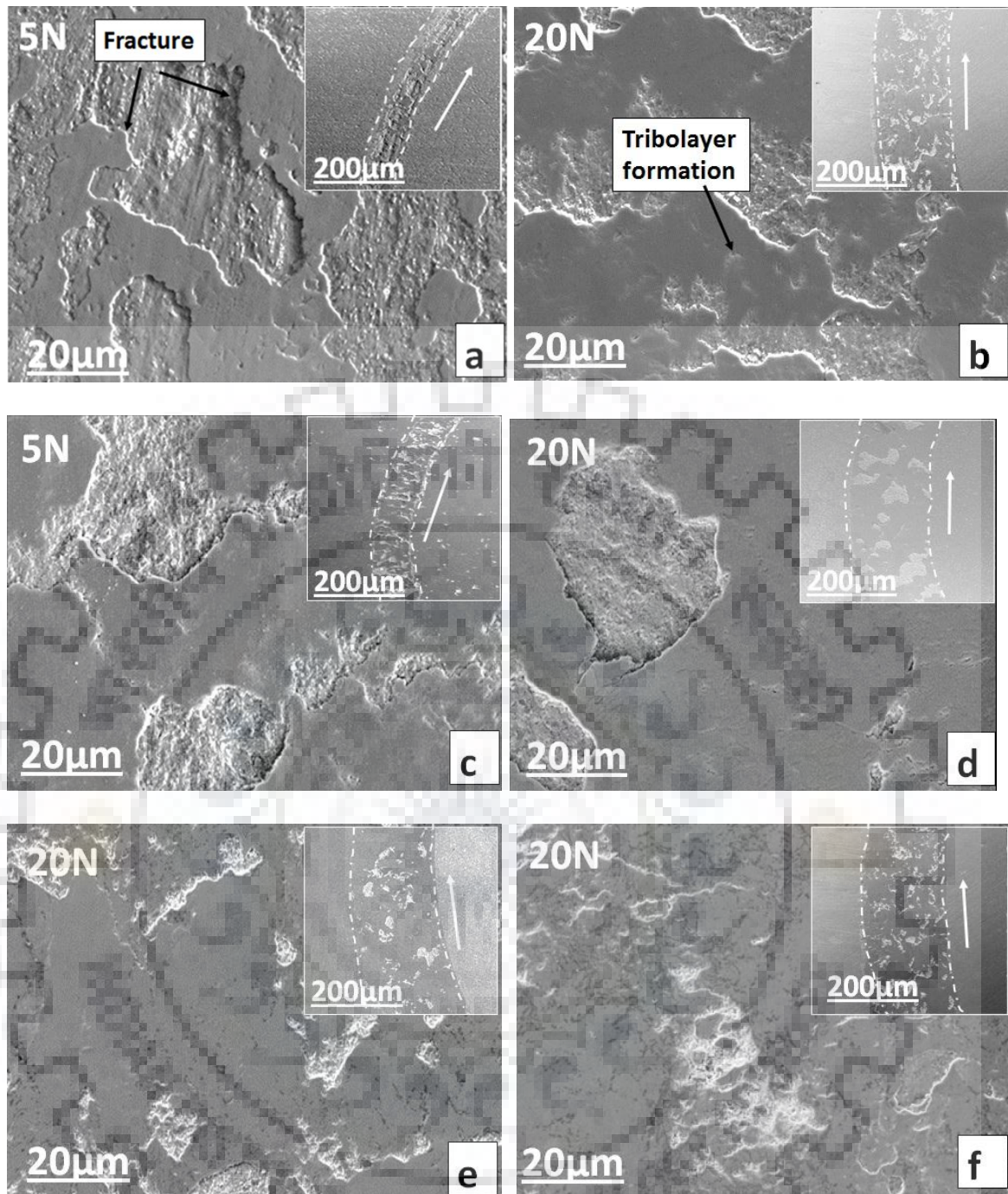
Figure 5-9 SEM images of worn cermets against cemented carbide balls: (a) Ti(CN)-5WC-20Ni at 5 N (b) Ti(CN)-5WC-20Ni at 20 N (c) Ti(CN)-5WC-20Ni-5TaC at 5 N (d) Ti(CN)-5WC-20Ni-5TaC at 20 N (e) Ti(CN)-5WC-10Ni-10Co at 20 N (f) Ti(CN)-5WC-10Ni-10Co-5TaC at 20 N load. Corresponding wear track images are shown in insets. The arrow indicating sliding direction in the inset also corresponds to the sliding direction in each primary figure.
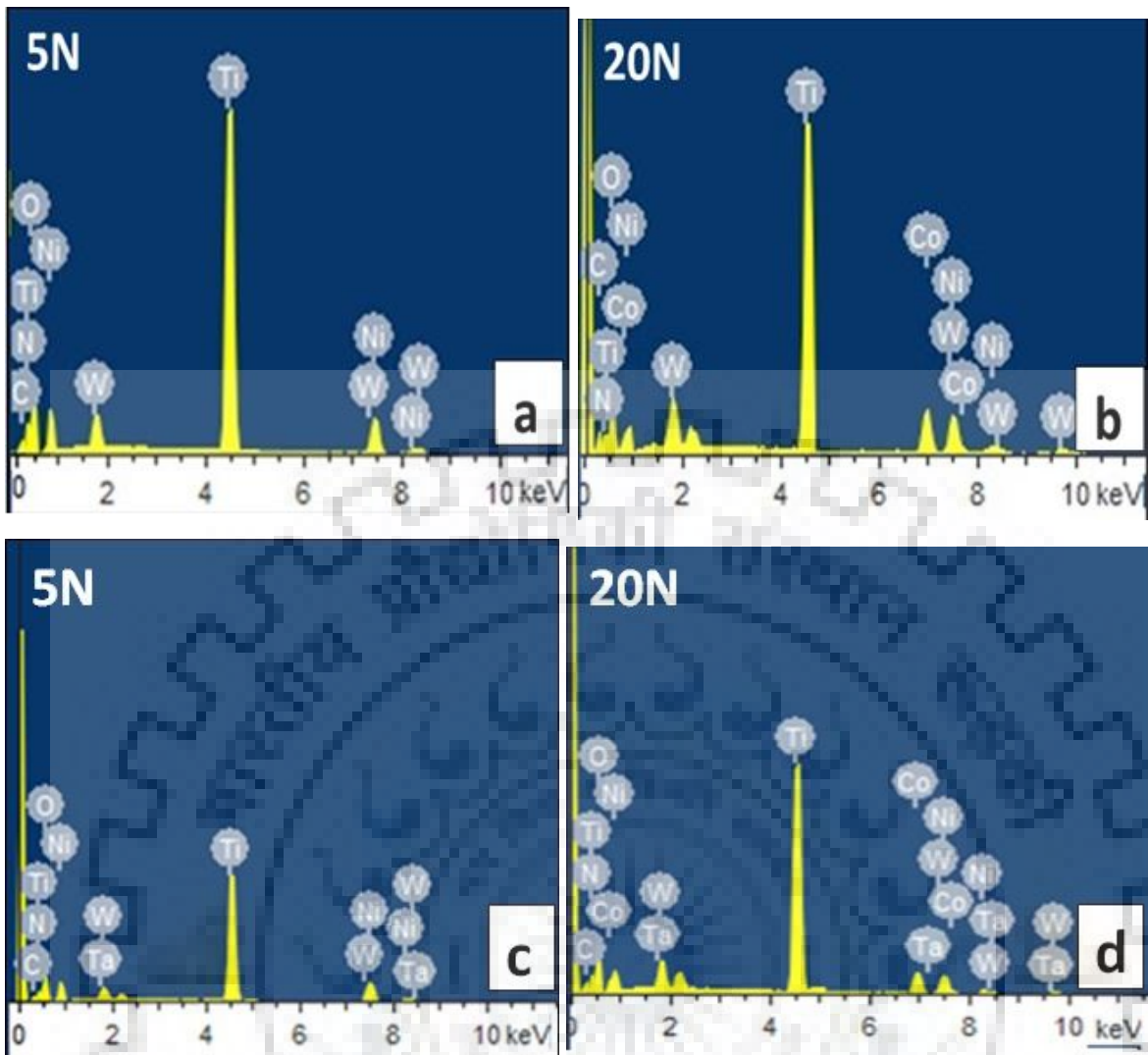
Figure 5-10   EDS analysis of tribolayer of Ti(CN) -5WC-20Ni cermets worn at 5N and 20N load (a,b). EDS analysis of tribolayer of Ti(CN)-5WC-20Ni-5TaC cermets worn at 5N and 20N load (c,d)

The wear scar of cemented carbide balls worn surface slid against Ti(CN)-5WC-10Ni-10Co-5TaC cermet at 5 N and 20 N is shown in **Figure 5-11 (a,b)**. Wear scar is almost circular in all the cases, whereas diameter increased with load. This is in contrast to the observation found against steel where the wear scar diameter decreased with increasing load. Presence of scratches indicates abrasion of balls by hard debris at the contact. Wear scar is accompanied with deep abrasion at 20 N load. EDS analysis obtained from the cemented carbide ball surface worn against Ti(CN)-5WC-10Ni-10Co-5TaC cermet at 20 N reveals the presence of W, Co, C, O and negligble presence of Ti (**Figure 5-11 (c)).** No layer on cemented ball surface is observed in the present study, as otherwise observed against steel. This can be attributed to the higher hardness of the counterbody used in the present study than steel.
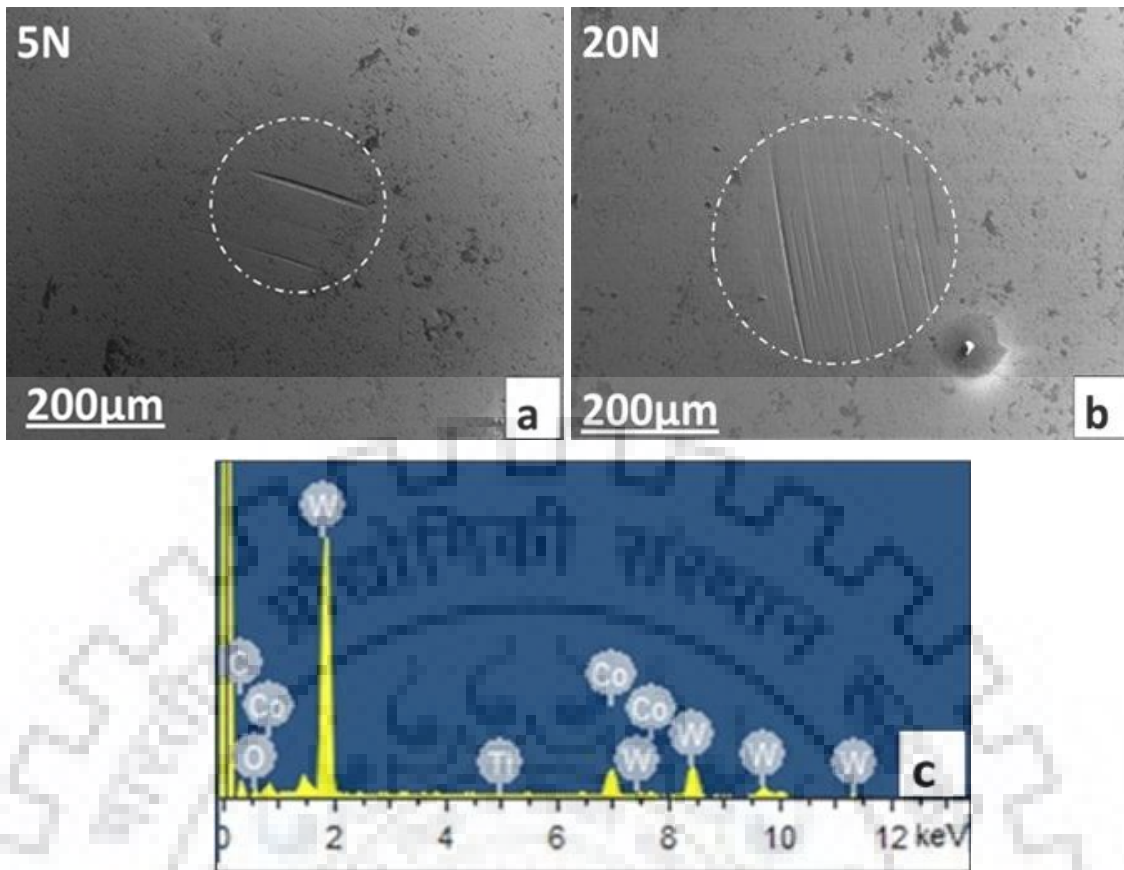
Figure 5-11 SEM images of cemented carbide balls worn surface slid against Ti(CN)-5WC-10Ni-10Co-5TaC cermet at 5 N and 20 N. EDS analysis of cemented carbide ball worn surface slid against Ti(CN)-5WC-10Ni-10Co-5TaC cermet at 20 N.

The influence of material and test parameters on the extent of material damage in sliding conditions can be realized. According to Evans and Marshall 1981, the wear in brittle material occurs by a lateral crack propagation which reaches to the surface. They showed that when sharp indenters slide over the brittle surface, the material removal occurs by the formation and propagation of lateral cracks. In this connection, the material removal can be quantified in terms of material parameters. The wear volume per unit sliding distance (V) of the interface can be considered as per the relation

$$V = \alpha \frac{P^{\frac{9}{8}}}{K_{Ic}^{\frac{1}{2}} H^{\frac{5}{8}}} \left(\frac{E}{H}\right)^{\frac{4}{3}} \tag{5.1}$$

where P is the normal load; K_{Ic}, E and H are the fracture toughness, elastic modulus and hardness of the brittle material, respectively; α is a material-independent constant.
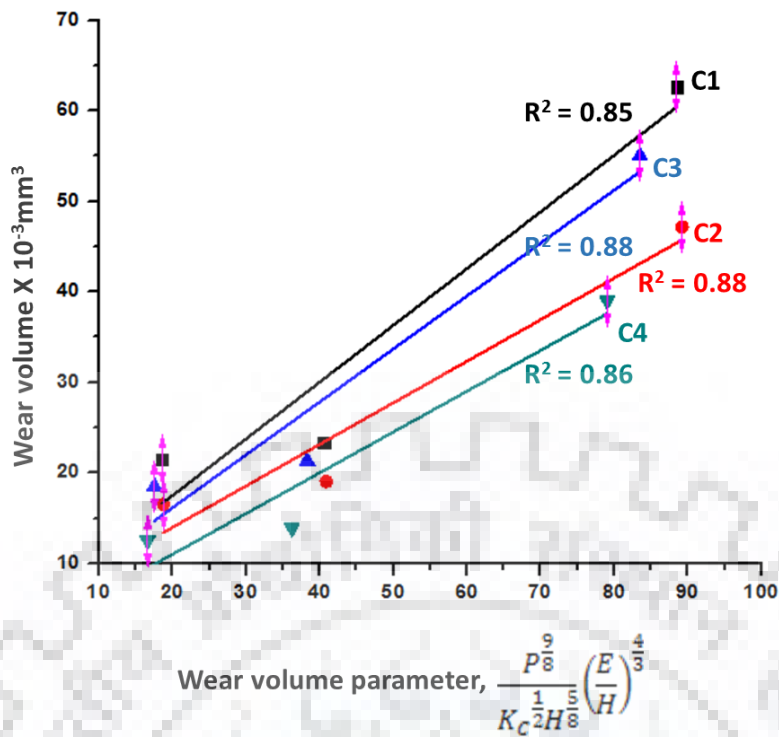
Figure 5-12. Analytically computed wear volume parameter vs. wear volume of conventionally sintered cermets against cemented carbide ball.

The wear volume parameter (calculated using the Evans and Marshall model) is plotted against experimentally measured wear volume of the conventionally sintered cermets worn against cemented carbide ball in **Figure 5-12.** The low coefficient of determination (R^2) in linear fit analysis indicates poor linear relation between the wear volume parameter and the experimentally measured wear volume for any cermet. This implies that the other wear mechanisms, (in addition to abrasion and cracking) also contributed to the removal of material with change in sliding test parameter (i.e. load) for the investigated cermets. Other part of the investigation, SEM-EDS analysis also shows change in dominant wear mechanism from abrasion and fracture to tribochemical layer removal with change in sliding load for all cermets (refer **Figure 5-9 and Figure 5-10).**

5.2.4 Wear debris evolution

In order to understand the relation between morphology of wear debris particles and tribological performance of the investigated Ti(CN) based cermets, debris particles from worn cermets surfaces were carefully collected and subjected to SEM-EDS analysis. Typical images of debris collected from Ti(CN)-5WC-20Ni and Ti(CN)-5WC-10Ni-10Co-5TaC cermets after sliding at 20 N load against cemented carbide balls are shown in **Figure 5-13 a-b.** Debris collected from worn cermet surface when slid against cemented

75

carbide average size of the wear debris between 0.1 and 0.3 µm. In general, collected debris particles generated from Ti(CN)-5WC-20Ni cermet are irregular in shape, as shown in **Figure 5-13 (a).** Debris generated for Ti(CN)-5WC-10Ni-10Co-5TaC is typically fine in size (**Figure 5-13 (b)).** EDS analysis of wear debris collected against cemented carbide ball shows the presence of Ti, W, C, N, Ni, Co and/or Ta. Presence of Co in EDS analysis for Ti(CN)-5WC-20Ni, Ti(CN)-5WC-20Ni-5TaC cermet debris particles is due to wear of counterbody cemented carbide ball. There is no such formation of oxide layer on worn scar of cemented carbide ball as noted in steel ball. In addition, the presence of oxygen indicates surface oxidation for cermet disc and/or ball. During sliding wear, initial Hertzian contact pressure deforms the binder phase comprising of Ni or Ni-Co and the applied load is carried by harder ceramic grains. Pirso et al. 2006, reported shifting of TiC ceramic grains underneath the surface that led to stress induced cracking and pull-out during sliding of TiC–Ni/Mo cermets against steel ball. The pulled-out grains tend to oxidize at the sliding contact. Accordingly, the worn surface of the cermets slid against cemented carbide is rich with hard oxides of tantalum or tungsten that result in high COF values.
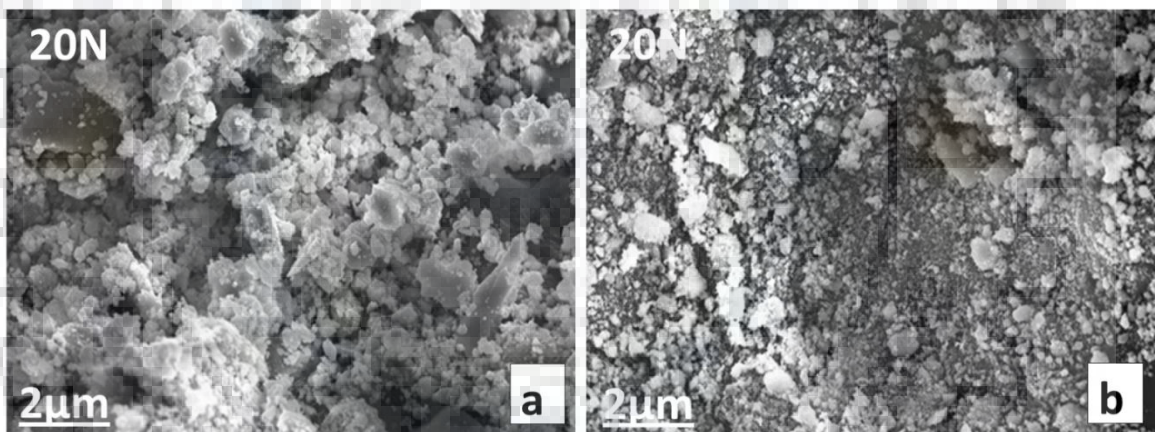
Figure 5-13 Typical SEM images of debris collected after sliding: (a) Ti(CN)-5WC-20Ni (b) Ti(CN)-5WC-10Ni-10Co-5TaC cermets against cemented carbide steel balls at 20 N load.

5.2.5 Contact temperature analysis

As it is now clear that oxides are present on the sliding surfaces because of the tribochemical reaction dominating at higher load, thermodynamic feasibility of these oxides products shall be discussed.

Contact temperature analysis is valid for the surfaces where a tribochemistry plays an important role and results in oxides of different elements from the cermet surface. The Gibbs free energy change (ΔG) for possible reactions as shown below, using commercial

software indicates that the change in (ΔG) of Ta_2O_5, WO_3, TiO_2 are negative, up to a very high temperature, as shown in **Figure 5-14**.

$$TiC + 2O_2 \text{ (g)} = TiO_2 + CO_2 \text{ (g)}$$

$$2TiN + 2O_2 \text{ (g)} = 2TiO_2 + N_2 \text{ (g)}$$

$$2TaC + 4.5O_2 \text{ (g)} = Ta_2O_5 + 2CO_2 \text{ (g)}$$

$$WC + 2.5O_2 = WO_3 + CO_2 \text{ (g)}$$
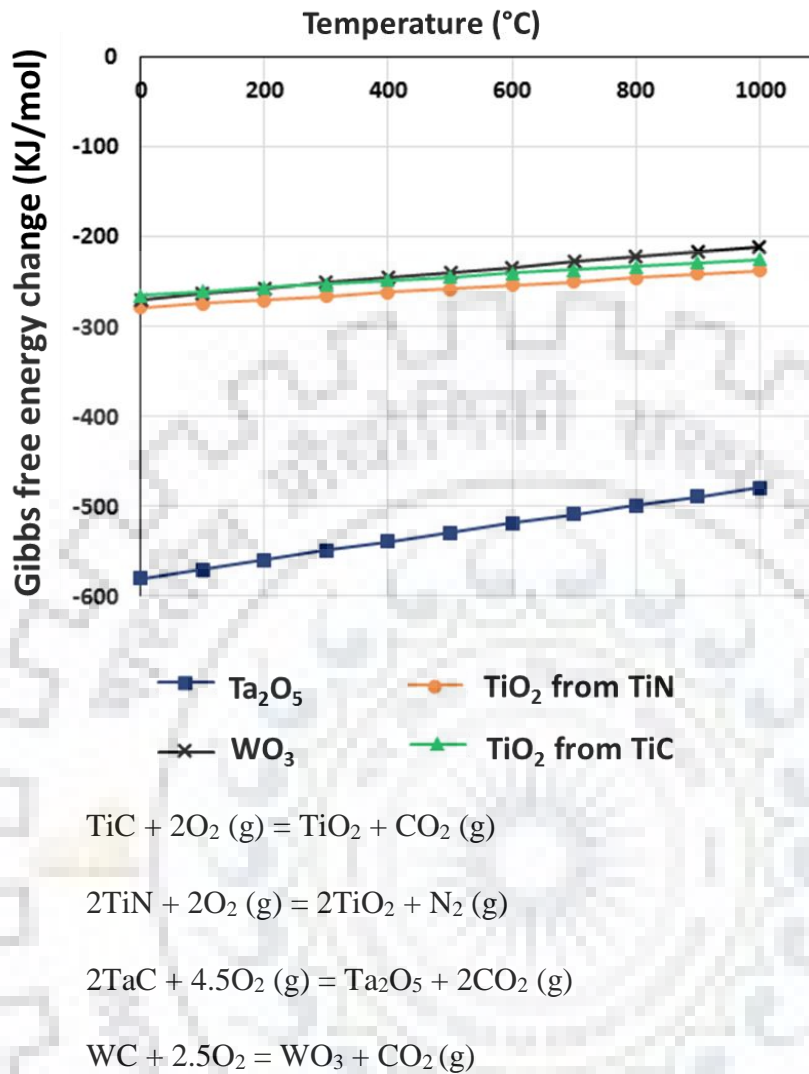
Figure 5-14. Gibbs free energy change (ΔG) for Ta_2O_5, TiO_2 and WO_3 as function of temperature.

During the sliding wear test conducted against cemented carbide ball for 40 min, rise in temperature is physically observed. The rise in contact temperature (ΔT_m) is estimated using the Archard's model (Archard, 1959; Archard and Rowntree, 1988) for the present sliding system as

$$\Delta T_m = \left\{ \frac{(\mu \, (\pi P_m)^{1/2}}{8K} \right\} * W^{1/2} v \tag{5.2}$$

where μ is the COF; P_m is the Hertzian contact stress at yield; W is the applied load; v is the sliding velocity; and k is the thermal conductivity of the cermet disc.

The maximum rise in contact temperature (ΔT_{max}) is calculated according to Archard and Rowntree, 1988 as,

$$\Delta T_{max} = 1.67 \, \Delta T_m \qquad\qquad (5.3)$$

The k of various cermet compositions was calculated by applying the rule of mixture. Values of maximum rise in contact temperature (ΔT_{max}) of Ti(CN) based cermets slid against varying load against harder cemented carbide ball are given in **Table 5-4**. ΔT_{max} is calculated in the range of 157-501°C for various cermets in the present case. It is observed that with increase in wear load maximum contact temperature is increased. It is reported that at high temperature, oxide layer depletes from the surface by wear (Kumar et al., 2008). Enhanced oxidation at high friction induced temperature results in high oxidation layer which do not retain on the surface and gets wear off from the surface. It is observed that cermet Ti(CN)-5WC-20Ni and Ti(CN)-5WC-10Ni-10Co cermet possess high wear. TaC behaves in a relatively ductile manner and deforms plastically before cracking (Rowcliffe and Warren, 1970). Among transition metal carbides, TaC is considered for the consistent mechanical behavior and it exhibits more plastic flow than any other carbide as its addition enhances the resistance to plastic deformation of (Ti,Ta,W)(CN)-Ni cermets [Rolander et al, 2001]. The potential toughness of TaC also yields stronger hard phase in cermet microstructure [Kiani et al., 2015; Rolander et al., 2001]. It attributes to the reason that Ti(CN)-5WC-20Ni-5TaC and Ti(CN)-5WC-10Ni-10Co-5TaC cermets having TaC addition retain oxide tribolayer and resulted in less wear.

Table 5-4. ΔT_{max} of Ti(CN) based cermets slid against varying load against harder cemented carbide ball

Cermet Composition	$\Delta \mathbf{T_{max}}$		
	5N	**10N**	**20N**
Ti(CN)-5WC-20Ni	263	341	501
Ti(CN)-5WC-20Ni-5TaC	231	296	385
Ti(CN)-5WC-10Ni-10Co	245	313	457
Ti(CN)-5WC-10Ni-10Co-5TaC	157	210	174

5.2.6 Friction and Ionic Potential

As per the crystal–chemical model, the frictional behavior can be correlated with the difference in ionic potential of the contacting compounds [Archard and Rowntree,

1988]. As noted in previous section, worn surfaces of investigated cermets are covered with oxide debris or layers consisting of oxides. For oxides with large difference in potential difference, cations are greatly protected by surrounding anions with poor bonding between cations in the system. Therefore, sliding interface with large difference in ionic potentials leads to poor adhesive interactions and less friction. During sliding of the investigated cermets against cemented carbide, oxides of titanium, tungsten, nickel, cobalt and/or tantalum are formed at the contact. Among the possible binary oxides, ionic potential difference for TiO_2-WO_3 combination is 3.0 and that of TiO_2-Ta_2O_5 combination is 4.4. As per the large difference in ionic potential for TiO_2-Ta_2O_5, sliding of the cermets containing TaC is easy with less friction. The steady state COF data for a given load (**Table 5-3**) is in accordance with this observation. The less friction at high load is attributed to the formation of layer, as explained in the previous section.

5.3 Effect of counterbody:

A comparative note on the effect of counterbody material on friction and wear behavior of the investigated Ti(CN) based cermets can be realized. Lower COF and wear rate are observed when Ti(CN) based cermets slid against steel. The difference in behavior can be related with the difference observed in microstructural features or mechanical properties of the investigated cermets, as explained in Chapter 4, section 4.3.3 and 4.4. However for a given load or the counterbody, it is observed that Ti(CN)-5WC-10Ni-10Co-5TaC (C4) cermet with refined size and least contiguity of ceramic phase exhibited highest hardness and higher indentation toughness and minimum wear, whereas Ti(CN)-5WC-20Ni cermet having longest mean free path of the binder phase exhibited maximum wear.

Further, one order magnitude difference between wear rates of cermet worn against steel and cemented carbide balls is observed. Wear rate of cermet is high when worn against cemented carbide. Difference in hardness of counterbody contributed to this behaviour. Cemented carbide ball has hardness of 17 GPa which is higher than the hardness of processed cermets, while steel ball has hardness of 7 GPa. Thus, the friction and wear characeristics of the investigated cermets are largely influenced by the hardness of the counterbody material.

A transition in wear mechanism occurred from fracture and grain pull-out at a low load of 5 N to the removal of tribochemical layer at a high load of 20 N when cermets were worn against steel. When worn against cemented carbide, characteristic grain pull-out and fracture of adhered material attributed to higher COF and wear at low load (5 N) while formation of continuous and adherent layer led to the reduction in friction and wear at high

load (20 N). Hard oxide debris particles were also responsible for high COF and wear rate against cemented carbide at 5 N. The maximum extent of transfer of oxides from balls results in the formation of a continuous and strongly adherent tribochemical layer on the Ti(CN)-5WC-10Ni-10Co-5TaC cermet surface.

There is a contrast in the wear scars of steel and cemented carbide balls. Typical SEM images of steel ball revealed that the wear scar size reduced at high load, whereas wear scar diameter on cemented carbide increased with load. Also, thin layers are found on the periphery of steel balls at high load, while no such layer observed in case of cemented carbide balls. Presence of scratches indicates abrasion of balls by hard debris at the contact. Debris collected from worn cermet surfaces slid against steel are larger in size than that obtained from surfaces slid against cemented carbide.

5.4 Effects of the microstructure and properties on the wear behavior of TiCN based cermets:

The present study necessarily indicates that the tribological characteristics of Ti(CN) based cermets are influenced by the microstructure and properties of TiCN based cermets. The SEM micrograph of the sintered cermets revealed the least carbide size of the Ti(CN)-5WC-10Ni-10Co-5TaC cermets and among all the four investigated cermets, Ti(CN)-5WC-10Ni-10Co-5TaC (C4) has the highest hardness of 16 GPa and indentation toughness of 9.25 MPa m$^{1/2}$. It is observed that the addition of TaC in Ti(CN)-WC-Ni/Co led to the minimum wear of the cermet and wear of counter ball slid against the least worn cermet is the maximum. During sliding, the deformation or removal of binder phase followed by the fracture of carbides. Ti(CN)-5WC-10Ni-10Co-5TaC cermet worn at high load reveals that the wear track is completely covered with a dense, continuous and strongly adhered layer. High hardness in C4 results in restricted deformation or removal of binder phase, while increased indentation toughness can be attributed to the limited fracture of carbides. Accordingly, the wear occurred for C4 cermet is the least.

5.5 Summary

The effect of TaC addition on tribological behaviour of sintered cermets against steel and cemented carbide counterbodies in unlubricated sliding conditions was investigated using a ball-on-disc wear tester at 5, 10 or 20 N. The following are major conclusions:

(a) Against steel, with change in sliding load from 5 to 20N, the coefficient of friction varied between 0.3 and 1.0 and the wear rate changed from 3×10^{-7} to 7×10^{-7} mm^3/Nm for the investigated cermets. The wear rate of steel balls varied from $7 \times$

10^{-5} mm^3/Nm to 3×10^{-4} mm^3/Nm. One order magnitude higher wear rate of cermet worn is observed against steel compared against cemented carbide balls.

(b) Against cemented carbide the steady state coefficient of friction (COF) varied from 0.25 to 1.17, and wear rate changes from 2.21×10^{-6} to 7.34×10^{-6} mm^3/Nm. Hard oxide debris particles were also responsible for high COF and wear rate against cemented carbide at low load. Against both counter bodies, the composition constituting of TaC and Co-Ni binder phase stabilized COF and reduced wear in the selected sliding conditions. The Ti(CN)-5WC-10Ni-10Co-5TaC cermet with maximum hardness, maximum indentation toughness exhibited minimum friction and wear.

(c) During sliding, the deformation or removal of binder phase followed by the fracture or pull-out of carbides. High hardness in Ti(CN)-5WC-10Ni-10Co-5TaC resulted in restricted deformation or removal of binder phase, while increased indentation toughness can be attributed to the limited fracture of carbides. Accordingly, the wear occurred for Ti(CN)-5WC-10Ni-10Co-5TaC cermet is the least against both steel and cemented carbide balls.

(d) Against steel, a transition in dominant wear mechanism occurred from fracture and grain pull-out at a low load in Ti(CN)-5WC-10Ni cermet to the removal of tribochemical layer at a high load in Ti(CN)-5WC-10Ni-10Co-5TaC cermet. Maximum extent of transfer of iron oxide from steel ball resulted in the formation of a continuous and strongly adherent tribochemical layer on the Ti(CN)-5WC-10Ni-10Co-5TaC cermet surface which resisted the wear and helps in pertaining layer remain attached.

(e) Against cemented carbide, the worn surface of the Ti(CN)-5WC-20Ni cermet worn at low load revealed grain pull-out and adhered layer, similar to that observed against steel ball. However, the layer formed against cemented carbide is thick and covers the worn surface. Ti(CN)-5WC-20Ni-5TaC cermet shows that wear track is completely covered with a dense, continuous and strongly adhered layer at high load.

(f) When sliding against cemented carbide, high contact temperature caused depletion of tribolayer from the surface and resulted in high wear. Contact temperature analysis at 20 N load indicated maximum contact temperature of 501°C for Ti(CN)-5WC-10Ni cermet and 174°C for Ti(CN)-5WC-10Ni-10Co-5TaC cermet. Large difference between ionic potentials of possible oxides during sliding against

81

cemented carbide at the contact resulted in less friction for the TaC added Ti(CN)-WC-Ni/Co cermets.

(g) The present study necessarily indicates that the tribological characteristics of Ti(CN) based cermets are influenced by both the compositions and as well as the sliding test parameters. The investigated cermets are worn to the maximum extent against hard cemented carbide ball and low load of 5 N, while Ti(CN)-5WC-10Ni-10Co-5TaC cermet exhibited superior wear resistance at a given load against any counterbody.

Tribological behavior of Spark plasma sintered cermets against silicon carbide ball

---

The salient observations on friction and wear properties of Spark plasma sintered Ti(CN) based cermets against hard silicon carbide ball as counterbody are discussed in this chapter.

6.1 Frictional behavior

A typical COF plot as a function of time is shown for the Ti(CN)-5WC-10Ni-10Co-5TaC, cermet in **Figure 6-1** and the average steady state COF values for the investigated cermets are shown as function of sliding load in **Figure 6-2.** The average steady state COF varied from 0. 3 to 1.1 with change in cermet composition and sliding load. Sliding against silicon carbide ball results in the formation of rough surface of contact which increases friction. Lower COF values from 0.2 to 0.8 are reported for the Ti(CN)-based cermets when slid against steel ball by previous investigators with varying cermet compositions and sliding conditions [Rigney, 1984; Arenas et al., 2003; Engqvist et al., 2000; Pirso et al., 2004a & 2004b; Meng et al. 2006; Östberg et al. 2006; Kumar et al., 2007; Kiani et al., 2015]. A drop in COF is observed when the applied sliding load is increased from 5 to 20 N for any cermet. At a given load, Ti(CN)-5WC-20Ni, cermet exhibited high COF values and Ti(CN)-5WC-10Ni-10Co-5TaC showed low COF values. Thus, the frictional behavior of the investigated cermets indicates strong influence of the addition of TaC in the cermet composition and load. Among these cermets containing TaC and Co-Ni binder phase is beneficial in reducing the friction in the selected sliding conditions.
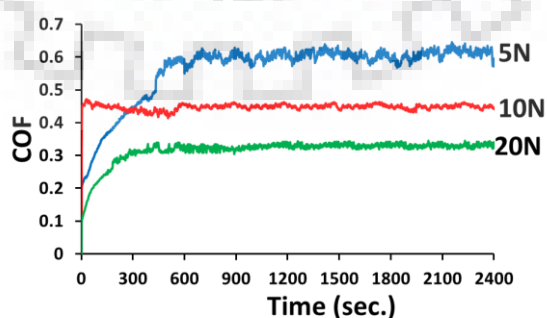
Figure 6-1: Coefficient of friction vs time for Ti(CN)-5WC-10Ni-10Co-5TaC cermet worn against silicon carbide ball at different loads
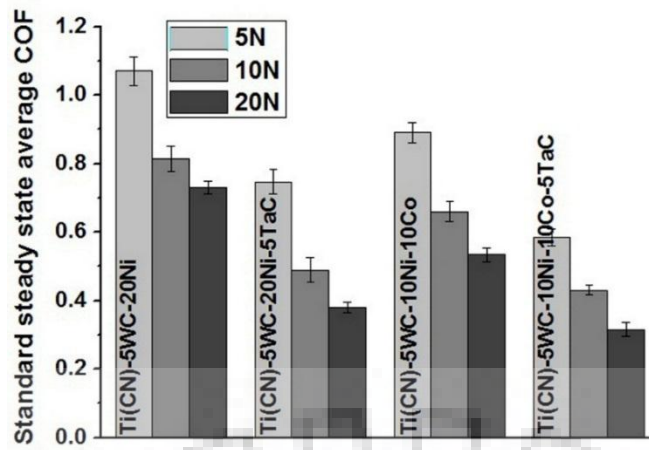
Figure 6-2: Average steady state coefficient of friction (COF) values of cermets as a function of composition and load.

6.2 Wear behavior

Wear rate of the investigated cermets slid against SiC ball varied from 4.7×10^{-7} mm^3/Nm to 2.2×10^{-6}. The Ti(CN)-5WC-20Ni cermet possess highest wear rate at a load of 5N, and the least wear rate is noted for Ti(CN)-5WC-10Ni-10Co-5TaC at a load of 10 N. Wear rates from 10^{-7} mm^3/Nm to 10^{-6} mm^3/Nm are reported for the Ti(CN)-based cermets by previous investigators (Rigney, 1984; Arenas et al., 2003; Engqvist et al., 2000; Pirso et al., 2004a & 2004b; Meng et al. 2006; Östberg et al. 2006; Kumar et al., 2007; Kiani et al., 2015). Wear rate of silicon carbide ball slid against investigated cermets varied from 0.4×10^{-6} to 1.4×10^{-6}. It is to note that the wear of ball slid against the least worn cermet is the maximum, whereas the wear of ball slid against the most worn cermet is the minimum. Specific wear rate as a function of load of investigated Ti(CN)-based cermets and silicon carbide balls are shown in **Figure 6-3.**
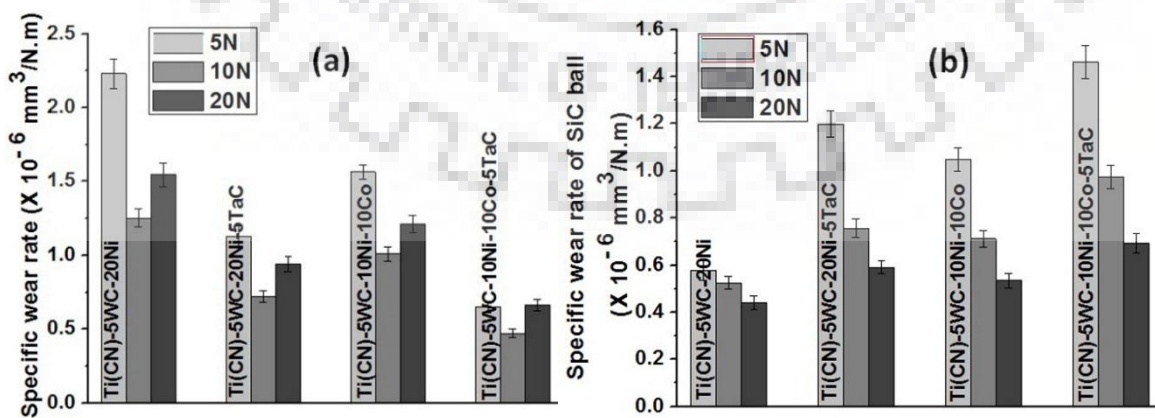
Figure 6-3: Wear rate of (a) cermets and (b) silicon carbide ball as function of composition and load.

84

6.3 SEM - EDS analysis of worn surfaces

Depending on the given sliding conditions, the dominant mechanisms involved in the wear process are studied. Representative SEM images of worn surfaces of investigated cermets are shown in **Figure 6-4 (a-h)**. The SEM image of C1 cermet of baseline Ti(CN)-5WC-20Ni composition worn at 5 N reveals severe wear with characteristic abrasion and grain pullout **(Figure 6-4 a)**. At 20 N load, the worn surface is significantly covered with a tribolayer **(Figure 6-4 b)**. The material is removed via microcracking of the layer. With the addition of TaC in baseline composition, the C2 cermet worn surface reveals the presence of a tribolayer at 5 N load **(Figure 6-4 c)**, as compared to C1 cermet. Tribolayer becomes dense on the worn surface at 20N **(Figure 6-4 d)**. Worn surface of Ti(CN)-5WC-10Ni-10Co (C3 cermet) reveals the formation of distinct tribolayer. However, cracking and grain pullout indicates easy removal of the layer and less protection from further wear at 5 N load **(Figure 6-4 e)**. Tribolayer is severely spalled at higher load of 20 N **(Figure 6-4 f)**. The worn surface of C4 cermet with Ti(CN)-5WC-10Ni-10Co-5TaC composition at 5N load shows thin and discontinues tribolayer which became thick, continuous, and strongly adhered at 20 N load **(Figure 6-4 g and h))**. Thus, the addition of Co and TaC in the baseline Ti(CN)-WC-Ni cermet composition resulted in the strongly adhered tribocontact. The presence of such layer in the tribocontact at high load decreases the friction between cermet and SiC ball. The data shown in **Figure 6-2** also reveals a decrease in COF with the load. Among transition metal carbides, TaC is considered for the consistent mechanical behavior and superior resistance against crack propagation. Resistance to crack propagation increases due to addition of TaC as it behaves plastically deformable before breaking, so relatively the toughness is increased (Rowcliffe and Warren, 1970; Rowcliffe and Hollox, 1971; Rolander et al., 2001). Thus, Ti(CN)-5WC-20Ni-5TaC and Ti(CN)-5WC-10Ni-10Co-5TaC cermets having TaC addition retain tribolayer in the selected sliding conditions and exhibit decrease in COF or wear.
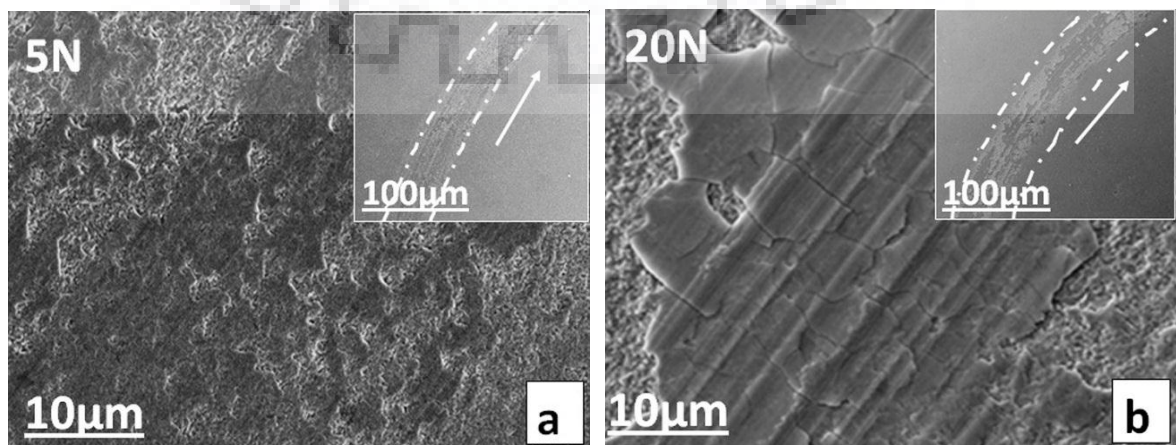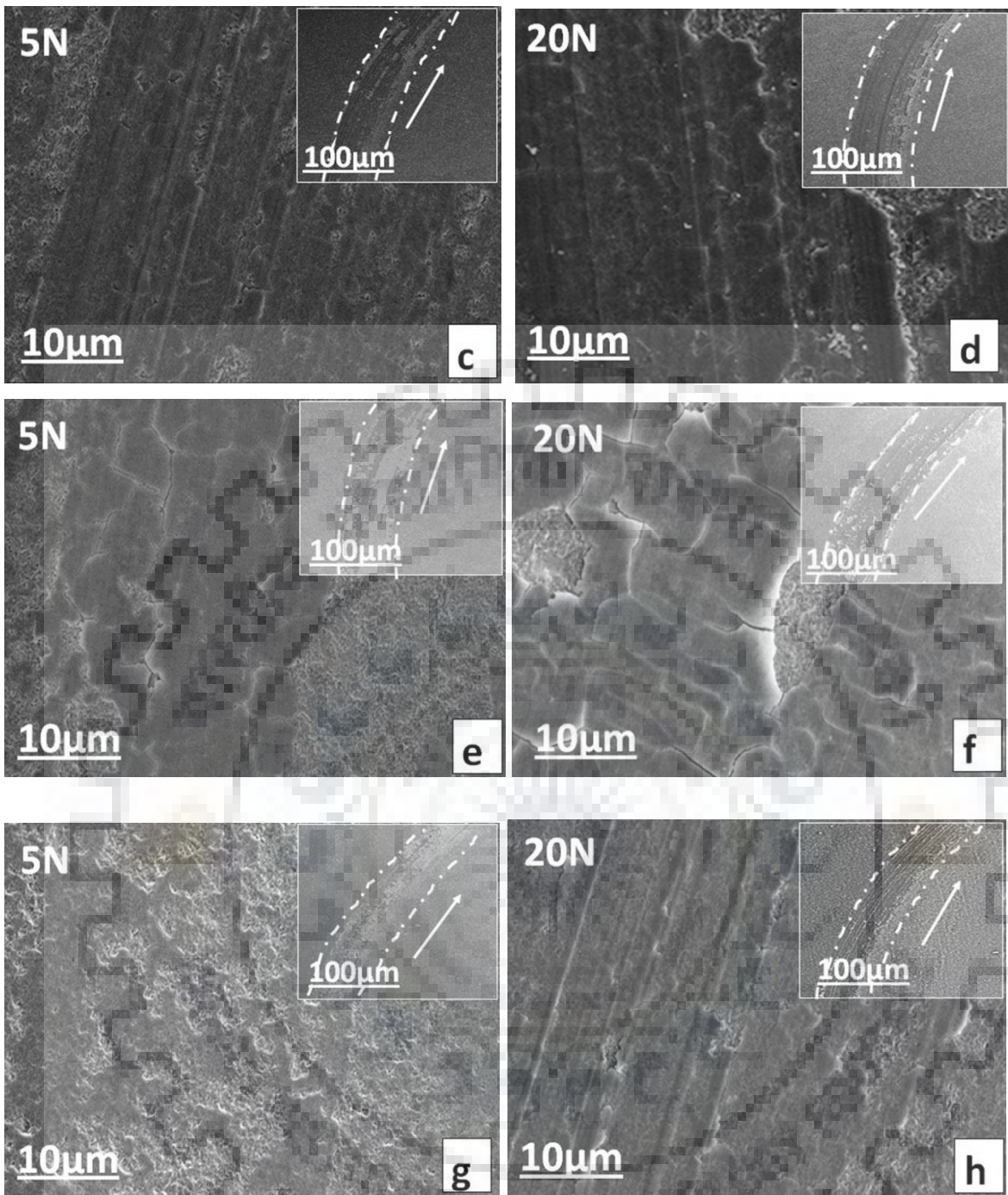
Figure 6-4: SEM images of (a) Ti(CN)-5WC-20Ni cermet worn at 5 N (b) Ti(CN)-5WC-20Ni cermet worn at 20 N (c) Ti(CN)-5WC-20Ni-5TaC cermet worn at 5 N (d) Ti(CN)-5WC-20Ni-5TaC cermet worn at 20 N (e) Ti(CN)-5WC-10Ni-10Co cermet worn at 5 N (f) Ti(CN)-5WC-10Ni-10Co cermet worn at 20 N (g) Ti(CN)-5WC-10Ni-10Co-5TaC cermet worn at 5 N and (h) Ti(CN)-5WC-10Ni-10Co-5TaC cermet worn at 20 N load. Corresponding wear track images are shown in insets. The arrow indicating sliding direction in the inset also corresponds to the sliding direction in each primary figure.

It is clear that the fracture, grain pull-out and microcracks is dominated by the formation and adherence of a layer on the surface with change in sliding load or cermet composition. In order to understand the chemistry of the layered surfaces, EDS studies are conducted for the worn surfaes of investigated cermet and ball. The EDS analysis of the worn surfaes at loads of 5, 10 and 20N is shown as insets in **Figure 6-5 (a-d).** In general, EDS analysis shows the presence of elements from cermet surfaces i.e. Ti, W, C, N, Ni, Co and/or Ta and from ball surface i.e. Si and C. In addtion, the presence of oxygen indicates that the layer consist of oxides.

SEM - EDS study is carried out for the worn ball surfaces to understand the wear mechanism and possibility of material transfer onto the counterbody. The wear scar of silicon carbide balls worn surface slid against Ti(CN)-5WC-10Ni-10Co-5TaC cermet at 5 N and 20 N is shown in **Figure 6-6**. Wear scar is almost circular in all the cases; diameter increased with load. Presence of scratches and abrasion during sliding wear developed at ball surfaces. Wear scar is accompanied with deep abrasion at 20 N load.
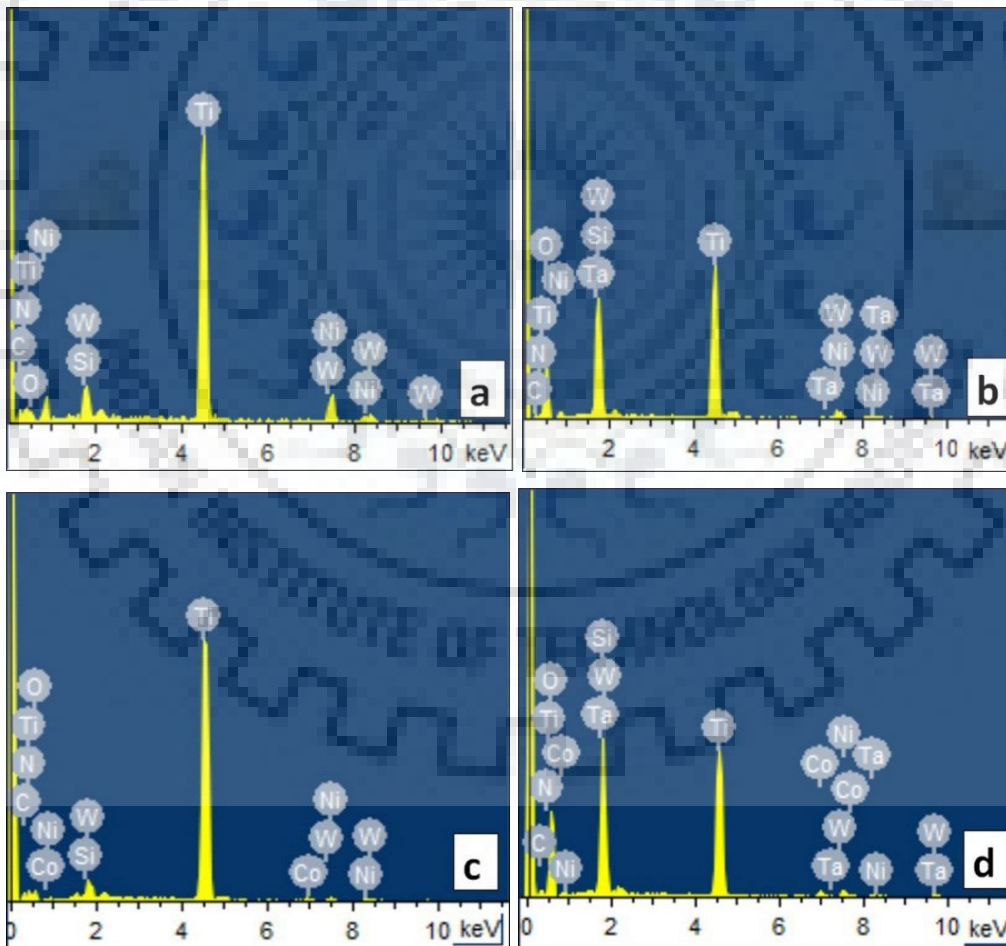
Figure 6-5: EDS analysis of (a) Ti(CN) -5WC-20Ni, (b) Ti(CN)-5WC-20Ni-5TaC, (c) Ti(CN) -5WC-10Ni-10Co and (d) Ti(CN)-5WC-10Ni-10Co-5TaC cermets worn at 20N load
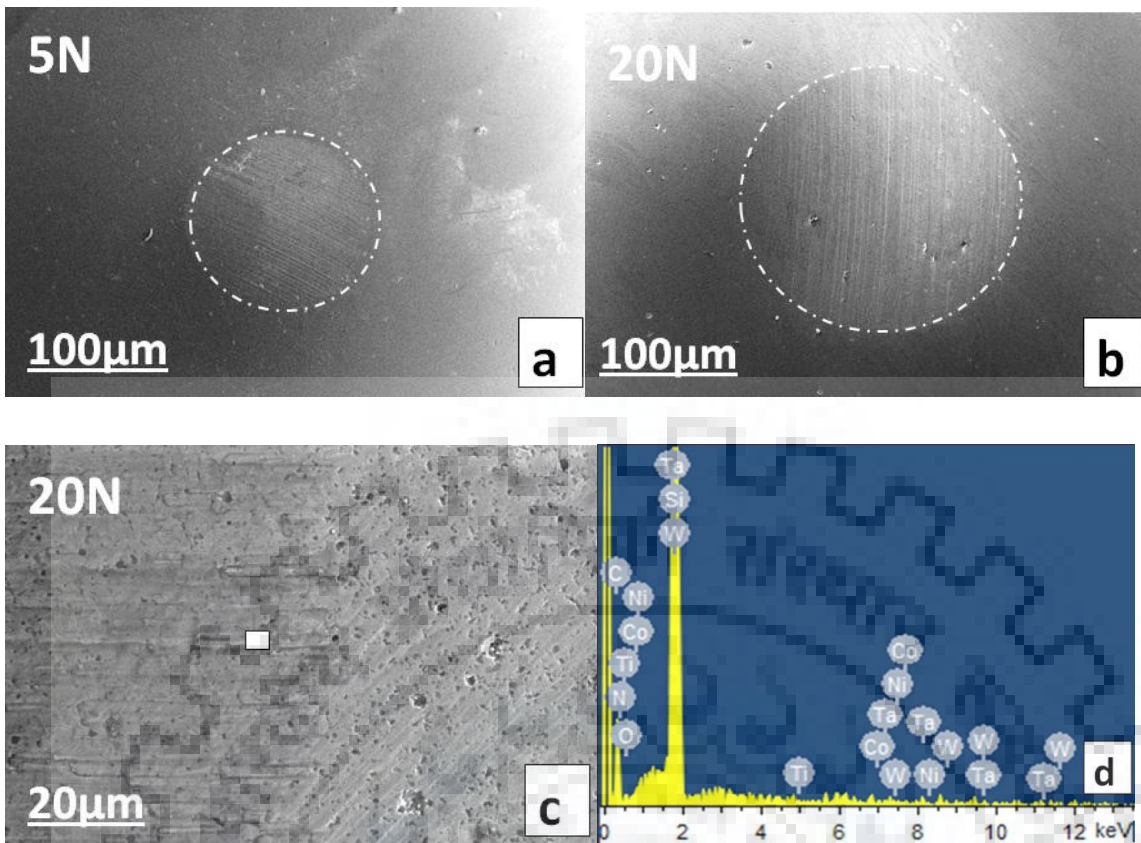
Figure 6-6: SEM – EDS images of silicon carbide balls worn surface slid against Ti(CN)-5WC-10Ni-10Co-5TaC cermet at 5 N and 20 N.

In order to understand the influence of mechanical properties, the experimentally measured wear volume of the spark plasma sintered cermets worn against SiC ball are plotted against the wear volume parameter (calculated using the Evans and Marshall, 1981) in **Figure 6-7.** As explained in section 5.2.3, the low coefficient of determination (R^2) indicates the domination of multiple wear mechanism, in addition to abrasion or fracture. Referring to **Figure 6-4 and Figure 6-5,** the dominant wear mechanisms changes from abrasion or fracture at low loads to tribochemical layer removal at high loads for all cermets.
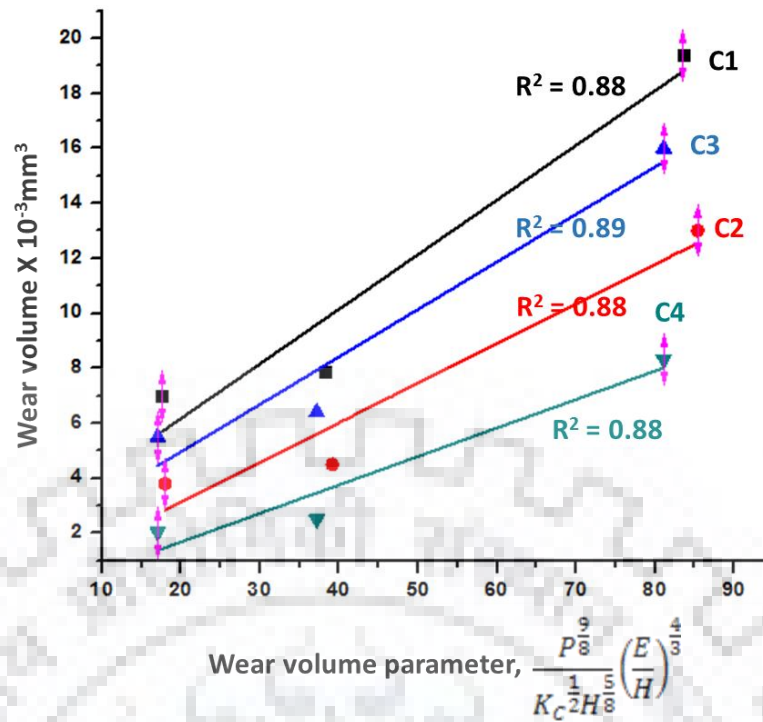
Figure 6-7. Analytically computed wear volume parameter vs. wear volume of spark plasma sintered cermets against silicon carbide ball.

6.4 Wear debris analysis

In order to understand the relation between morphology of wear debris particles and tribological performance of the investigated Ti(CN) based cermets slid against silicon carbide ball at 20 N load, debris particles from worn cermets surfaces are carefully collected and subjected to SEM-EDS analysis **(Figure 6-8 (a,b,c))**. Size of the debris particles is measured by image analysis and results are obtained from 150-180 readings from images of collected debris of each cermet composition. SEM images of wear debris collected from worn Ti(CN)-5WC-20Ni Cermets shows irregular sized particles **Figure 6-8 (a)** whereas SEM images of wear debris collected from worn Ti(CN)-5WC-10Ni-10Co-5TaC Cermets shows refined sized particles **Figure 6-8 (b)**. SEM images of sintered Ti(CN)-5WC-10Ni-10Co-5TaC cermet shows refined crystallite size so the debris formation during sliding is also refined. Debris particles are crushed at high load. The average size of the wear debris for C1, C2, C3, C4 compositions are 1.0, 0.6, 0.8, 0.6 μm, respectively. A maximum wear debris particle size of 1.0 μm is found for Ti(CN)-5WC-20Ni cermet which is for maximum wear at 20 N load. Least wear debris particle size of 0.565 μm is found for Ti(CN)-5WC-10Ni-10Co-5TaC cermet. EDS analysis of debris collected from worn surface of Ti(CN)-5WC-20Ni cermet is shown in **Figure 6-8 (c)**. EDS analysis of wear debris of Ti(CN)-5WC-20Ni cermet cofirms the presence of following

elements i.e. Ti, W, C, N and Ni, presence of Si is due to wear of SiC ball. In addition, the presence of oxygen along with these elements observed in EDS analysis of debris particles indicates oxidation at the contact surface of cermet disc and ball. Sliding wear of Ti(CN) based cermets against harder silicon carbide ball results in wear of material in form of debris. Moreover, sliding in ambient conditions of temperature and humidity also favors formation of oxides leading to hard debris formation.
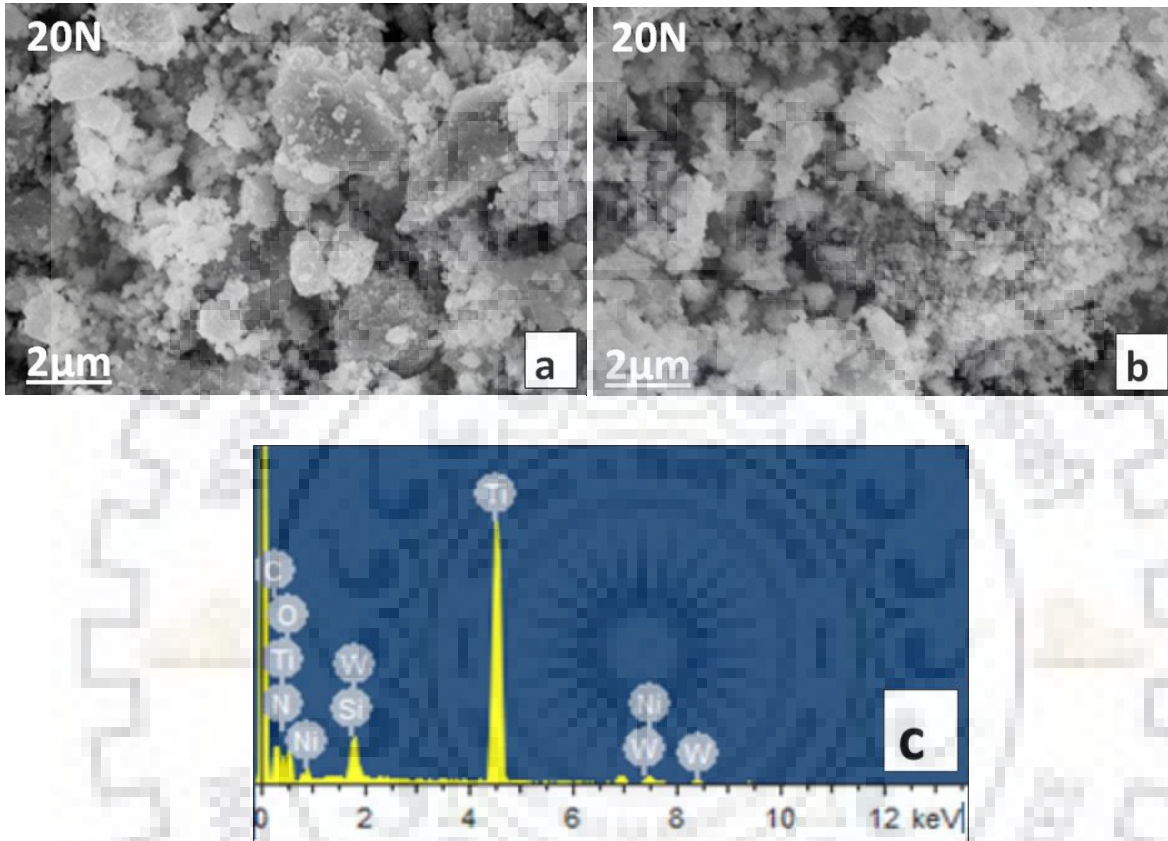
Figure 6-8: Typical SEM images of debris collected after sliding at 20 N load against silicon carbide ball (a) Ti(CN)-5WC-20Ni (b) Ti(CN)-5WC-10Ni-10Co-5TaC Cermets. (c) Point EDS analysis of debris collected from worn surface of Ti(CN)-5WC-20Ni cermet.

6.5 Summary

The friction and wear characteristics of sintered cermets are studied against hard counterbody SiC ball in dry sliding conditions. Present study was conducted to explore the potential of new cermet material in severe wear conditions against hard material in context of dry machining conditions. Following are the major conclusions:

1. With change in sliding load from 5 to 20N, the coefficient of friction varied between 0.3 to 1.1 and wear rate of cermets varied from 4.7×10^{-7} mm^3/Nm to 2.2×10^{-6} mm^3/Nm and of worn SiC ball from 0.4×10^{-6} mm^3/Nm to 1.4×10^{-6}

mm^3/Nm. The Ti(CN)-5WC-10Ni-10Co-5TaC cermet exhibits minimum COF and minimum wear rate at a high sliding load of 20 N.

2. It is observed that the worn surfaces of the investigated cermets are generally characterized by microcracking, tribolayer formation and spalling when slid against SiC ball. The Ti (CN)-5WC-10Ni-10Co-5TaC cermet exhibits worn surface covered with a thick, continuous and strongly adhered tribolayer.

3. Debris collected after the wear testing are irregular for Ti(CN)-5WC-20Ni and refined for Ti (CN)-5WC-10Ni-10Co-5TaC cermet.

Chapter-7

Machining studies of Ti(CN) based cermet tools

This chapter deals with the study of cutting forces and dominant crater wear mechanisms responsible for material removed from the cutting edge of Ti(CN) based cermet tools during machining of 304 stainless steel.

Consistent performance of tools is essential to meet the requirements of modern machining process. For efficient performance, cutting tool needs to have certain characteristics: hardness and strength of the cutting tool must be maintained at elevated temperatures; high toughness of cutting tool is needed so that tools do not chip or fracture especially during interrupted cutting operations; wear resistance is required for attaining acceptable tool life. In recent years, Ti(CN) based cermets are considered for cutting tool applications because of the combination of high hardness, improved toughness, superior wear resistance and thermal shock resistance, chemical stability at high temperatures and superior surface finish [Zhang, 1993; Ettmayer et al., 1995; Ahn and Kang, 2001]. Ti(CN) based cermets consist of hard Ti(CN) grains bonded by metallic binder phase (normally Ni or Co) formed during liquid phase sintering at high temperatures. The ceramic phase gives wear resistance, while toughness is contributed by the binder phase [Zhang, 1993; Watanabe et al., 1996; D' Errico et al., 1997; Pastor, 1998; Zhang, 1998].

The improvement in machining performance is possible by designing novel compositions of Ti(CN) based cermets and understanding dominant wear mechanisms. The principal aim of the present investigation is to explain the dominant crater wear mechanisms responsible for material removed from the cutting edge while machining. Ti(CN)-5wt.%WC-20wt.%Ni and Ti(CN)-5wt.%WC-10wt.%Ni-10wt.%Co-5wt.%TaC cermets were subjected to dry turning at 133 rpm for 180 sec or 435 rpm for 60 sec spindle speed against stainless steel rod of initial diameter (d_i) – 24.9 mm. Turning operations were performed 3-5 times at 0.5 mm/rev feed rate and 0.9 mm depth of cut. Cutting force was studied as function of cermet composition, processing type and cutting speed. Dominant mechanisms of material removal from rake face of the tools are elucidated. Results are compared with performance of commercially available cemented carbide tip. In the given conditions of machining, material removal rate (MRR) is found to vary by one order i.e from 1.5 x 10^{-5} m^3/min to

4.6 x 10^{-6} m^3/min. Material removal rate calculated by the following equation [Singh et al., 2016]:

MRR= $\pi D_{avg} dfN$ (7.1)

$D_{avg} = (D_o + D_i)/2$ (mm)

D_i, D_o are initial and final diameters of the steel rod

d= depth of cut (mm)

f=feed (mm/rev)

N=spindle speed (rpm)

7.1 Cutting force

Table 7-1 shows average of cutting force evolved during orthogonal cutting of the 304 stainless steel workpiece for the investigated cermets in selected machining operations. Higher cutting force evolved at lower speed (133 rpm) and as cutting speed increases (435 rpm) generated cutting force decreased. The effect of cermet processing and composition on cutting force is significant at high speed (435 rpm). Spark plasma sintered cermets exhibited less cutting force at high speed.

It is observed that at lower speed, cutting edge of the tool tends to plough into workpiece surface and as the cutting speed increases, cutting becomes steady with a consequent reduction in the cutting force. At 133 rpm, higher cutting forces of 1270 N and 1250 N are obtained during turning of commercial carbide tip and conventionally sintered Ti(CN)-5WC-20Ni cermet tools, whereas lowest cutting force of 1210 N evolved during turning for Spark plasma sintered Ti(CN)-10Ni-10Co-5WC-5TaC cermet (**Table 7-1**). Compared to the cutting forces at 135 rpm less cutting forces are evolved at 435 rpm. At 435 rpm, higher cutting forces of 1065 N and 1060 N evolved during turning for commercial carbide tip and conventionally sintered Ti(CN)-5WC-20Ni cermet whereas lowest cutting forces of 990 N is evolved during turning for Spark plasma sintered Ti(CN)-10Ni-10Co-5WC-5TaC cermet (**Table 7-1**).

Table 7-1: Turning parameters and generation of cutting force at 0.9 mm depth of cut and 0.5 mm/rev feed rate

Cermet	Processing technique	Stainless steel rod (304 Grade) (initial diameter, d_i - 24.9 mm; final diameter, d_f - 24 mm)	
		F_c, N at 133 rpm for 180 sec	F_c, N at 435 rpm for 60 sec
Ti(CN)-20Ni-5WC	Conventional	1250±15	1060±10
Ti(CN)-10Ni-10Co-5WC-5TaC		1220±10	1020±5
Ti(CN)-20Ni-5WC	SPS	1245±15	1040±10
Ti(CN)-10Ni-10Co-5WC-5TaC		1210±10	990±5
Commercial carbide tip	Not known	1270±15	1065±10

7.2 Crater wear mechanisms

After turning at 133 and 435 rpm, worn tool edges were examined using scanning electron microscope and typical images of worn rake surfaces are shown in **Figures 7-1 (a-h)**. Detailed analysis with respect to dominant wear mechanisms is given in **Table 7-1**. The process of material removal during machining is complicated with simultaneous occurrence of various mechanisms. The worn tool surface of conventionally sintered Ti(CN)-5WC-20Ni cermet shows cracks, grain pullout and fracture **(Figure 7-1 (a))** at 133 rpm and the intensity of crack, grain pullout, and fracture increased at 435 rpm **(Figure 7-1 (b)).** During machining, hard asperities or wear particles act as sharp indenters and generate cracks, which on further propagation and intersection lead to grain pull-outs on the cermet tool surface. Friction induced heat at the nose tip is also high at high speed. Thermal cracking is therefore highly possible at high speeds. Worn tool surface of Spark plasma sintered Ti(CN)-5WC-20Ni cermet show abrasive tracks over most of the contact length and grain pull-out with presence of shallow grooves at lower speed of 133 rpm **(Figure 7-1 (c))** and grain pull-out in clusters and abrasion at higher speed of 435 rpm

(Figure 7-1 (d)). The fractured material is prone to oxidation at contact temperatures. Thus oxides of constituents of cermet or steel are likely to evolve at the contact surface. Harder tungsten oxide formed during machining plough into the workpiece. Abrasive ridges or grooves formed in **Figure 7-1 (d)** are attributed to high stresses generated at the tool-chip interface during machining. Similar observation of grooves was also reported on Al_2O_3–Ti(CN) tool surface, while machining hardened steel (Senthil kumar et al., 2003). The worn tool surface of conventionally sintered Ti(CN)-5WC-10Ni-10Co-5TaC cermet show shallow grooves and grain pull-out at 133 rpm (not shown as Figure) while increased grain pull-outs regions are observed at 435 rpm (**Figure 7-1 (e)**). Worn tool surface of Spark plasma sintered Ti(CN)-5WC-10Ni-10Co-5TaC cermet revealed grain pull-out on the tool face and discontinuous adhesion beneath the tool face at 133 rpm (not shown as figure), while grain pull-out and continuous adhesion beneath the tool face are observed at 435 rpm (**Figure 7-1 (f)**). Adhesion occurred mainly due to the material transfer through diffusion process during machining. Presence of adhered layer beneath the tool face protected the tool from getting damage by continous rubbing with generated chips and workpiece. Addition of TaC added Ti(CN)-WC-Ni/Co cermet tool resulted in resistance of crack or fracture during machining. The characteristic wear mechanisms observed during turning of Ti(CN)-5WC-10Ni-10Co-5TaC cermet are grain pull-out whereas those observed in Ti(CN)-20Ni-5WC cermet are grain pull-out, cracking and fracture. **Figures 7-1 (g and h)** are images of worn tool tip surfaces of commercial cemented carbide tip showing severe abrasion with pull-outs and cracking at 133 rpm and severe abrasion ridges and grain pull out at 435 rpm. Large amount of ploughing into the workpiece during machining led to severe abrasion. Cutting forces generated at the nose tip interface are also high for commercial cemented carbide tip whereas less forces observed for the investigated cermets. Among the Ti(CN) based cermets, Spark plasma sintered Ti(CN)-5WC-10Ni-10Co-5TaC is promising by having decreased severity in wear.

EDS analysis was done at various locations of tool surfaces after machining and results are shown in **Figures 7-2 (a-d).** In general, EDS analysis reveals the presence minor peaks of Ti, W and Ta and dominant peaks of Fe and O. Presence of Fe, Cr, Si, S, P, Mn and O on the worn tool edge confirms presence of oxides. This confirms the fact that material transfer takes place as a result of chemical affinity between the steel workpiece and the cermet tool. Typical images of chips (not shown in Figure) collected after turning operation shows that at lower cutting speed of 133 rpm the width of chip is higher than that obtained at 435 rpm. It might be because the tool tend to plough in to the workpiece to large extent at low cutting speed resulting in increased width.
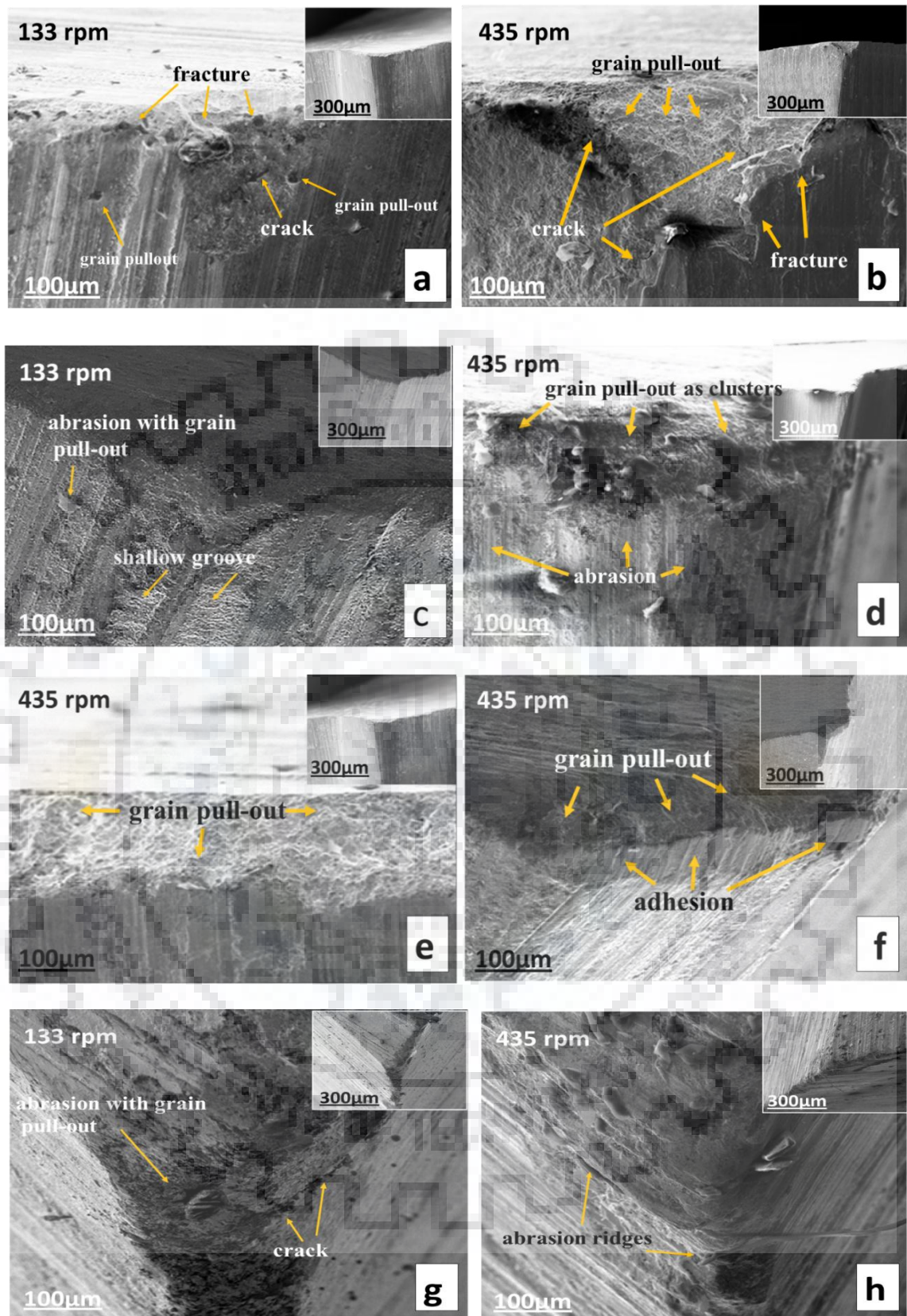
Figure 7- 1. SEM images of worn tool tip surfaces of

(a, b) Ti(CN)-5WC-20Ni cermet processed via conventional at 133 rpm and 435 rpm

(c, d) Ti(CN)-5WC-20Ni cermet processed via SPS at 133 rpm and 435 rpm

(e ,f) Ti(CN)-5WC-10Ni-10Co-5TaC cermet processed via conventionally sintering and SPS at 435 rpm

(g, h) Commercial cemented carbide tip at 133 rpm and 435 rpm
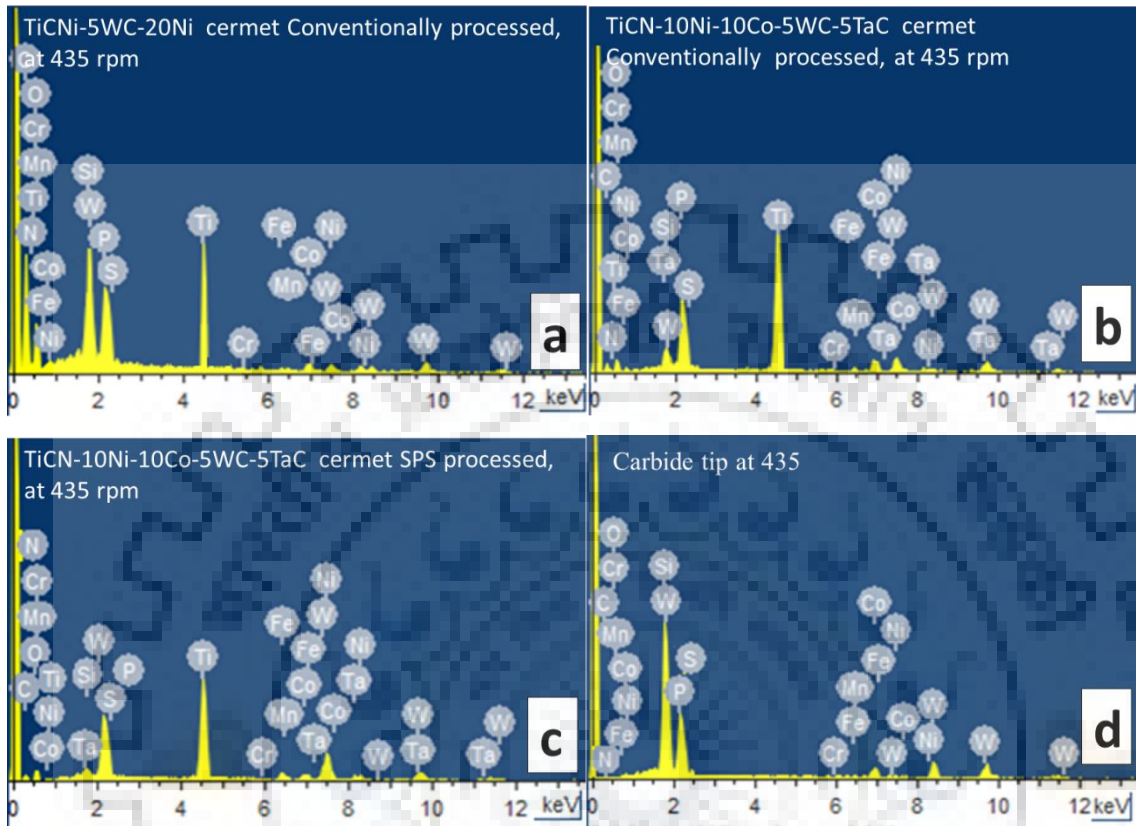
Figure 7- 2. EDS analysis of worn tool tip surfaces of

(a) Ti(CN)-5WC-20Ni cermet processed via SPS at 435 rpm

(b) Ti(CN)-5WC-10Ni-10Co-5TaC cermet processed via conventional at 435 rpm

(c) Ti(CN)-5WC-10Ni-10Co-5TaC cermet processed via SPS at 435 rpm

 (d) Commercial cemented Carbide tip at 435 rpm

Table 7-2. Dominant wear mechanisms in turning of the investigated cermets.

Cermet	Processing technique	Dominant crater wear mechanisms	
		133 rpm, 3 min.	**435 rpm, 1 min.**
Ti(CN)-20Ni-5WC	Conventional	grain pull-out, cracking and fracture	grain pull-out, cracking and severe fracture
Ti(CN)-10Ni-10Co-5WC-5TaC		shallow groove	grain pull-out

Ti(CN)-20Ni-5WC	SPS	abrasion and grain pull-out, shallow narrow grooves	abrasion and clusters of grain pull-out
Ti(CN)-10Ni-10Co-5WC-5TaC		grain pull-out	grain pull-out and continous adhesion beneath the tool face
Commercial carbide tip	Not known	severe abrasion and pull-outs	severe abrasive ridges, grain pull-out

7.3 Effects of the microstructure and properties on the machining performances of TiCN based cermets

Among the investigated materials highest cutting force is observed in commercial cemented carbide tip and conventionally sintered Ti(CN)-5WC-20Ni cermet while lowest cutting force is obtained in spark plasma sintered Ti(CN)-5WC-10Ni-10Co-5TaC cermet at a given speed. At higher speed, Spark plasma sintered TaC added Ti(CN)-WC-Ni/Co cermet tool is capable of reducing the cutting force significantly. Improved mechanical properties are attributed for Spark plasma sintered Ti(CN)-10Ni-10Co-5WC-5TaC cermet tool. Refined carbide size is attributed for improved mechanical properties with the addition of TaC in Ti(CN)-WC-Ni/Co cermet. Further, it is reported that addition of TaC improves the interrupted cutting performance by imparting hot hardness and thermal shock resistance (Kang, 1996; Rolander et al. 2001). Among transition metal carbides, TaC is considered for the consistent mechanical behavior and superior resistance against crack propagation (Rowcliffe and Warren, 1970; Rowcliffe and Hollox, 1971; Rolander et al., 2001). Thus, the cutting performance of Ti(CN)-WC-Ni/Co cermet is observed to improve with the addition of TaC.

7.4 Summary

Present work deals with designing a new Ti(CN) based cermet composition for the improved performance in machining. Ti(CN) based cermet composition Ti(CN)-5WC-20Ni and Ti(CN)-5WC-10Ni-10Co-5TaC (in wt.%) processed via conventional and SPS techniques were selected for turning operations performed for 0.5 mm/rev feed rate and 0.9 mm depth of cut at 133 rpm for 180 sec and 435 rpm for 60 sec against 304 stainless steel

rod of external diameter of 25 mm. Results were compared with commercially available cemented carbide tip tool performance. The study reveals the following major conclusions:

1. Higher cutting forces are resulted at lower speed (133 rpm) compared to higher speed (435 rpm). At lower speed, cutting edge of the tool tends to plough into workpiece surface to a larger extent and as the cutting speed increases, cutting becomes steady with a consequent reduction in the cutting force. Among the investigated tool materials, lower cutting force is observed in Spark plasma sintered Ti(CN)-5WC-10Ni-10Co-5TaC cermet and higher cutting force observed in commercial cemented carbide tip tool and Ti(CN)-5WC-20Ni cermet tool.

2. The worn tool surface of conventional Ti(CN)-5WC-20Ni cermet showed cracks, grain pull-out and fracture at 133 rpm, while the intensity of crack, grain pull-out, and fracture increased at 435 rpm. Hard asperities or wear particles act as sharp indenters and generate cracks, which on further propagation and intersection lead to grain pull-outs on the cermet tool surface. Worn tool surface of conventionally sintered and Spark plasma sintered Ti(CN)-5WC-10Ni-10Co-5TaC cermet revealed increased resistance against crack or fracture. Presence of adhered layer beneath the tool face of Spark plasma sintered Ti(CN)-5WC-10Ni-10Co-5TaC cermet protected the tool from getting damage by continous rubbing during machining.

3. Worn surfaces of cemented carbide tip tool revealed deeper abrasion at 133 rpm, whereas and deeper abrasion and grain pull-out are observed at 435 rpm. Ploughing harder tungsten oxide into the workpiece during machining led to deeper abrasion.

4. The present study demonstrates superior performance of the newly designed Ti(CN) based cermet tools than commercial cemented carbide tools. The Spark plasma sintered Ti(CN)-5WC-10Ni-10Co-5TaC cermet is preferred for tool for machining hard steel.

Chapter-8

Conclusions and future scope

The important conclusions drawn from the present doctoral thesis work are described. Also future directions where studies can be extended are suggested.

8.1 Conclusions

The important contributions of the present work include designing novel Ti(CN) based compositions with or without addition of TaC in Ti(CN)-WC-Ni/Co cermet for improved performance in wear and machining conditions. Ti(CN) based cermets were processed via two techniques: (i) conventional sintering technique and (ii) spark plasma sintering (SPS). The microstructural and mechanical properties of sintered cermets were studied. Further, wear behavior and machining performance of the sintered cermets were investigated. The important conclusions obtained from processing of cermets, tribology and machining studies are separately listed.

Processing of Ti(CN) based cermets via conventional sintering and spark plasma sintering

Four compositions of TiCN-WC-Ni/Co cermets with or without TaC were prepared by conventional sintering (compacted at 100 MPa and sintered at 1550°C for 2 h) and spark plasma sintering (1400°C and 70 MPa for 3 min). Following are the major findings.

- Ti(CN)-5WC-20Ni, Ti(CN)-5WC-20Ni-5TaC, Ti(CN)-5WC-10Ni-10Co, and Ti(CN)-5WC-10Ni-10Co-5TaC prepared by spark plasma sintering resulted in higher densities than conventional sintering.
- While all cermets revealed Ti(CN) core and (Ti,W and/or Ta)CN rim structure, Spark plasma sintered cermets consisted refined carbide size. Spark plasma sintered Ti(CN)-5WC-10Ni-10Co-5TaC cermet has the least contiguity of the ceramic phase and largest binder mean free path among all investigated cermets.
- Higher hardness and higher indentation toughness are obtained for Spark plasma sintered cermets. Addition of TaC in Ti(CN)-WC-Ni/Co cermets resulted in high hardness and indentation toughness. Refined size and least fraction of adjacent ceramic phase are attributed for improved properties of TaC added Ti(CN)-WC-Ni/Co cermet sintered via SPS route.

100

Tribological study of conventional sintered Ti(CN) based cermets against steel and cemented carbide

The effect of TaC addition on the tribological behavior of Ti(CN)-5 wt% WC-20 wt% Ni/Co cermets was investigated against commercially available bearing grade EN-31 steel balls and cemented carbide balls in dry unlubricated conditions at different load. Major conclusions are as given.

- During sliding, the deformation or removal of binder phase is followed by the fracture or pull-out of carbides. The Ti(CN)-5WC-10Ni-10Co-5TaC cermet with maximum hardness, maximum indentation toughness exhibited minimum friction and wear.

- Hard oxide debris particles were responsible for high COF and wear rate against cemented carbide than steel at low load. Against steel, dominant wear mechanism changed from fracture and grain pull-out at a low load in Ti(CN)-5WC-10Ni cermet to the removal of tribochemical layer at high load in Ti(CN)-5WC-10Ni-10Co-5TaC cermet. Maximum extent of transfer of iron oxide from steel ball resulted in the formation of a continuous and strongly adherent tribochemical layer on the Ti(CN)-5WC-10Ni-10Co-5TaC cermet surface; against cemented carbide ball, transfer of tungsten oxide from ball observed on the layer. Also, high contact temperature caused depletion of tribolayer from the surface and resulted in high wear against cemented carbide.

- This part of the study necessarily indicates that the tribological characteristics of Ti(CN) based cermets are influenced by both the composition of the cermet and as well as the sliding test parameters.

Tribological study of Spark plasma sintered Ti(CN) based cermets against silicon carbide

In order to estimate the potential of Spark plasma sintered Ti(CN) based cermets having improved mechanical properties, the sliding wear behavior was studied against hard SiC ball in dry unlubricated conditions at 5, 10 or 20 N load. Major conclusions are as follows.

- One order magnitude higher wear rate of cermet or ball is observed when sliding load increased from 5 to 20 N.

- Among investigated materials, cermet containing TaC and Co-Ni binder phase exhibited stabilized friction and reduced wear in the selected sliding conditions.
- Worn surfaces of the investigated cermets are generally characterized by microcracking, tribolayer formation and spalling when slid against SiC ball.

Machining study of processed Ti(CN) based cermets

Ti(CN) based cermet composition Ti(CN)-5WC-20Ni and Ti(CN)-5WC-10Ni-10Co-5TaC (in wt.%) processed via conventional and SPS techniques were selected for turning operations at 0.5 mm/rev feed rate and 0.9 mm depth of cut at 133 rpm for 180 sec, and 435 rpm for 60 sec against 304 stainless steel rod of external diameter of 25 mm. Results were compared with commercial available cemented carbide tip tool performance. The study revealed the following major conclusions:

- At lower speed, cutting edge of the tool tends to plough into workpiece surface to a larger extent and as the cutting speed increases, cutting becomes steady with a consequent reduction in the cutting force. Spark plasma sintered Ti(CN)-5WC-10Ni-10Co-5TaC cermet exhibited lower cutting force than commercial cemented carbide tool or Ti(CN)-5WC-20Ni cermet tool.
- At higher cutting speed, intensity of cracking, grain pull-out, and fracture observed in conventional Ti(CN)-5WC-20Ni cermet tool; whereas increased resistance against crack or fracture is observed in conventionally sintered and Spark plasma sintered Ti(CN)-5WC-10Ni-10Co-5TaC cermet tools. Damage is further restricted in Spark plasma sintered Ti(CN)-5WC-10Ni-10Co-5TaC cermet tool due to formation of adhered layer beneath the tool face.
- Formation of harder tungsten oxide led to deeper abrasion and grain pull-out at higher speed in commercial cemented carbide tool during turning.
- This part of the study essentially reveals superior performance of the newly designed Ti(CN) based cermet tools than commercial cemented carbide tools. Based on results obtained on machining study, the Spark plasma sintered Ti(CN)-5WC-10Ni-10Co-5TaC cermet is preferred for tool for machining hard steel.

As a closure, the outcome of the present thesis can be realized in terms of (i) design of cermet composition for the given wear conditions and (ii) physics of degradation mechanisms as function of cermet composition and wear conditions. Among the investigated materials, the Ti(CN)-5WC-10Ni-10Co-5TaC cermet composition is optimum for superior performance in sliding wear conditions against any counterbody, load as well

as high speed dry machining conditions against steel workpiece. Secondly the degradation mechanisms changed from fracture and grain pull-out or abrasion to adhesion or formation and removal of a tribochemical layer. The wear or machining performance of the cermet is dependent on the stability of the tribochemical layer. Also, the chemistry of the tribochemical layer is influenced by the material transfer in the given wear or machining conditions.

8.2 Suggestions for Future Work

Based on the results obtained following are the suggestions:

1. Sintering conditions in both conventional and SPS can be optimized in future studies to obtain full density and controlled microstructure in the investigated cermets. The characteristics of ceramic powders can also be varied to control the sintering, resulted mechanical properties and wear or machining performance.

2. Further, processing work can be extended by varying TaC content in Ti(CN)-WC-Ni/Co cermets. Accordingly optimization of the sintering conditions must be obtained. Its influence on the physical and mechanical properties can be studied.

3. Sliding wear behavior in water or oil lubrication can also be investigated to assess the performance of newly designed Ti(CN) based cermets as tools in wet machining conditions. Wear parameters in terms of speed, temperature, humidity etc. can also be varied.

4. Considering the potential tribological applications of the investigated cermets, study can be further extended to understand erosion wear mechanisms.

5. Machining studies can be extended to harder workpieces like titanium alloys. Machining speed and parameters like feed rates can be varied. Flank wear mechanisms can also be studied.

6. The potential of the investigated cermets in non-conventional machining viz. electrical discharge machining is also recommended for future study.

7. Considering salient observations of change in wear mechanisms with varying test parameters or compositions of cermets, it would be interesting to study the subsurface analysis of worn cermets to determine the source of wear damage.

1. A. A. Khan, S. S. Hajjaj. Capabilities of cermets tools for high speed machining of austentic stainless steel, Journal of Applied Sciences. 2006; 6(4):779-784.

2. A. Bellosi, R. Calzavarini, M. G. Faga, F. Monteverde, C. Zancolo, G. E. D'Errico. Characterisation and application of titanium carbonitride-based cutting tools, Journal of Materials Processing Technology, 2003; 143-144:527-532.

3. A. Borrell, M. D. Salvador, V.G. Rocha, A. Fernandez, M. A. Aviles, F. J. Gotor. Bulk TiCxN1x–15%Co cermets obtained by direct spark plasma sintering of mechanochemical synthesized powders, Materials Research Bulletin. 2012; 47(12):4487-4490.

4. A. C. A. de Melo, J. C. G. Milan, M. B. da Silva, Á. R. Machado. Some observations on wear and damages in cemented carbide tools, Journal of the Brazilian Society of Mechanical Sciences and Engineering. 2006; 28(3):269-277.

5. A. Devillez, S. Lesko, W. Mozer. Cutting tool crater wear measurement with white light interferometery, Wear. 2004; 256(1-2):56-65.

6. A. G. de la Obra, F. J. Gotor, E. Chicardi. Effect of the impact energy on the chemical homogeneity of a (Ti,Ta,Nb)(C,N) solid solution obtained via a mechanically induced self-sustaining reaction, Journal of Alloys and Compounds. 2017a; 708:1008-1017.

7. A. G. de la Obra, M. A. Avilés, Y. Torres, E. Chicardi, F. J. Gotor. A new family of cermets: chemically complex but microstructurally simple, International Journal of Refractory Metals and Hard Materials. 2017b; 63:17-25.

8. A.G. Evans and D.B. Marshal. Wear mechanisms in ceramics; Fundamentals of Friction and Wear of Materials, Edited by D.A. Rigney, ed., ASM, Materials Park, OH, 1981, 439–52.

9. A. G. Fried Krupp. Hard alloy for work instruments and tools; French Patent No. 715148, 1931.

10. A. G. King, W. M. Wheidon. Ceramics in machining process, Academic press, New York, 1966.

11. A. R. Machado, J. Wallbank, 1990, Machining of titanium and its alloys - a review, Proceedings of the Institution of Mechanical Engineers, Part B: Journal of Engineering Manufacture. 1990; 204(1):53-60.

12. A. R. Machado. Machining of Ti6Al4V and Inconel 901 with a high pressure coolant system, PhD Thesis, University of Warwick, Coventry, England. 1990.

13. A. Senthil Kumar, A. Raja Durai, T. Sornakumar. Machinability of hardened steel using alumina based ceramic cutting tools, International Journal of Refractory Metals & Hard Materials. 2003; 21:109-117.

14. A. Singh, H Singh, R Kumar. Review on Effects of Process Parameters in Hard Turning of Steels, IJIRST –International Journal for Innovative Research in Science & Technology. 2016; 3(6): 30-35.

15. A. T. Santhanam. Application of transition metal carbides and nitrides in industrial tools. In: Oyama ST. The chemistry of transition metal carbides and nitrides. London: Chapman & Hall; 1996; 28-52.

16. B. Bharat. Introduction to tribology, Second Edition, John Wiley & Sons 2013; ISBN: 9781119944539.

17. B. Basu, K. Balani. Advanced structural ceramics, John Wiley & Sons. 2011; ISBN: 978-0-470-49711-1.

18. B. Bhushan. Principles and applications of tribology, John Wiley & Sons. 1999; ISBN: 9781119944546.

19. B. Basu, M. Kalin. Tribology of ceramics and composites: A Materials Science Perspective, ISBN 978-0-470-52263-9, John Wiley & Sons, 2011.

20. B.V. Manoj Kumar, B. Basu, O. Vizintin, M. Kalin. Tribochemistry in sliding wear of Ti(CN)–Ni-based cermets, Journal of Material Research. 2008; 23(5):1214-1227.

21. B.V. Manoj Kumar, J. Ram Kumar, B. Basu. Crater wear mechanisms of Ti(CN)–Ni–WC cermets during dry machining, International Journal of Refractory Metals and Hard Materials. 2007; 25: 392-399.

22. C. Jin, C. C. Onuoha, Z. N. Farhat, G. J. Kipouros, K. P. Plucknett. Microstructural damage following reciprocating wear of TiC-stainless steel cermets, Tribology International. 2017a; 105:201–218.

23. C. Jin, M. Gaier, Z. Memarrashidi, C. C. Onouha, Z. N. Farhat, K.P. Plucknett. Using combined microscopy techniques to assess sliding wear damage in high performance cermets, Chapter, In book: Microscopy and imaging science: practical approaches to applied research and education, Publisher: Formatex Research Center. 2017b; 490-499. ISBN-13: 978-84-942134-9-6.

24. C. Liu, N. Lin, Y. H. Hea. Influence of Mo2C and TaC additions on the microstructure and mechanical properties of Ti(C, N)-based cermets, Ceramics International. 2016; 42(2): 3569-3574.

25. C. Y. H. Lim, S. C. Lim, K. S. Lee. Wear of TiC-coated carbide tools in dry turning, Wear 1999; 225–229 Part 1:354-367.

26. C. Zhang, E. Narimatsu, K. Komeya, J. Tatami, T. Meguro. Control of grain morphology in Ca-α sialon ceramics by changing the heating rate, Materials Letters. 2000; 43(5): 315-319.

27. D. A. Rigney, L. H. Chen, M. G. S. Naylor, A. R. Rosenfield. Wear processes in sliding systems, Wear. 1984; 100(1-3):195-219.

28. D. Jain, K. M. Reddy, A. Mukhopadhyaya, B. Basu. Achieving uniform microstructure and superior mechanical properties in ultrafine grained TiB_2-$TiSi_2$ composites using innovative multi stage spark plasma sintering, Material Science Engineering A. 2010; 528:200-207.

29. D. J. Rowcliffe, G. E. Hollox. Plastic flow and fracture of tantalum carbide and hafnium carbide at low temperatures, Journal of Materials Science. 1971; 6(10): 1261-1269.

30. D. J. Rowcliffe, W. J. Warren. Structure and properties of tantalum carbide crystals, Journal of Materials Science. 1970; 5(4):345-350.

31. D. K. Shetty, I. G. Wright, P. N. Mincer, A. H. Clauer. Indentation fracture of WC-Co cermets. Journal of Materials Science. 1985; 20: 1873-1882.

32. D. Moskowitz, M. Humenik Jr. Cemented titanium carbide cutting tools, Modern Developments in Powder Metallurgy. 1966; 3:83-94.

33. D. Sarkar, B.V. Manoj Kumar, S. Ahn, S. Kang, B. Basu. Fretting wear behavior of Ti(CN)-based advanced cermets, Key Engineering Materials. 2004; 264-268:1115-8.

34. D. S. Park, Y. D. Lee. Effect of carbides on the microstructure and properties of ti(c,n)-based ceramics, Journal of. American Ceramic Society. 1999; 82(11):3150–3154.

35. E. Chicardi, J. M. Cordoba, F. J. Gotor, High temperature oxidation resistance of (Ti,Ta)(C,N)-based cermets. Corrosion Science. 2016a; 102:125-136.

36. E. Chicardi, J. M. Córdoba, F. J. Gotor. Kinetics of high-temperature oxidation of (Ti,Ta)(C,N)-based cermets, Corrosion Science. 2016b; 102:168-177.

37. E. M. Trent, P. K. Wright. Metal cutting, Butterworth/ Heinemann, Oxford. 2002; ISBN 0-7506-7069-X.

38. E. T. Jeon, J. Joardar, S. Kang. Microstructure and tribo-mechanical properties of ultrafine Ti (CN) cermets, International Journal of Refractory Metals & Hard Materials. 2002; 20(3):207-211.

39. F. Arenas, C. Rondón, R. Sepúlveda. Friction and tribological behavior of (Ti, V)C–Co cermets, Journal of Materials Processing Technology. 2003; 143–144:822–826.

40. F. Monteverde, A. Bellosi. Oxidation behavior of titanium carbonitride based materials, Corrosion Science. 2002; 44(9):1967-1982.

41. F. Ping, X. W. Hao, Z. Yong, Y. L. Xin, X. Y. Hua. Spark plasma sintering properties of ultrafine Ti (C, N)-based Cermet, Journal of Wuhan University of Technology - Material Science. 2004; 19(1):69-72.

42. F. Qi, S. Kang. A study on microstructural changes in Ti(CN)–NbC–Ni cermets, Materials Science and Engineering A. 1998; 251(1-2):276–285.

43. G. Byrne, E. Scholta, Environmentally clean machining processes - a strategic approach, CIRP Annals - Manufacturing Technology. 1993; 42(1):471-474.

44. G. E. D'Errico, S. Bugliosi, D. Cuppiui, E. Guglielmi. A study of cermets' wear behavior, Wear. 1997; 203-204:242-246.

45. G. E. D'Errico, S. Bugliosi, R. Calzavarini, D. Cuppini. Wear of advanced ceramics for tool materials, Wear. 1999; 225–229:267–272.

46. G. Quercia, I. Grigorescu, H. Contreras, C. D. Rauso, D. G. Campos. Friction and wear behavior of several hard materials, International Journal of Refractory Metals & Hard Materials. 2001; 19(4-6):359-369.

47. G. Ostberg, K. Buss, M. Christensen, S. Norgren, H. O. Andrena, D. Mari, G. Wahnstrom, I. Reineck, Effect of TaC on plastic deformation of WC–Co and Ti(C,N)–WC–Co, International Journal of Refractory Metals & Hard Materials. 2006; 24(1-2):145-154.

48. H. A. Zhang, D. K. Yan, S. W. Tang. Preparation and properties of ultrafine Ti(CN) matrix cermets by vacuum microwave sintering, Rare Metals. 2010; 29(5), 528-532.

49. H. Czichos. Review on wear research -activities in the F.R.G., Wear. 1984; 100(1984):579-589.

50. H. C. Lee and J. Gurland. Hardness and Deformation of Cemented Tungsten Carbide, Materials Science and Engineering. 1978; 33(1):125-133.

51. H. Engqvist, H. Hogberg, G.A. Botton, S. Ederyd, N. Axen, Tribofilm formation on cemented carbides in dry sliding conformal contact, Wear. 2000; 239(2):219–228.

52. H. K. Tonshoff, H. G. Wobker, C. Cassel. Wear characteristics of cermet cutting tools, CIRP Annals - Manufacturing Technology. 1994; 43(1):89-92.

53. H. Liu, Y. D. Xu, H. Li, M. H. Chen, J. Zhou, F. Xie, H. D. Yang. Cutting and wearing characteristics of TiC-based cermets cutters with nano-TiN addition, Journal of Materials Processing Technology. 2005; 161(3):478-484.

54. H. Matsubara, T. Sakuma. Microstructure and mechanical properties of titanium carbonitride base cermets, Sintering '87. 1988; 2:1269-1274.

55. H. Opitz, W. Konig. On the wear of cutting tools, advances in machine tool design and research, Proceedings of the 8th International MTDR Conference. 1967; 173-190.

56. H. Pastor. Present status and development of tool materials: Part 1 cutting tools, International Journal of Refractory Metals and Hard Materials. 1987; 6(4):196-209.

57. H. Pastor. Titanium-carbonitride-based hard alloys for cutting tools, Material Science and Engineering A. 1988; 105-106:401-409.

58. H. Thoors, H. Chandrasekaran, O. Patrik. Study of some active wear mechanisms in a titanium-based cermet when machining steels, Wear. 1993; 162-164 Part A: l-11.

59. H. Wei, H. Lei, G. Zhong, H. Yu, P. Feng. Effect of carbon content on microstructure, mechanical properties and wear resistance of Ti(C,N)-based cermets, Applied Mechanics and Materials. 2014; 697:41-45.

60. H. Zhang, J. Yan, X. Zhang, S. Tang. Properties of titanium carbonitride matrix cermets, International Journal of Refractory Metals and Hard Materials. 2006; 24(3):236-239.

61. H. Zhang, S. Tang, J. Yan, X. Hu. Cutting performance of titanium carbonitride cermet tools, International Journal of Refractory Metals & Hard Materials. 2007; 25(5-6):440-444.

62. I. Hussainova. Effect of microstructure on the erosive wear of titanium carbide-based cermets, Wear. 2003; 255(1-6):121–128.

63. I. M. Hutchings, P. Shipway. Tribology: friction and wear of engineering materials, Butterworth Heinemann Publications. 1992; ISBN: 0081009518.

64. J. A. Arsecularatne, L. C. Zhang, C. Montross. Wear and tool life of tungsten carbide, PCBN and PCD cutting tools, International Journal of Machine Tools and Manufacture. 2006; 46(5):482-491.

65. J. A. Williams. Wear and wear particles—some fundamentals, Tribology International. 2005; 38(10):863–870.

66. J. Bijwe, C. M. Logani, U. S. Tewari. Influence of fillers and fibre reinforcement on abrasive wear resistance of some polymeric composites, Wear. 1990; 138(1-2):77-92.

67. J. Bijwe, R Rattan. Influence of weave of carbon fabric in polyetherimide composites in various wear situations, Wear, 2007: 263(7), 984-991.

68. J. Bijwe, R. Rattan, M. Fahim. Abrasive wear performance of carbon fabric reinforced polyetherimide composites: influence of content and orientation of fabric, Tribology International. 2007: 40(5), 844-854.

69. J. B. Dahmus, T. G. Gutowski. An environmental analysis of machining, Proceedings of IMECE04. 2004; 643-652.

70. J. Dusza, L. Parilak, M. Slesar, Fracture characteristics of ceramic and cermet cutting tools, Ceramics International. 1987; 13(3):133-137.

71. J. F. Archard, Contact and rubbing of flat surfaces, Journal of Applied Physics. 1953; 24(8): 981.

72. J. F. Archard, R. A. Rowntree. Metallurgical phase transformations in the rubbing of steels, Proceedings of the Royal Society of London. Series A, Mathematical and Physical Sciences. 1988; 418 (1855):405-424.

73. J. F. Archard. The temperature of rubbing surfaces, Wear. 1959; 2(6):438–455.

74. J. Gong, X. Pan, H. Miao, Z. Zhao. Effect of metallic binder content on the microhardness of Ti(CN)-based cermets, Materials Science and Engineering: A. 2003; 359(1-2):391-395.

75. J. H. Eom, Y. W. Kim. Low temperature processing of silicon oxycarbide-bonded silicon carbide, Journal of. American Ceramic Society. 2010; 93(9):2463-2466.

76. J. K. Lancaster. A review of the influence of environmental humidity and water on friction, lubrication and wear, Tribology international. 1990; 23(6):371-389.

77. J. L. Basse. Binder extrusion in sliding wear of WC-Co alloys, Wear. 1985; 105(3):247-256.

78. J. M. Córdoba, E. Chicardi, R. Poyato, F. J. Gotor, V. Medri, S. Guicciardi, C. Melandri. Spark plasma sintering of $Ti_xTa_{1-x}C_{0.5}N_{0.5}$-based cermets: effects of processing conditions on chemistry, microstructure and mechanical properties, Chemical Engineering Journal. 2013; 230:558-566.

79. J. Meng, J. Lu, J. Wang, S. Yang, Tribological behavior of Ti(CN)-based cermets at elevated temperatures, Materials Science and Engineering: A. 2006; 418(1-2):68-76.

80. J. M. Vieira, A. R. Machado, E. O. Ezugwu, 2001. Performance of cutting fluids during face milling of steels, Journal of Materials Processing Technology. 2001; 116(2-3):244-251.

81. J. Pirso, M. Viljus, S. Letunovits, Friction and dry sliding wear behavior of cermets, Wear. 2006; 260(7-8):815-824.

82. J. Pirso, M. Viljus, S. Letunovits, Sliding wear of TiC–NiMo cermets, Tribology International. 2004a; 37(10):817–824.

83. J. Pirso, S. Letunovits, M. Viljus, Friction and wear behaviour of cemented carbides, Wear. 2004b; 257(3-4):257-265.

84. J. Salem, G. Hilmas, W. Fahrenholtz. Mechanical properties and processing of ceramic binary, ternary, and composite systems, Ceramic Engineering and Science Proceedings. 2009; 29(2):179-187.

85. J. Wang, Y. Liu, J. Ye, S. Ma, Jia Pang. The fabrication of multi-core structure cermets based on (Ti,W,Ta)CN and Ti(CN) solid-solution powders, International Journal of Refractory Metals & Hard Materials. 2017; 64:294–300.

86. J. Xiong, Z. X. Guo, M. Yang, B. L. Shen. Preparation of ultrafine TiC0.7N0.3-based cermet, International Journal of Refractory Metals & Hard Materials. 2008; 26(3), 212-219.

87. J. Xiong, Z. Guo, B. Shen, D. Cao. Fracture origin and intrinsic strength of ultra-fine TiC0.7N0.3-based cermet, International Journal of Refractory Metals & Hard Materials. 2007; 25:256-262.

88. J. Y. Kim, Y. W. Kim, M. Mitomo, G. D. Zhan, J. G. Lee. Microstructure and mechanical properties of alpha-silicon carbide sintered with yttrium-aluminum garnet and silica, Journal of. American Ceramic Society. 1999; 82(2):441-444.

89. J. Zackrisson, H. O. Andren. Effect of carbon content on the microstructure and mechanical properties of (Ti,W,Ta,Mo)(C,N)-(Co,Ni) cermets, International Journal of Refractory Metals & Hard Materials. 1999; 17:265-73.

90. J. Zackrisson, U. Rollander, H. O. Andren. Development of cermet microstructures during sintering, Metallurgical and Materials Transactions A. 2001; 32(1):85-94.

91. J. Zhang, C. L. Liu, Z. H. Hu. Influence of carbon contents on structure and properties of Ti(CN)-based cermets, Powder Metallurgy Technology. 1997; 15:122-125.

92. K. H. Zum Gahr. Microstructure and wear of materials, Elsevier, Oxford. 1987; ISBN: 0-444-42754-6.

93. K. L. Jhonson. Surface interaction between elastically loaded bodies under tangential forces, Proceedings of the Royal Society London. 1955; A230 (1183):531-548.

94. K. M. Reddy, N. Kumar, B. Basu. Inhibition of grain growth during final stage of multistage spark plasma sintering of oxide ceramics, Scripta Materialia. 2010a; 63(6):585-588.

95. K. M. Reddy, N. Kumar, B. Basu. Innovative multi-stage spark plasma sintering to obtain strong and tough ultrafine grained ceramics, Scripta Materialia. 2010b; 62(7):435-438.

96. L. E. Toth. Transition Metal Carbides and Nitrides. New York: Academic Press; 1971.

97. L. Ning, Z. Xingzhong, L. Canlou, H. Zhenhua, C. K. Huazhong, T. Shupei Addition of carbon contents on the microstructure and mechanical properties of cermets with high content of nickel, Cemented Carbide. 1994; 11:144-7.

98. L. R. Krishna, A. S. Purnima, G. Sundararajan. A comparative study of tribological behavior of microarc oxidation and hard-anodized coatings, Wear. 2006: 261(10), 1095-1101.

99. L. R. Krishna, K. R. C. Somaraju, G. Sundararajan. The tribological performance of ultra-hard ceramic composite coatings obtained through microarc oxidation, Surface and Coatings Technology. 2003:163-164, 484-490

100. L. R. Krishna, P. Gupta, G. Sundararajan. The influence of phase gradient within the micro arc oxidation (MAO) coatings on mechanical and tribological behavior, Surface and Coatings Technology. 2015; 269:54-63.

101. M. Alvarez, J. M. Sanchez. Spark plasma sintering of Ti(C,N) cermets with intermetallic binder phases, International Journal of Refractory Metals & Hard Materials. 2007; 25(1):107–118.

102. M. Nouari, A. Ginting. Wear characteristics and performance of multi-layer CVD-coated alloyed carbide tool in dry end milling of titanium alloy, Surface & Coatings Technology. 2006; 200 (18-19):5663-5676.

103. M. Rynemark. Investigation at 1750°C of equilibria in the Ti-W-C-N System, International Journal of Refractory Metals & Hard Materials. 1991; 10:185-193.

104. M. Sokovic, K. Mijanovic. Ecological aspects of the cutting fluids and its influence on quantifiable parameters of the cutting processes, Journal of Materials Processing Technology. 2001; 109(1-2):181-189.

105. M. Tobioka, Y. Shimizu, K. Isobe, N. Kitagawa, T. Nomura, K. Takahashi. High toughness cermet and a process for the production of the same. Patent EP 0259192 A2 1988.

106. M. W. Chase, NIST-JANAF Thermochemical Tables. 4th ed. 1998.

107. N. H. Cook. Tool wear and tool life, Journal of Engineering for Industry. 1973; 95(4):931-938.

108. N. Liu, C. L. Han, Y. D. Xu, S. Chao, M. Shi, J. P. Feng. Microstructures and mechanical properties of nano TiN modified TiC-based cermets for the milling tools, Materials Science and Engineering A. 2004; 382(1):122-131.

109. N. Liu, S. Chao, H. D. Yang. Cutting performances, mechanical property and microstructure of ultrafine grade Ti(CN)-based cermets, International Journal of Refractory Metals & Hard Materials. 2006; 24:445-52.

110. N. M. Parikh, M. Humenik. Cermets: II, wettability and microstructure studies in liquid-phase sintering, Journal of the American Ceramic Society. 1957; 40(9):315-320.

111. N. Narutaki, Y. Yamane, S. Tashima, H. Kuroki. A new advanced ceramic for dry machining, CIRP Annals - Manufacturing Technology. 1997; 46(1):43-48.

112. N. P. Suh. An overview of the delamination theory of wear, Wear. 1977; 44(1):l-16.

113. N. P. Suh. The delamination theory of wear, Wear. 1973; 25(1):111-124.

114. O. Guillon, J. G. Julian, B. Dargatz, T. Kessel, G. Schierning, J. Rathel, M. Herrmann. Field-assisted sintering technology/spark plasma sintering: mechanisms, materials, and technology developments, Advanced Engineering Materials. 2014; 16(7):830–49.

115. P. Ettmayer, H. Kolaska, W. Lengauer, K. Dreyer. Ti(C,N) Cermets – metallurgy and properties, International Journal of Refractory Metals and Hard Materials. 1995; 13(6):343-351.

116. P. Ettmayer, W. Lengauer. The story of cermet, Powder metallurgy international. 1989; 21(2):37-38.

117. P. Lindahl, A. E. Rose, P. Gustafson, U. Rolander, H. O. Andre. Effect of pre-alloyed raw materials on the microstructure of a (Ti, W)(C, N)–Co cermet, International Journal of Refractory Metals and Hard Materials. 2000; 18:273-279.

118. P. Li, J. Ye, Y. Liu, D. Yang, H. Yu. Study on the formation of core–rim structure in Ti(CN)-based cermets, International Journal of Refractory Metals & Hard Materials. 2012; 35:27–31.

119. P. Ramkumar, L. Wang, T. J. Harvey, R. J. K. Wood, K. Nelson, E. Yamaguchi, J. J. Harrison, H. E. G. Powrie. The effect of diesel engine oil contamination on friction and wear, World Tribology Congress III. 2005; 537-538.

120. P. Ramkumar, T. J. Harvey, R. J. K. Wood, K. Nelson, H. E. G Powrie. The effects of diesel contaminants on tribological performance on sliding steel on steel contacts, Proceedings of the Institution of Mechanical Engineers, Part J: Journal of Engineering Tribology. 2011; 225:779 -797.

121. P. S. Sreejith, B. K. A. Ngoi. Dry machining: machining of the future, Journal of Materials Processing Technology. 2000; 101(1-3):287-291.

122. R. H. R. Castro. Overview of conventional sintering, Sintering, Engineering Materials 35, 2012.

123. R. J. K Wood, P. Ramkumar, L. Wang, T. J. Wang, K. Nelson, E. S. Yamaguchi, J. J. Harrison, H. E. G Powrie, N. Otin. Electrostatic monitoring of the effects of carbon black on lubricated steel/steel sliding contacts, Tribology and Interface Engineering Series. 2005; 48:109-121.

124. R. Kieffer, P. Ettmayer, M. Freudhofmeier. Novel types of nitrides and carbonitrides of hard metals, Metall. 1971; 25, 1335–1342.

125. R. L. Smith, G. E. Sandland. An Accurate Method of Determining the Hardness of Metals with Reference to those of a High Degree of Hardness. Proceedings of the Institution of Mechanical Engineers. 1922; 102(1):623-641.

126. R. M. German. Sintering theory and practice, ISBN: 978-0-471-05786-4, John Wiley & Sons, 1996.

127. R. Terao, J. Tatami, T. Meguro, K. Komeya. Fracture behavior of AlN ceramics with rare earth oxides, Journal of the European Ceramic Society. 2002; 22(7):1051-1059.

128. S. Cardinal, A. Malchere, V. Garnier, G. Fantozzi. Microstructure and mechanical properties of TiC–TiN based cermets for tools application, International Journal of Refractory Metals & Hard Materials. 2009, 27(3), 521-527.

129. S. Chaoa, N. Liua, Y. Yuana, C. Hana, Y. Xua, M. Shia, J. Fen. Microstructure and mechanical properties of ultrafine Ti(CN)-based cermets fabricated from nano/submicron starting powders, Ceramics International. 2005; 31(6):851–862.

130. S. Dolinsek, B. Sustarsi, J. Kopa. Wear mechanisms of cutting tools in high-speed cutting processes, Wear. 2001; 250(1-12):349-356.

131. S. Kiani, J. M. Yang, S. Kodambaka. Nanomechanics of refractory transition-metal carbides: a path to discovering plasticity in hard ceramics, Journal of. American Ceramic Society. 2015; 98(8):2313-2323.

132. S. M. A. Suliman, M. I. Abubakr, E. F. Mirghani, Microbial contamination of cutting fluids and associated hazards, Tribology International. 1997; 30(10):753-757.

133. S. Park, S. Kang. Toughened ultrafine (Ti,W)(C,N)-Ni cermet, Scripta Materialia. 2005; 52(2):129-133.

134. S. Y. Ahn, S. Kang. Formation of core/rim structures in Ti(C,N)-WC-Ni cermets via a dissolution and precipitation process, Journal of the American Ceramic Society. 2000; 83:1489-94.

135. S. Y. Ahn, S. Kang. Effect of various carbides on the dissolution behavior of Ti(C0.7N0.3) in a Ti(C0.7N0.3)-30 Ni system, International Journal of Refractory Metals & Hard Materials. 2001; 19:539-545.

136. S. Zhang, C. D. Qin, L. C. Lim. Solid solution extent of WC and TaC in Ti(C,N) as revealed by lattice parameter increase, International Journal of Refractory Metals & Hard Materials. 1993-1994; 12(6):329-333.

137. S. Zhang, G. Q. Lu. Effect of the green state on the sintering of Ti(C,N)-based cermets, Journal of Materials Processing Technology. 1995; 54(1-4):29-33.

138. S. Zhang. Material development of titanium carbonitride based cermets for machining applications, Key Engineering Materials. 1997, 138-140:521-544.

139. S. Zhang. Titanium carbonitride-based cermets: processes and properties, Materials Science and Engineering: A. 1993; 163(1):141-148.

140. S. Zhou, W. Zhao, W. Xiong. Microstructure and properties of the cermets based on Ti(C,N), International Journal of Refractory Metals & Hard Materials. 2009; 27(1):26-32.

141. T. Kayaba, K. Hokkirigawa, K. Kato. Analysis of the abrasive wear mechanism by successive observations of wear processes in a scanning electron microscope, Wear. 1986; 110(3-4):419-430.

142. T. L. Stewart, K. P. Plucknett. The effects of Mo_2C additions on the microstructure and sliding wear of $TiC_{0.3}N_{0.7}$-Ni_3Al cermets, International Journal of Refractory Metals and Hard Materials. 2015; 50:227-39.

143. T. Watanabe, T. Doutsu, T. Nakanishi. Sintering properties and cutting tool performance of Ti(C,N)- based ceramics, Key Engineering Materials. 1995, 114, 189-190

144. U. Rolander, G. Wein, M. Zwinkels. Effect of Ta on structure and mechanical properties of (Ti,Ta,W)(C,N)-Co cermets, International Journal of Refractory Metals & Hard Materials. 2001; 19(4-6):325-328.

145. V. L Tretyakov, V. L Mashevskaya. Effect of tantalum on the properties and structure of hard alloys based on titanium carbonitride, Powder Metallurgy and Metal Ceramics. 1999; 38(1-2):64–67.

146. V. P. Astakhov. The assessment of cutting tool wear, International Journal of Machine Tools & Manufacture. 2004; 44(6):637-647.

147. V. R. Dizaji, M. Rahmani, M. F. Sani, Z. Nemati, J. Akbari. Microstructure and cutting performance investigation of Ti(C, N)-based cermets containing various types of secondary carbides, International Journal of Machine Tools & Manufacture. 2007; 47:768-772.

148. W. F. Hastings, P. L. B. Oxley. Predicting tool life from fundamental work material properties and cutting conditions, CIRP Annals. 1976; 25(1):33-38.

149. W. W. Gruss. Cermets. In: Metals Handbook. 9th ed. 1989. p. 90-97.

150. W.T. Kwona, J.S. Park, S.W. Kimb, S. Kang. Effect of WC and group IV carbides on the cutting performance of Ti(C,N) cermet tools, International Journal of Machine Tools and Manufacture. 2004; 44(4): 341–346

151. X. S. Li, I. M. Low. Ceramic cutting tools – an introduction, Key Engineering Materials. 1994; 96:1-18.

152. Y. Kang, S. Kang. WC-reinforced (Ti,W)(CN), Journal of the European Ceramic Society. 2010; 30(3):793-798.

153. Y. Koren, T. R. Ko, A. G. Ulsoy, K. Danai. Flank wear estimation under varying cutting conditions, Journal of Dynamic Systems, Measurement, and Control. 1991; 113(2):300-307.

154. Y. Liu, Y. Z. Jin, H. J. Yu, J. W. Ye. Ultrafine (Ti,M)(C,N)-based cermets with optimal mechanical properties, International Journal of Refractory Metals & Hard Materials. 2011; 29(1):104-107.

155. Y. Peng, H. Miao, Z. Peng. Development of Ti(CN)-based cermets: mechanical properties and wear mechanism, International Journal of Refractory Metals & Hard Materials. 2013; 39:78-89.

156. Y. S. Kim, W. T. Kwon, M. Seo, S. Kang. Tool performance of new wear-resistant cermets, International Journal of Precision Engineering and Manufacturing. 2012; 13(6), 941-946.

157. Y. W. Kim, S. H. Kim, I. H. Song, H. D. Kim, C. B. Park. Fabrication of open-cell, microcellular silicon carbide ceramics by carbothermal reduction, Journal of. American Ceramic Society. 2005; 88(10):2949-2951.

158. Yokoo, Y. lyori, H. Cermet alloys and composite mechanical parts made by employing them. US Patent 4983212 A. 2016.

159. Y. Zheng, S. Wang, M. You, H. Tana, W. Xiong. Fabrication of nanocomposite Ti(C,N)-based cermet by spark plasma sintering, Materials Chemistry and Physics. 2005; 92(1):64-70.

160. Z. Guo, J. Xiong, W. Wan, G. Dong, M. Yang, Effect of binder content on the erosive wear of Ti(C,N)-based cermet in SiO_2 particle-containing simulated seawater, International Journal of Applied Ceramic Technology. 2014; 11(6):1045–1053.

161. Z. M. Shi, Y. Zheng, W. J. Liu. Wear mechanism of ti(c, n)-based cermet cutting tools in the machining of normalized medium carbon steel AISI1045, Key Engineering Materials. 2007; 353-358:792-795.